THE
PHYSICAL REVIEW
A Journal of Experimental and Theoretical Physics Established by E. L. Nichols in 1893
VOL. 49, NO. 10 MAY 15, 1936 SECOND SERIES

The Absorption of Cosmic-Ray Showers in Lead

C. G. MONTGOMERY AND D. D. MONTGOMERY, *Bartol Research Foundation of the Franklin Institute*
(Received March 25, 1936)

The absorption in lead of the shower rays which produce the bursts of cosmic-ray ionization is measured by two methods. The first method consists in observing the ionization produced above and below a lead absorber placed across the center of an ionization chamber; the second is to observe the probability that a burst of ionization in a chamber is accompanied by a simultaneous discharge of three Geiger-Müller counters over one of which has been placed an absorber. The results of the two methods are in good accord and may be stated in the form that the probability that a ray of a shower will penetrate a thickness of lead decreases linearly with the thickness, becoming zero at approximately 11 cm. The experiments serve to emphasize again the high energies that are involved in a large shower. The results are applied to observations on the effect of shielding on the ionization observed in the stratosphere.

SINCE the first experiments of Rossi,[1] in 1932, on the measurement by means of Geiger-Müller counters, of the absorption of cosmic-ray showers, many refinements have been made, particularly by H. Geiger[2] and his collaborators and by J. C. Street,[3] which have led to a better understanding of the phenomena involved. However, since these showers occur with a large range of sizes and degrees of complexity, additional information can be obtained by observing the behavior of showers of definite size, as may be done with an ionization chamber, instead of observing only the integrated effect of showers of all sizes, as is done in counter experiments. The experiments here described were begun in collaboration with Professor W. F. G. Swann, and some preliminary reports have been published.[4] The absorption in lead of large showers (of the order of a hundred rays, or more) has been measured by two methods in which the ionization that a shower produces is measured before the shower is absorbed.

FIRST METHOD

The principle of this ionization method is to measure the ionization which a given shower produces before and after passing through a thickness of material. Since, presumably, the ionization which a shower produces is proportional to the number of rays which it contains, the observed difference is a measure of the number of rays which are stopped within the material. To measure this, a large cylindrical ionization chamber, 150 cm high and 90 cm in diameter, was used. The chamber was constructed of welded steel of approximately 18 mm thickness. It was divided into two halves, see

[1] B. Rossi, Zeits. f. Physik **82**, 151 (1933).
[2] H. Geiger and O. Zeiller, Zeits. f. Physik **97**, 300 (1935) and earlier papers.
[3] R. H. Woodward and J. C. Street, Phys. Rev. **47**, 800 (1935) and earlier papers.
[4] W. F. G. Swann and C. G. Montgomery, Phys. Rev. **43**, 782 (1933); **44**, 52 (1933). W. F. G. Swann, "Report on the Work of the Bartol Research Foundation," 1933–1934, J. Frank. Inst. **218**, 173 (1934).

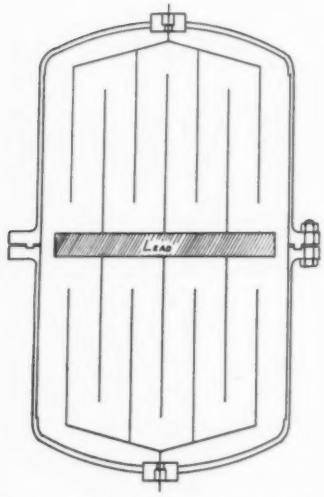

FIG. 1. Diagram of double ionization chamber with absorber in place, showing the electrode arrangement.

Fig. 1, each of 538 liters volume, and each provided with an independent electrode system and guard ring. The electrodes were concentric sheet iron cylinders with conical caps, separated by approximately 10 cm. To collect the ions, the electrodes were maintained at a potential of about 500 volts, and the time of collection of the ions was less than one second. These conditions insure that the statistical fluctuations of the cosmic-ray currents are small.[5] The potential of each electrode system was recorded photographically by allowing the image of an illuminated slit reflected from a galvanometer mirror to fall upon a moving strip of photographic paper. Each galvanometer measured the changes in the plate current of an FP-54 pliotron in the usual manner. The chamber contained nitrogen at 6.8 atmospheres pressure. The capacities of the electrodes were determined by inserting known resistances in the circuits and measuring the time constants of the decay of potential differences between the electrodes. The capacity of each system was found to be about 500 cm.

The thick steel walls of the chamber and the surrounding material served as a source of showers. The ionization which these showers produced was measured in each half of the chamber and the frequency distribution of the shower sizes obtained. Then, to absorb the showers, a circular plate of lead, 7 cm thick and 80 cm in diameter, was inserted between the two halves of the chamber, and the frequency distribution of the sizes of the showers in each half redetermined. Only those showers which produced more than 4×10^6 ions in each half of the chamber were measured. This amount of ionization would be produced by the passage of about 150 high speed electrons through the chamber, if the value for the specific ionization is taken as 60 ions per centimeter.[6] The observations were extended over two 35-hour periods, during each of which more than 200 showers were observed. Since the root-mean-square fluctuation in the cosmic-ray ionization in the time necessary for the galvanometer to deflect was only 6×10^5 ions, the showers of the sizes measured were quite unaffected by these fluctuations. It is of interest to note that the fluctuations in the two halves of the vessel are not statistically independent, but show a correlation caused by the passage of cosmic-ray electrons through both halves. The correlation coefficient is approximately 0.2.[7]

The interpretation of shower observations is complicated by the fact that the showers which emerge from a piece of material are not all of equal size, but are of many sizes whose frequency distribution covers a wide range. In the present experiment, there is the further complication that showers of equal size produce different amounts of ionization, the amounts depending upon their points of origin and their path lengths in the chamber. Thus, we observe three kinds of showers: those which produce amounts of ionization above the limit of measurement in the lower half only, those whose ionizations are above the limit in the top half only, and those which produce measurable amounts of ionization in both halves. Table I gives the numbers of

TABLE I. *Numbers of bursts observed in 35 hours.*

	Both Halves	Upper Half Only	Lower Half Only	Total
Without lead	49	89	78	216
With lead	24	142	102	268

[5] C. G. Montgomery and D. D. Montgomery, Phys. Rev. **47**, 430 (1935).

[6] W. F. G. Swann, Phys. Rev. **44**, 961 (1933).

[7] Cf. W. S. Pforte, Zeits. f. Physik **72**, 511 (1931).

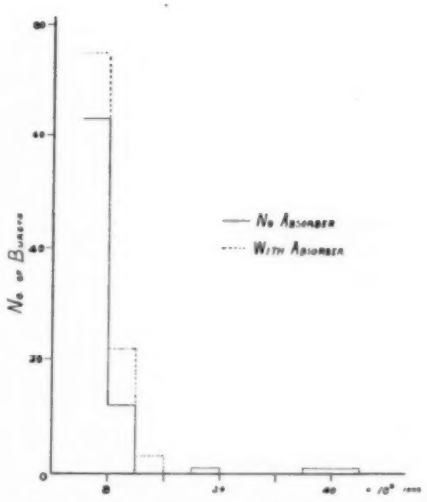

FIG. 2. Frequency distribution of bursts which occurred in the lower half only.

bursts of these three classes observed in 35 hours, with and without a lead absorber.

The effect of introducing the lead is twofold. As well as acting as an absorber of showers produced above it, the lead acts as an additional source of showers. The showers produced in it show themselves most prominently, of course, in the lower half of the chamber. Thus, if we consider the showers which occur in the lower half of the vessel only, we see that more showers are observed with the lead present than without the lead. Fig. 2 shows the distribution in size of the bursts of ionization which occur in the lower half only. However, the difference between the two curves does not represent all the showers which the lead has produced. Certain showers whose points of origin were in the upper half of the chamber but whose sizes, in the absence of the lead, were above the limit of measurement in the lower half only, are now absorbed by the lead and become too small in the lower half to be measured. Therefore, the number of these showers should be added to the difference between the two curves in Fig. 2 to obtain the total number of showers produced by the lead.

The phenomenon in which we are at present most interested is the absorbing effect of the lead upon the showers which pass through it. We see from Table I that the number of showers which produce more than 4×10^6 ions in both the upper and lower halves of the vessel are considerably reduced by the presence of the lead. This reduction in number is to be regarded as the effect of the lead in reducing the size of the showers and making some of them fall below the limit of measurement in the lower half. We may obtain an estimate of the amount of this reduction in size in the following way. Fig. 3 shows the frequency distributions of the ratios of the amounts of ionization produced in the lower half of the vessel to those produced in the upper half by the showers under consideration, with and without the lead absorber. When no lead is present, most of the showers occurring in the upper half of the chamber produce, in the lower half, an amount of ionization only slightly less than in the upper half. This slight difference is to be ascribed to the spreading of the shower rays from their point of origin and their passing out through the side walls of the vessel. When the lead is present, the maximum in the distribution of ratios of sizes shifts to smaller values, since the sizes of the showers in the lower half of the vessel have been reduced without alteration of the sizes in the upper half. We may take the ratio of the positions of the maxima of the two curves as an estimate of the most probable value of the fraction of the rays of a shower which are able to pass through the lead.[8] This value is 0.35/0.85, or 0.4.

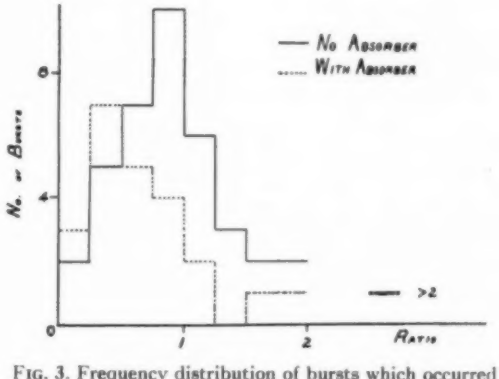

FIG. 3. Frequency distribution of bursts which occurred in both halves of the vessel, with respect to the ratio of the size in the lower half to that in the upper.

[8] It is conceivable that there are showers produced in the lead which proceed upward as well as downward. However, the agreement between the two methods of estimating the absorption in lead indicate that such showers, if present, are relatively few in number.

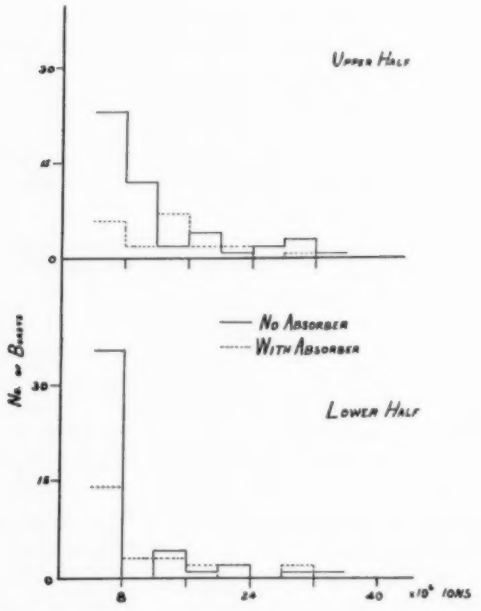

FIG. 4. Frequency distributions of bursts which occurred in both halves of the chamber.

Having obtained a numerical estimate of the reduction which the lead brings about in the size of a shower, we may use it to calculate the number of showers which we should expect to be reduced to a size below the limit of measurement in the lower half of the vessel. This expected reduction, by the lead, of the number of showers which are measurable in both halves of the chamber, may then be compared to the observed reduction. Fig. 4 shows the frequency distribution of the sizes of showers which are above the limit of measurement in both halves of the vessel, with and without the lead present. The lead removes all showers which would have produced less than $4/0.4\times10^6$, or 10×10^6 ions in the lower half of the chamber. Let us take this number of showers to be equal to the number below 10×10^6 ions which *did* occur when no lead was present. This number is 37. The observed decrease is 25. These showers, the bottom components of which have been absorbed, are still observable in the top half of the chamber, and thus the introduction of the lead should cause a corresponding increase in the number of showers observed in the upper half *only*. Fig. 5 shows that there is such an increase and within the limits of the experimental error it is the number expected.

Thus the observations may all be consistently explained if the absorbing effect of the 7 cm of lead is that it reduces the number of rays in a shower passing through it by a factor of 1/0.4. This estimate of the absorbing power of a lead plate may be compared with the absorption effects as measured by a second method, described below.

SECOND METHOD

A second method of measuring the absorption in lead of a cosmic-ray shower is based upon measurements of the probability that a shower of a given size will simultaneously discharge several Geiger-Müller counters. In previous papers,[9] it has been shown that, with reasonable assumptions, it is possible to compute and measure this probability. Suppose now that an absorber is interposed between the source of showers and one of the Geiger-Müller counters. The probability that a ray of the shower will set off that counter will then be decreased, and the probability that a ray of the shower can pass through the absorber can be derived. Fig. 6 shows the experimental arrangement used. The source of showers consisted of a tray, L, 41.5 cm square, containing lead shot to a depth equiva-

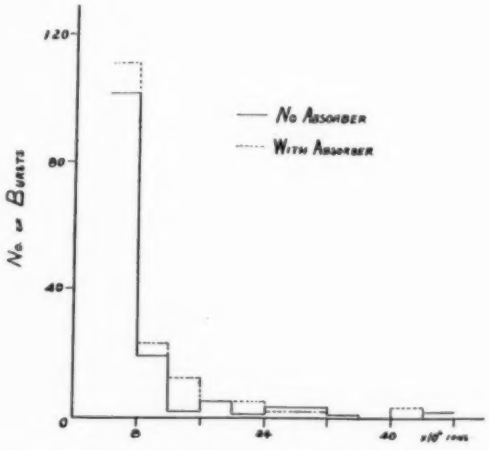

FIG. 5. Frequency distribution of bursts which occurred in the upper half only.

[9] C. G. Montgomery and D. D. Montgomery, Phys. Rev. **48**, 786 (1935); J. Frank. Inst. **221**, 59 (1936).

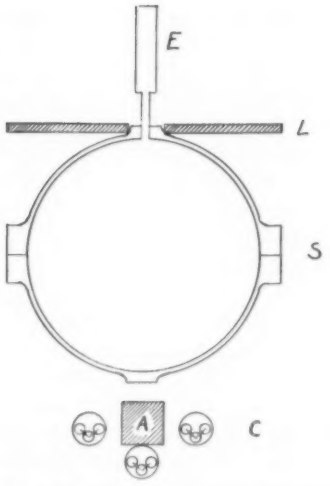

FIG. 6. Experimental arrangement used in the second method.

lent to one centimeter of solid lead. The showers were detected by means of the magnesium ionization chamber, S, and the vacuum tube electrometer, E. The shower rays passing out of the chamber fell upon three Geiger-Müller counters, C, arranged in a "cradle." Over the center counter was placed an absorber, A, of solid lead. A simultaneous discharge of the three counters made an imprint upon the same photographic paper that recorded the bursts of ionization caused by the shower. The fraction of the number of bursts of ionization which were accompanied by a discharge of the set of counters was determined for different thicknesses of the absorber, A. Table II gives the total numbers of bursts of ionization observed in the chamber and the number of bursts with which a simultaneous discharge of the counters occurred. The bursts of ionization are divided, according to size, into five groups. During the course of these observations, the high resistances associated with the counters had two different values. The series of observations labeled I were taken with a lower value of these resistances than the series labeled II. The counter efficiencies in the series I were therefore higher than in II, but the data were treated in such a way, as explained below, that the efficiencies of the counters entered only as a small correction, and the final results are strictly comparable.

The efficiencies of the counters were determined in the usual manner. The counters were arranged so that they formed a telescope pointing in the vertical direction. The number of triple coincidences and the individual counting rates of each counter were measured with and without radium in the vicinity. From these data the recovery time of a counter was computed and hence the efficiency for any given value of the individual counting rate. The efficiency for a counter with no lead over it was 95 percent for the observations in series I, 85 percent in series II.

In order to derive from the above observations a value for the probability that a ray of a shower will penetrate the absorber, we must apply the formulae previously calculated.[9] If N is the number of rays in a shower, p the *a priori* probability that a ray of the shower will pass through a counter in the absence of the absorber, p' the probability that a ray will penetrate the absorber, and E_0 and E_A the efficiencies of a counter without and with an absorber over it respectively, then it can be shown that the probability that the occurrence of a shower will be accompanied by a simultaneous discharge of the three counters is:

$$P=E_0^2E_A[1-2(1-p)^N-(1-pp')^N+(1-2p)^N +2(1-p-pp')^N-(1-2p-pp')^N].$$

For values of N and p which are here under

TABLE II. *Bursts of various sizes observed for different thicknesses of lead absorber.* Rows labeled A give the number of bursts accompanied by counts. Rows labeled B give the total number of bursts.

	Size of Burst ($\times 10^{-6}$ ion pairs)		1.1 to 2.0	2.0 to 3.0	3.0 to 5.0	5.0 to 10.0	10.0 to 20.0
	No Pb	A	117	38	18	16	2
		B	755	105	36	22	3
Series I	2.54 cm Pb	A	92	27	16	17	5
		B	632	97	44	28	5
	5.08 cm Pb	A	54	20	17	10	4
		B	533	102	45	15	4
	No Pb	A	62	30	24	12	8
		B	509	101	35	15	9
Series II	7.62 cm Pb	A	32	18	12	4	3
		B	412	92	46	15	6

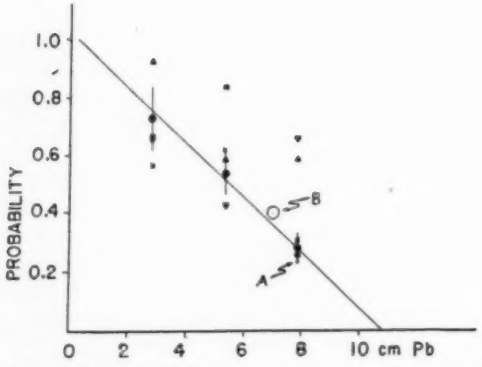

FIG. 7. The probability that a ray of a shower will penetrate a given thickness of lead. *A*, mean value uncorrected for efficiency; *B*, observations by first method. ϕ weighted mean values; Δ, 1.1 to 2.0×10^6 ion pairs; ▽, 2.0 to 3.0×10^6 ion pairs; ×, 3.0 to 5.0×10^6 ion pairs; □, 5.0 to 10.0×10^6 ion pairs.

consideration, it is sufficient to employ the approximate expression:

$$P=E_0^2E_A(1-e^{-Np})^2(1-e^{-Npp'}). \qquad (1)$$

If we designate by P_A and P_0 the observed fraction of the bursts of ionization which were accompanied by a simultaneous discharge of the three counters with and without the absorber, respectively, we can solve Eq. (1) for p' thus:

$$p'=\log\,(1-P_A/E_AP_0^{\frac{1}{2}})/\log\,(1-P_0^{\frac{1}{2}}/E_0).$$

We notice that the value of p' so derived is independent of N and hence independent of the value of the specific ionization of a shower ray. The values of p' were calculated in this way for the first four groups of shower sizes in Table II, and are plotted in Fig. 7. The values of p' that we calculate are, of course, relative to the value of p' for the condition of no absorber, which value has been taken as unity. Now, even when no absorber is present, a ray of the shower, to discharge a counter, must pass out through the wall of the ionization chamber and through the wall and shield of the counter. The amount of material which it must traverse is 2.9 g/cm², which is equivalent to 2.5 mm of lead. Hence the abscissae in Fig. 7 have been displaced by this amount. The probable error for each value of p' was estimated in the usual way from the number of bursts observed and accordingly the weighted mean value of p' for each thickness of lead was computed. These mean values with their probable errors are also recorded in Fig. 7. The values of p' so obtained are largely independent of the efficiency of the counters. The point labeled *A* in Fig. 7 is the value computed assuming the efficiency of the counters to be 100 percent. It differs very little from the value computed when the actual efficiencies were taken into account, although the error introduced by assuming 100 percent efficiency would be greatest for this particular thickness of lead.

We see that, within the limits of the experimental error, p' decreases linearly with the thickness of the absorber and is independent of the size of the shower. The point labeled *B* in Fig. 7 represents the value of p' obtained by the ionization method described in the first section. The agreement between the two methods is thus very satisfactory. If we extrapolate the observations to obtain the maximum range of a shower in lead, we find a value of 11 cm.

DISCUSSION

In the counter experiments on the absorption of showers, the number of counts observed[3] decreases very sharply with the introduction of a lead absorber a few millimeters thick, and then as the thickness of the absorber is increased, the number of counts decreases much more gradually. Of course, it is not possible to express the results of the counter observations directly in terms of the probability that a shower ray will penetrate the absorber, since the frequency distribution in size of the showers counted is not known, and hence the results of the present experiment may not be directly compared with the counter observations. Unfortunately the ionization chamber used for our experiments is so thick that the sharp initial decrease in the probability of penetration, if it were present, could not be observed. The measured probabilities of a shower ray penetrating a given thickness of lead, as given in Fig. 7, are relative values calculated by choosing as unity the probability when no additional absorber other than the chamber itself was present. However, the very gradual falling off of the number of showers, observed in counter experiments, as large thicknesses of lead are added is in good accord with the experiments here described.

These experiments emphasize again the fact that very large amounts of energy must be involved in the production of showers. Using Anderson's[10] value of the energy loss of electrons in lead, we see that at least half of the rays of the shower which emerge from the chamber have energies greater than 3×10^8 electron volts, and that the total energy in the showers which we observe must often exceed 3×10^{10} electron volts. It is also apparent that such penetrating powers as we observe are incompatible with the simple identification of the position of the maximum of a Rossi curve with the range of the shower particles.

An interesting consequence of these experiments is the quantitative agreement with the observations on the ionization produced in shielded and unshielded chambers in the stratosphere. As we go to higher and higher elevations, the contribution to the ionization of the extremely penetrating (primary) cosmic rays becomes smaller and smaller relative to the contribution of the secondary (shower) particles produced in the atmosphere. Thus we should expect that the percentage decrease in the ionization brought about by shielding the chamber should approach the value observed in the present experiments for the probability that a shower ray will be stopped in the shield. Bowen, Millikan, and Neher[11] have published a curve showing the variation with elevation of the decrease in ionization caused by a 6.5-cm lead shield, derived from their measurements and those of Compton and Stevenson.[12] The percentage decrease approaches the value of 68 percent as the elevation increases. The probability that a shower ray will be stopped in this shield thickness is 62 percent. Thus the observations are in accord with the interpretation suggested here.

The authors wish to express their gratitude to Professor W. F. G. Swann, in collaboration with whom a portion of these experiments were carried out, and whose interest and guidance throughout the course of this investigation have been invaluable.

[10] C. D. Anderson and S. H. Neddermeyer, Papers and Discussions, International Conference on Physics, London, 1934, I, p. 171.

[11] I. S. Bowen, R. A. Millikan and H. V. Neher, Phys. Rev. **46**, 646 (1934).

[12] A. H. Compton and R. J. Stevenson, Phys. Rev. **45**, 441 (1934).

MAY 15, 1936 PHYSICAL REVIEW VOLUME 49

Coincidence Counter Studies of Cosmic-Ray Showers

R. H. WOODWARD, *Harvard University*

(Received March 28, 1936)

It has been found that the production curves (counting rate against thickness of lead) of electron-produced and of photon-produced showers are similar and that the average penetrating power of the rays from electron-produced and from photon-produced showers is the same. Shower production curves have been obtained at four elevations and analysis of the curves shows that the absorption per nucleus of the shower-producing radiation (photons) is approximately proportional to the square of the atomic number. Coefficients for lead (0.33 cm^{-1}), iron, and air have been determined, and a comparison with theory is given. Also the penetrating power of the shower rays emerging from a block of lead has been measured and found to be independent of the elevation and of the thickness of the lead from which the rays emerge.

1. INTRODUCTION

THE cloud chamber photographs of Anderson *et al.*[1] and Blackett and Occhialini[2] have shown that cosmic-ray showers consist of groups of from two to several score electrons which are accompanied by numerous low energy photons. The shower-producing rays are usually non-ionizing, although the photographs of Stevenson and Street[3] show that ionizing rays may produce

[1] C. D. Anderson, R. A. Millikan, S. Neddermeyer and W. Pickering, Phys. Rev. **45**, 352 (1934).

[2] P. M. S. Blackett and G. P. S. Occhialini, Proc. Roy. Soc. **A139**, 699 (1933).

[3] E. C. Stevenson and J. C. Street, Phys. Rev. **48**, 464 (1935).

showers (possibly through the intermediary of nonionizing rays). Many of the shower electrons radiate from a single point. There is a high probability, however, that the production of one shower will be accompanied by the simultaneous production of other showers, the several shower foci usually being unconnected by tracks of ionizing rays. Either in the production of a shower or in a primary process nonionizing rays, photons, are created which themselves are capable of producing showers.

Geiger and Fünfer[4] have proposed a convenient nomenclature which we shall adopt in this discussion:

A-rays. The primary charged particles which lose energy through ionization and the radiation of B-rays (photons) in nuclear collisions. The latitude effect of showers[5, 6] requires that they be related to a primary corpuscular radiation.

B-rays. The shower producing photons.

C-rays. Shower electrons created in groups by B-rays.

D-rays. Low energy photons produced in the absorption of C-rays.

E-rays. Low energy electrons from photo and Compton collisions of the D-rays. The D- and E-rays account for the back scattering reported by Fünfer.[7] The distinction between A-, C-, and E-rays is not clearly defined. Their properties may be similar, and there may be overlapping of energies of different groups. Likewise the B- and D-rays may behave in similar fashions. But in general the classes are arranged in order of decreasing energy.

The study of showers by the coincidence counter method has been made by Rossi[8] and many others, and the results of these experiments have been discussed in detail by Geiger.[9] In general, curves of the type shown in Fig. 2 are obtained. Such a curve relating the counting rate N to the thickness X of material can be roughly expressed as the difference of two exponentials,

$$N = C(e^{-\mu X} - e^{-\nu X}). \qquad (1)$$

Here μ may be considered as the absorption coefficient of the primary radiation and ν that of the secondary radiation or *vice versa*, and consequently there are two possible interpretations of the curve. The initial rise may represent the coming into equilibrium of a secondary radiation ($\nu \sim 0.7$ per cm of lead) with a more penetrating shower-producing radiation ($\mu \sim 0.3$ cm^{-1}), the absorption of which accounts for the fall of the curve beyond the maximum. The alternative interpretation is that the shower-producing radiation is rapidly absorbed ($\nu \sim 0.7$ cm^{-1}), while the secondary radiation is the more penetrating ($\mu \sim 0.3$ cm^{-1}). Direct measurements (see sections 2 and 4) of the absorption of the secondary rays emerging from a block of lead show that most of these rays are not penetrating, being absorbed to a large extent in two millimeters of lead. Furthermore it does not seem plausible that the secondary radiation, which on the average must be considerably less energetic, should be more penetrating than the primary radiation. For these reasons we prefer the former interpretation and in our discussion shall disregard the possibility of the latter.

2. A Comparative Study of Electron and Photon-Produced Showers

The production of cosmic-ray showers has been studied by the arrangement shown in Fig. 1. The counters in each of four groups were connected in parallel so that each group acts as a single counter. Iron blocks were placed below and at the sides of the lower counters to reduce the number of cross-scattered rays. The triple coincidence counting rates N_{123} between groups 1, 2, and 3, and N_{234} between groups 2, 3, and 4 were recorded simultaneously for various thicknesses of the lead in position A. A coincident discharge of groups 1, 2, and 3 requires ionization above the lead, whereas a discharge of groups 2, 3, and 4 is

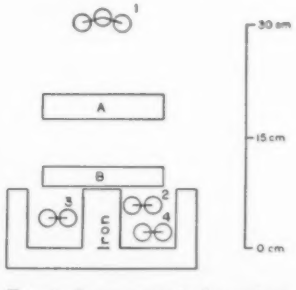

Fig. 1. Arrangement of counters.

[4] H. Geiger and E. Fünfer, Zeits. f. Physik **93**, 543 (1935).
[5] T. H. Johnson, Phys. Rev. **47**, 318 (1935).
[6] T. H. Johnson and D. N. Read, Abstract 2, New York Meeting of Am. Phys. Soc., Feb., 1936.
[7] E. Fünfer, Zeits. f. Physik **83**, 92 (1933).
[8] B. Rossi, Zeits. f. Physik **82**, 151 (1933).
[9] H. Geiger, Ergeb. d. Exakt. Naturwiss. **14**, 42 (1935).

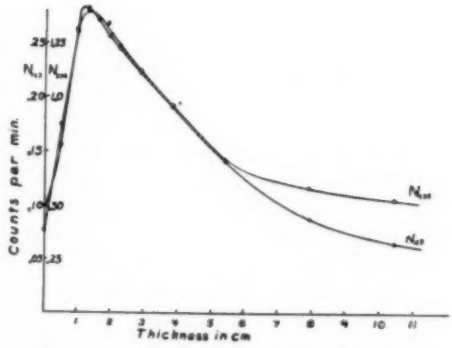

FIG. 2. Curves of shower production in lead.

independent of the nature of the radiation above the lead. As shown in Fig. 2, the variation of the counting rate N_{234} with thickness of lead is similar to that of N_{123}, the factor of five between the scales presumably depending on the geometry of the arrangement. Stevenson and Street[10] have shown that about 70 percent of the coincidences of type N_{123} due to showers produced in the lead actually arise from incident electrons. Most of the coincidences of type N_{234} involving no selection in favor of incident electrons are due to an incident photon radiation.[1] It is surprising, therefore, that the curves are so nearly similar, for in each case the shape of the curve and the position of the maximum are dependent upon the relative absorptions of the incident and secondary radiations. However, there is evidently a real difference in the curves at great thicknesses of lead. The significance of this difference will be discussed in section 3.

The absorption of the C-, D-, and E-rays which actually discharge the lower counters has been measured by placing plates of absorbing material of various thicknesses in position B, so that they absorb the rays produced in the block A but do not themselves produce many showers capable of discharging the triple sets of counters. Fig. 3 shows a schematic diagram of the arrangement together with a plot of four pairs of absorption curves which were obtained by placing various thicknesses of lead or aluminum in positions B under thicknesses 0, 0.476, 1.59, and 7.94 cm of lead at A. The thickness of aluminum is plotted on such a scale that equal distances along the abscissa represent equal numbers of extranuclear electrons per cm² in the lead and aluminum. The nature of the absorption curves is nearly similar for the two types (N_{123} and N_{234}) of coincidences discussed above, and only one set of curves is given. This indicates that there is no distinction between the photon and electron-produced showers as regards to penetrating power of the secondaries. The interpretation of the curves is complicated by the fact that the lead and aluminum in positions B are not pure absorbers; i.e., there are coincidences due to the production of showers and also there is possibly an increase of the efficiency of the photons (D-rays) in discharging the lower counters. These effects account for the peaks in the absorption curves, and corrections for them are unreliable. However, the initial rapid fall of the curves, which probably is not greatly influenced by these effects, shows that most of the shower rays are absorbed in two millimeters of lead. Also the curves show that the penetrating power of the shower rays does not change appreciably as the thickness of the lead block A is increased. The absorption per extranuclear electron is less rapid for aluminum than for lead, indicating that the absorption of shower rays depends not only on extranuclear electrons but also on the nuclei.

[10] E. C. Stevenson and J. C. Street, Phys. Rev. **49**, 425 (1936).

3. The Variation of the Rate of Shower Production with Elevation

The coincidence rate with no lead in positions A and B is a considerable fraction of the maximum change due to the introduction of lead, and it is

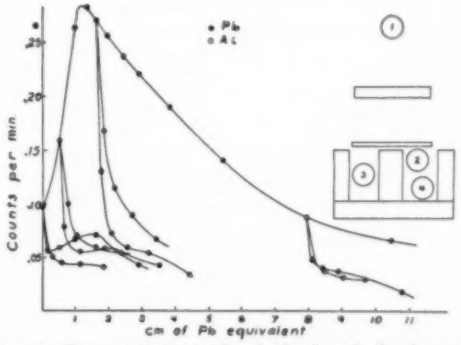

FIG 3. Curves of absorption in lead and aluminum of shower rays from lead. The thickness of aluminum is expressed in equivalent cm of lead on a scale of equal numbers of electrons per cm².

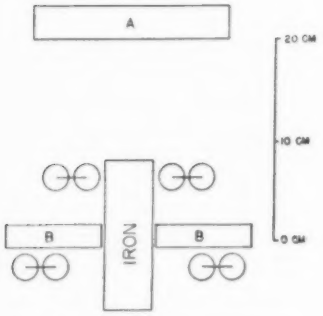

FIG. 4. Arrangement of counters.

not clear how corrections can be made for the variation of this "background"[11] rate with the introduction of lead at *A* and *B*. This difficulty, together with the fact that lead at *B* does not behave as a perfect absorber renders a quantitative treatment of the data obtained with the arrangement of Fig. 1 uncertain. The arrangement of counters shown in Fig. 4 was designed to minimize these difficulties. Quadruple coincidences between the four pairs of counters were recorded for various thicknesses of lead placed above the counters at *A*. The zero reading is too low to distort the measurements and the quadruple coincidence counting rate due to showers produced in the absorbing plates at *B* is negligible; i.e., no distortion of the absorption curves is observed. With this arrangement the previous measurements have been repeated at Cambridge and at three higher elevations. The results with the probable errors are tabulated in Table I and the principal curves are plotted in Fig. 5. All measurements were taken under canvas, and corrections were made for barometric fluctuations and for change of the efficiencies[12] of the counters with altitude and with thickness of lead. The accidental counting rate was negligible (order of 0.0001 per min.). The four curves are similar within the limits of experimental error. The increase of the rate of shower production with elevation is in satisfactory accord with other coincidence counter observations.[5, 13, 14] However it is in serious disagreement with the ionization chamber observations of C. G. and D. D. Montgomery.[15] They find that the frequency of cosmic-ray bursts increases by a factor of 26.6 from sea level to Pike's Peak (4300 m), whereas our coincidence rates increase by a factor of only 8.5 from sea level to Mt. Evans (4300 m). As a possible explanation for the discrepancy, we suggest that the small showers (an average of 3 or 4 rays per shower) recorded by the counter set increase with altitude less rapidly than the large bursts (estimated at 100 or more rays per burst) recorded by their ionization chamber. The results obtained at the same stations (Cambridge, Denver, Echo Lake, and Mt. Evans) by R. T. Young[16] with a small ionization chamber seem to support this explanation. He finds that while the small bursts (10 to 15 rays) increase by a factor of 9.0 between sea level and Mt. Evans, the large bursts (greater than 30 rays) increased by a factor of 22.

Gilbert[17] has reported that the peak of the shower production curve shifted from 1.6 cm of lead at sea level to 2.2 cm at an elevation of 3500 m. Although there is an indication of such a shift of the peak in our curves, it is certainly smaller, if it exists at all. Here again the explanation may lie in the different types of showers

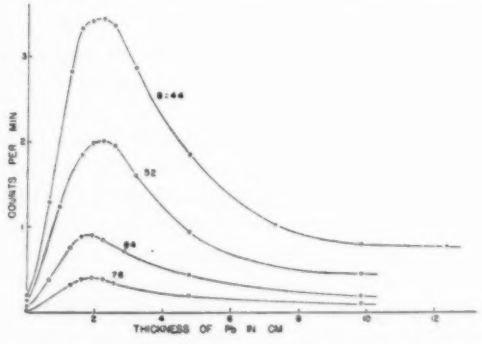

FIG. 5. Shower production curves at Mt. Evans (4300 meters), Echo Lake (3250 m), Denver (1620 m), and Cambridge (60 m).

[11] Supplementary tests have shown that not more than ten percent of this rate is due to accidental coincidences. The major part is no doubt due to showers from the air or light wooden roof above the counter set.

[12] J. C. Street and R. H. Woodward, Phys. Rev. **46**, 1029 (1934).

[13] B. Rossi and S. de Benedetti, Ricerca Scient. 5-II, 379 (1934).

[14] J. A. Priebsch, Zeits. f. Physik **95**, 102 (1935).

[15] C. G. Montgomery and D. D. Montgomery, Phys. Rev. **47**, 429 (1935).

[16] R. T. Young, Abstract 10, New York Meeting Am. Phys. Soc., Feb. 1936.

[17] C. W. Gilbert, Proc. Roy. Soc. **A144**, 559 (1934).

TABLE I. *Quadruple coincidence counts for various thicknesses of lead placed above the counters at A and for various altitudes.* Column 1 gives the position A in cm of lead; column 2, the position of B in cm of lead; columns 3, 6, 9, and 12 give the coincidence counts per minute, N; columns 4, 7, 10, and 13 give the probable error as defined by $0.67[\Sigma(\Delta N)^2/n(n-1)]^{\frac{1}{2}}$; columns 5, 8, 11, and 14 give the probable error as defined by $0.67c^{\frac{1}{2}}/T$.

Barometric Pressure Elevation		76 cm 60 meters			64 cm 1620 meters			52 cm 3250 meters			44 cm 4300 meters		
1	2	3	4	5	6	7	8	9	10	11	12	13	14
0.00	0.00	0.014	0.0017	0.0010	0.066	0.007	0.004	0.138	0.005	0.006	0.206	0.012	0.008
.63	.00				.39	.004	.012				1.28	.017	.033
.95	.00							1.23	.007	.005			
1.27	.00	.320	.0062	.0048	.75	.019	.014				2.82	.037	.035
1.59	.00	.388	.0064	.0054	.89	.017	.012	1.84	.032	.028	3.35	.020	.040
1.91	.00	.398	.0072	.0051	.91	.011	.012	1.98	.040	.025	3.38	.034	.027
2.22	.00	.398	.0065	.0064	.85	.011	.012	2.00	.026	.025	3.44	.038	.030
2.54	.00	.345	.0075	.0061				1.97	.019	.027	3.35	.040	.044
2.85	.00				.72	.018	.013						
3.18	.00							1.59	.017	.034	2.86	.054	.037
4.77	.00	.197	.0037	.0047	.43	.014	.012	0.93	.007	.028	1.84	.039	.030
7.30	.00										1.02	.017	.034
9.85	.00	.102	.0021	.0036	.20	.006	.007	.46	.030	.019	0.79	.009	.018
12.40	.00										.77	.007	.030
0.00	.63				.043		.006						
.00	5.08	.011		.0017	.030		.006	.071		.009	.105		.008
.63	.32										.62		.024
.63	1.59										.39		.021
.63	5.08										.19		.010
1.91	.16	.259		.0057	.60		.015						
1.91	.32	.161		.0042	.37		.012	.85		.028	1.54		.042
1.91	.63	.115		.0047	.19		.008	.60		.029			
1.91	1.11	.069		.0042									
1.91	1.59	.063		.0033	.14		.007	.39		.024	.63		.041
1.91	5.08	.013		.0015	.035		.004	.17		.010	.29		.016

recorded. Gilbert's arrangement of counters required three rays to produce a coincidence whereas ours required only two. It is evident from a comparison of the results of sections 2 and 3 that there is a shift of the peak due to the use of different geometrical arrangements. Probably this shift is not significant, for the distortion caused by the variation of the initial counting rate with the introduction of lead may well explain the entire difference. It is to be expected that the superposition of an initial decreasing curve upon the production curve will shift the peak to a smaller thickness.

The intensity of the single corpuscular radiation was measured by recording double coincidences between one of the upper pairs of counters in the arrangement of Fig. 4 and the pair below it. Corrections have been made for accidental coincidences. However, the coincidence rate due to showers probably is considerable, and, since the solid angle subtended by the counters is large, the observed counting rate is not truly representative of the vertical intensity. The ratio of the shower intensity to this measured corpuscular intensity increases markedly with altitude as shown in Table II, even though the factors mentioned above tend to make this increase less evident.

TABLE II. *Ratio of showers to corpuscular intensity at different altitudes.*

Barometric pressure (cm)	44	51	64	76
Relative shower intensity	8.5	5.0	2.25	1.00
Relative corpuscular intensity	3.6	2.5	1.46	1.00
Ratio of showers to corpuscular intensity	2.4	2.0	1.5	1.0

Although the theory as so far developed is unsatisfactory in treating multiple pair formation by photons, it is of interest to compare the theoretical predictions for single pair formation with the experimentally determined absorption of photons in shower production. Oppenheimer[18] has presented an argument which would lead to a lower limit for the nuclear cross section for pair formation by photon encounter.

[18] J. R. Oppenheimer, Phys. Rev. **47**, 44 (1935).

$$\sigma \sim (28/9)\alpha Z^2\rho^2 \ln (1/\alpha^2 Z^{\frac{1}{3}}\epsilon),$$
$$\sigma \sim 0 \quad \text{for} \quad \epsilon > \alpha^{-2}Z^{-\frac{1}{3}}, \tag{2}$$

where

$\alpha = e^2/\hbar c$, $\rho = e^2/mc^2$, $\epsilon =$ Energy of photon$/mc^2$.

As a basis of comparison we shall consider the absorbing power of a material as a function of its atomic number. Since the effect of the logarithmic factor is not large, a first comparison can be made by neglecting it. Then the absorption per nucleus of absorbing material should be proportional to the square of the atomic number, and for comparison, the atmospheric layers between stations have been expressed in equivalent cm of lead on the Z^2 scale. Fig. 6 is a logarithmic plot of the counting rate against the total equivalent thickness of lead. Each curve rises approximately linearly, falls approximately linearly, and then levels off. Presumably the linear portion of each curve beyond the peak represents the absorption of the B-radiation in lead. It is parallel to the corresponding portion of each of the other curves and approximately parallel to the line drawn through the peaks of the curves and representing the absorption of the B-radiation in air.[19] This

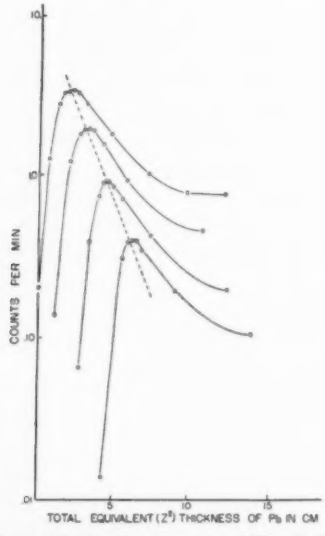

FIG. 6. Logarithmic plot of curves of Fig. 5. The atmospheric layers are expressed in equivalent cm of lead on the basis of an absorption per nucleus proportional to Z^2.

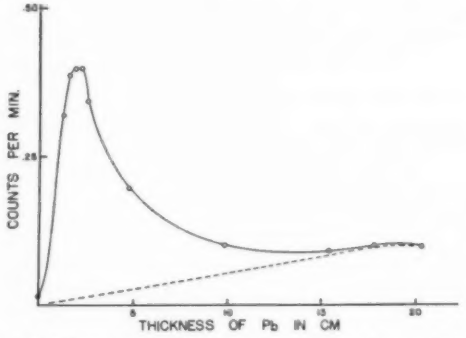

FIG. 7. Shower production curve at sea level extended to 20 cm of lead.

indicates that on the scale of the square of the atomic number the coefficients of absorption are roughly the same for lead and air. However, we do not wish to attach too much significance to the facts that the portions of the curves appear to be linear on a logarithmic plot and that the coefficients depend on the square of the atomic number. The shape of a logarithmic plot is very sensitive to the addition or subtraction of a constant value and the departure of the curves from linearity at great thicknesses of lead requires some explanation if this analysis is to apply. We considered the possibility that this departure might be due to rays which fall obliquely on the sides of the lead block and produce showers without traversing the entire thickness of the block. To test this we built up lead wedges on the sides to absorb rays coming in obliquely. Since the lead wedges produced no appreciable decrease in the counting rate, we concluded that this effect was too small to account for the departure of the curves from linearity. However, consideration of the experiments of Ackemann[20] and Hummel[21] leads to an explanation of the difficulty. By an experiment similar to theirs we have verified the existence of a second maximum at 18 cm of lead as shown in Fig. 7. The experiments of Kulenkampff[22] have given an explanation of the second maximum. He finds that it arises from a very penetrating B-radiation which produces a penetrating C-

[19] W. F. G. Swann, Phys. Rev. **48**, 641 (1935), has proposed an alternative interpretation, based on the assumption that the increase of shower production with elevation may be attributed to an increase (with energy) of the probability that a primary ray (either directly or indirectly) will produce a shower rather than to an increase in abundance of shower-producing rays.

[20] M. Ackemann, Naturwiss. **22**, 169 (1934).

[21] J. N. Hummel, Naturwiss. **22**, 170 (1934).

[22] H. Kulenkampff, Physik. Zeits. **22**, 785 (1935).

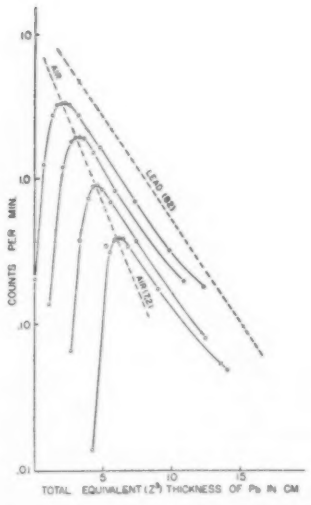

FIG. 8. Curves similar to the dashed curve of Fig. 7 have been subtracted from the curves of Fig. 6.

radiation. We suggest that the showers of the second maximum arise from this C-radiation, and that the variation with thickness of lead is represented by the dashed curve of Fig. 7.[23] We have assumed, as is strongly indicated by the curves of Fig. 5, that similar maxima would be found at higher elevations, bearing approximately the same ratio to the first maxima. Thus from each set of data we subtract the counting rate due to showers of this type, and obtain the curves of Fig. 8. Beyond the maxima the plots are now nearly straight and all have approximately the same slope, corresponding to an absorption coefficient of about 0.33 per cm of lead. This is to be compared with a coefficient of 0.53 per cm of equivalent lead for the absorption of the atmosphere. We estimate the probable error to be 0.04 cm^{-1} for each, which is considerably less than their difference. The ratio of the coefficients (μ air/μ lead = 1.6) may be compared with the ratio of the logarithmic term for air and for lead given by Oppenheimer (Eq. (2)). The computed value for an energy of 300 MEV is 1.4. More recently an expression for the absorption coefficient for high energy photons has been suggested by Nordheim.[24]

$$\mu=\frac{Nz^2r_0^2}{137}\frac{28}{9}\ln\frac{137}{Z^{5/6}}\left(\frac{137mc^2}{\epsilon}\right)^{\frac{1}{2}}, \qquad (3)$$

where $r_0=e^2/mc^2$ and N = number of atoms per cm^3. This expression gives a ratio of 5.0 for the logarithmic terms for air and lead. Although the experimental errors are large, the indication is that the dependence of the nuclear cross section on Z is somewhat stronger than that given in Oppenheimer's expression and weaker than Nordheim's. The experimental coefficient 0.33 per cm of lead is to be compared with 0.77 cm^{-1} predicted by Oppenheimer and 0.20 cm^{-1} predicted by Nordheim. The computations were made for an estimated average energy of 300 MEV.[25] The uncertainty in the estimated energy is large and might possibly account for the discrepancy either way.

To substantiate our conclusion that the absorption of high energy photons depends at least to a first approximation on the square of the atomic number, we have made measurements of the absorption of the B-radiation in iron at sea level. For this purpose we have placed at A

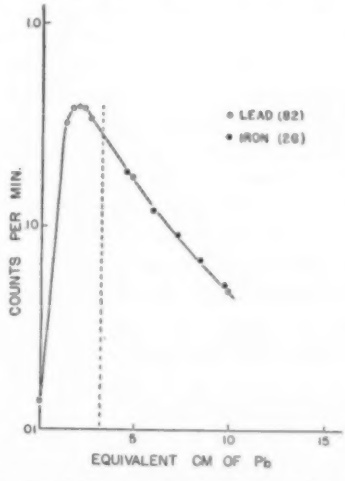

FIG. 9. Curves similar to those in Fig. 8 of the absorption of B-rays in lead and in iron (on top of 3.2 cm of lead).

[23] The difference between curves N_{123} and N_{234} (of section 2, Fig. 3) can now be explained as due to the contribution of showers of the type which cause the second maximum to the rate N_{234}, but not to the rate N_{123}, since this requires an ionizing ray above the lead.

[24] L. W. Nordheim, Phys. Rev. **49**, 189 (1936).

[25] This estimate is made from a consideration of the average number of rays per shower, reference 10, the average energy of the shower rays (C. D. Anderson and S. H. Neddermeyer, Int. Conf. Physics, London, October 1934), and the importance of secondary photons, reference 9, in the phenomenon.

(Fig. 4) 3.2 cm of lead, an amount sufficient to bring the C-radiation into equilibrium with the B-radiation. Iron placed on top of the lead acts essentially as an absorber of the B-radiation. The counting rates for lead and iron corrected for the second maximum and plotted against the total equivalent thickness of lead should lie along the same line, and it is found that within experimental error they do (Fig. 9). However, the correction for the second maximum here is rather uncertain. We take its position at 30 cm of iron as given by Kulenkampff[22] and assume that the magnitude of the first and second maxima for iron are in the same ratio as those for lead. For the case of iron and lead the deviation from the Z^2 relationship (i.e., the logarithmic term) is too small to be detected by this experiment.

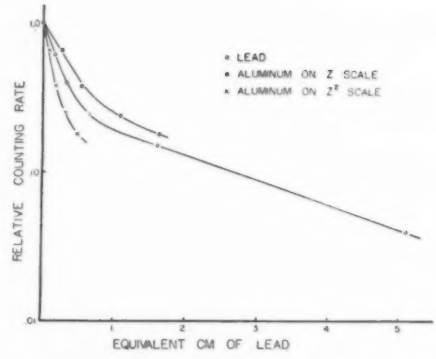

FIG. 10. Absorption of shower rays in lead and aluminum. The thickness of aluminum is expressed in equivalent cm of lead on the basis of an absorption per nucleus proportional to Z and Z^2.

4. Absorption of the Radiation Produced in Cosmic-Ray Showers

By placing plates of lead and aluminum in position B of Fig. 4 we have measured the absorption of the shower radiation from lead (probably a mixture of C-, D- and E-rays) in these two materials. Small corrections have been made for the initial counting rate (with no lead at A). It is found that within the experimental limits of the investigation the penetration of the rays is independent of the thickness of the lead at A and of the elevation. Since this is so, we have plotted curves for lead and aluminum (Fig. 10) which represent averages of all the data on absorption. Two curves are given for aluminum. For one the thickness is taken equivalent to lead on the Z scale and the other on the Z^2 scale. Since one of these curves lies above and the other below the lead curve, it is seen that the dependence upon Z is between the first and second power.

The logarithmic plot shows that at least empirically the shower radiation can be considered as made up of two components with coefficients 5.0 and 0.4 per cm of lead. But, if the shower production curve is to be represented by Eq. (1), the absorption coefficient ν of the shower radiation is determined by the value of the coefficient μ of the B-radiation and the position of the peak, and is thus found to be about 0.7 per cm of lead. This does not agree with the coefficient of either of the components deduced from direct measurements. It will be noted that since the absorption takes place in both plates at B, the measured coefficient is too large by a factor of two. However, the absorption probably enters in the same way in block A and in Eq. (1). The coefficient 0.4 may possibly apply to a C-radiation capable of producing large numbers of soft D- and E-rays which are more effective in actuating the counters. Further cloud chamber studies are required to clear up this point.

In conclusion the author wishes to express his gratitude to Dr. J. C. Street, whose advice and inspiration have made this investigation possible. Also it is a pleasure to acknowledge the cooperation of Professor J. C. Stearns and of the University of Denver in affording laboratory facilities. Transportation of the apparatus was generously provided by the city of Denver through the courtesy of Mr. G. E. Cranmer and Mr. R. R. Vail.

On the Geomagnetic Analysis of Cosmic Radiation

G. LEMAITRE AND M. S. VALLARTA,* *University of Louvain and Massachusetts Institute of Technology*

(Received March 30, 1936)

The results of an extensive study of trajectories asymptotic to a certain family of periodic orbits in the earth's magnetic field, carried out by means of Bush's differential analyzer, are presented in this paper. The theory of the region of full light, or main cone, is fully discussed. Attention is then restricted to the section of the main cone in the plane of the geomagnetic meridian and it is shown that the north-south asymmetry furnishes the most direct approach to the analysis of the energy spectrum in a wide region, independently of the particles' sign. Further it is shown that the general shape and the minimum of the north-south asymmetry discovered by Johnson in the course of his Mexican experiments are fully accounted for by the action of the earth's field.

1. INTRODUCTION

RECENT experiments by the method of multiple coincidences carried out by Johnson[1] in Mexico (geomagnetic latitude 29°N) and by Clay[2] in Java (geomagnetic latitude 18°S) have shown that in the northern geomagnetic hemisphere the intensity of cosmic radiation in the geomagnetic meridian is, for equal zenith angles, greater from the south than from the north; conversely in the southern hemisphere it is greater from the north than from the south.[3] That this is a consequence of the action of the earth's magnetic field on the motion of charged particles was pointed out by the present authors as early as 1932.[4] Shortly afterwards Bouckaert[5] was able to calculate this north-south asymmetry for geomagnetic latitudes up to 20° and moderate zenith angles. Considerable difficulties stand in the way of extending these calculations to higher latitudes and larger zenith angles. The use of Bush's differential analyzer,[11] which was made available to us to carry out the investigation reported here, has made it possible to include in the present analysis latitudes as high as 40° and, in most cases, zenith angles as far as the horizon. Thus with the completion of these researches the problem of determining the allowed main cone, or region of full light, for the latitudes mentioned is essentially solved.

The chief results of our present research are, first, that the north-south asymmetry, already discussed in a previous paper,[6] depends for each latitude on a narrow band of energy. Therefore, as further shown in the sequel, the experimental study of this asymmetry provides a direct workable method for the analysis of the spectral distribution of corpuscular cosmic radiation, independent of the latter's sign. Second, we show that the minimum of the north-south asymmetry found by Johnson at a geomagnetic latitude 29°N and at about 45° zenith angle, as well as the general features of his experimental results, are fully accounted for by the action of the earth's field. In fact the theory predicts a slight reversal of the sign of the asymmetry for zenith angles between 45° and 55° which depends on the existence of a very narrow energy band. This reversal begins at latitudes around 20° for for zenith angles about 70° and eventually broadens out so as to include the whole region between the zenith and 40° at latitudes around 35°. Contrary to our earlier[6] suggestion it is not necessary to invoke atmospheric absorption in order to account for this minimum.

The results we wish to present here must be considered as preliminary insofar as a critical examination of their precision is concerned. There is in fact ground for suspecting that our method of finding asymptotic trajectories leads to slightly too large a value for the aperture of

* At present Visiting Professor of the C.R.B. Educational Foundation at the University of Louvain.

[1] T. H. Johnson, Phys. Rev. **47**, 91 (1935).

[2] J. Clay, Physica **8**, 867 (1935).

[3] A northern excess in Eritrea (geomag. lat. 11.5°N) at a zenith angle of 45°, slightly larger than the rather large experimental error, has been reported by B. Rossi, Ricerca Scient. **5**, 583 (1934).

[4] G. Lemaitre and M. S. Vallarta, Phys. Rev. **43**, 87 (1933).

[5] L. Bouckaert, Ann. de la Soc. Sci. de Bruxelles, **A54**, 174 (1934).

[6] G. Lemaitre, M. S. Vallarta and L. Bouckaert, Phys. Rev. **47**, 434 (1935). Full references bearing on our application of Liouville's theorem to the present problem are given in the footnote on p. 435.

the main cone. The whole question as to the precision of our present results cannot be finally settled before more rigorous calculations of asymptotic trajectories in which we are now engaged are carried through to completion; we hope to return to this question shortly.

2. Outline of the Theory of the Allowed Cone

Let us now review briefly the statement of our problem and our method of attack. We start from the assumption of an isotropic distribution of charged particles at very large distances from the earth. Because of the action of the earth's magnetic field some of these particles are shot back to infinity, others are allowed to reach the earth. We have then shown[4, 7] that at any point a given distance from the earth's magnetic center all particles of a given energy reaching that point must come within a cone, generally of very involved shape, which forms the boundary between the region where all directions are allowed—the full light region, to borrow from the terminology of optics—and the region where only some or no direction are allowed. In any allowed direction, however, we have shown that[6] the intensity is precisely the same as would exist in the absence of the field and hence the same as it is at infinity.

The problem is thus to determine the generators of the cone. These generators, as shown by one of us[7] following ideas already outlined in our first paper,[4] may be of either of two kinds. The trajectories of the first kind are asymptotic to a periodic orbit, in fact asymptotic to periodic orbits forming a family first studied by Störmer.[8] This family has been calculated in detail by one of us,[9] as well as trajectories asymptotic to the members of this family in the immediate vicinity of the equatorial plane.[7] It was there shown, moreover, that some of these trajectories are doubly asymptotic, i.e., asymptotic to the same periodic orbit in the past as well as in the future. It follows further that asymptotic trajectories in the vicinity of these doubly asymptotic orbits separate again into trajectories going to infinity and trajectories returning to the earth. The latter may return infinitely near the first asymptotic trajectory; further among them is an infinite number of other doubly asymptotic trajectories. One of us has carried out the analysis of this maze of trajectories in the immediate vicinity of the equator.[7] The consequence is that the full light region is surrounded by an infinity of infinitely narrow bands of extremely complicated structure. This region we have called, borrowing again from the language of optics, the region of penumbra.

We have thus been led to distinguish among the trajectories of the first kind those which directly reach the earth, i.e., without returning to the vicinity of the periodic orbit. These asymptotic trajectories form the generators of what we have called the main cone or region of full light. As mentioned above the latter is surrounded by the penumbra. The distinction between full light and penumbra is of course only a matter of convenience and in no wise is to be looked upon as fundamental.

In addition to the trajectories of the first kind which are asymptotic to a periodic orbit there are also trajectories of the second kind which can form part of the boundary of the main cone.[7] These trajectories are tangent to the earth before reaching the point of observation. They limit a part of the main cone because of what we might call, again to borrow from the vocabulary of optics, the shadow of the earth.

We have finally to recall briefly some of the properties of the differential equations of motion of a charged particle in the earth's dipole field to which the above discussion applies. These equations have been first set up, studied and made generally well known by Carl Störmer to whom the results we are about to recall are also due.

First by suitably defining the units of time and length one may study at once trajectories of different particles and correspondingly different energies. For a given particle and for each energy the standard earth's radius is represented by a certain length which measures the energy of the particle. We suggest that this unit of length be called in the future a Störmer unit, or briefly a Störmer, in honor of its discoverer. For high energy particles this length is very nearly proportional to the square root of the energy.

[7] G. Lemaitre, Ann. de la Soc. Sci. de Bruxelles **A54**, 165 (1934).
[8] C. Störmer, Zeits. f. Astrophys. **1**, 237 (1930).
[9] G. Lemaitre, Ann. de la Soc. Sci. de Bruxelles **A54**, 194 (1934).

Second, the motion of a particle may be resolved into two components: one in the meridian plane and the other a rotation of the meridian plane around the magnetic axis. The calculation of this last motion has no bearing on our problem and consequently is left out in the sequel.[10] If r and λ are polar coordinates fixing the position of the particle in the meridian plane then the space trajectory intersects this plane at an angle θ given by Störmer's equation

$$\sin\theta = -2\gamma_1/(r\cos\lambda) + (\cos\lambda)/r^2. \quad (1)$$

The constant γ_1 is a constant of the motion; it is the component of momentum of the particle conjugate to the ignorable coordinate of the meridian.

For purposes of calculation it is convenient as noted by Störmer to introduce a new variable x by the transformation

$$e^x = 2\gamma_1 r. \quad (2)$$

If now x and λ are looked upon as rectangular coordinates a conformal map of the meridian plane is obtained where the radius vector r becomes a line parallel to the λ axis and the circles $r=$const. become lines parallel to the λ axis. As already explained above the earth is represented on this map by a line parallel to the λ axis for each value of the energy r in Störmer units. The angle η between a trajectory and the zenith direction is therefore read off directly on the conformal map since it is the slope defined by

$$\tan\eta = d\lambda/dx. \quad (3)$$

Finally in terms of an independent variable σ, function of the time, the equations of motion become

$$d^2x/d\sigma^2 = \tfrac{1}{2}\partial P/\partial x, \qquad d^2\lambda/d\sigma^2 = \tfrac{1}{2}\partial P/\partial\lambda, \quad (4)$$

where

$$P = (dx/d\sigma)^2 + (d\lambda/d\sigma)^2 = e^{2x}/16\gamma_1^4 - (e^{-x}\cos\lambda - 1/\cos\lambda)^2 \quad (5)$$

and from (1) and (2) it is readily seen that the locus of the points for which $\theta = 0$ is given by

$$x = 2\log\cos\lambda \quad (6)$$

and represents on the conformal map those points of the cone lying on the meridian plane.

3. The Determination of Asymptotic Trajectories

The capacity of the differential analyzer[11] now available at the Massachusetts Institute of Technology is just sufficient to integrate the system of differential equations (4). An ingenious set of machine connections was devised for this problem by S. H. Caldwell, but for lack of space the details of operation must be omitted here. Besides a preliminary attempt in the winter of 1932 the work was carried out at two different periods. During the first period (December, 1933) we found about a score asymptotic trajectories for $1/16\gamma_1^4 = 0.07$, $\gamma_1 = 0.972$. The initial slopes were calculated from the first terms of an analytical expansion of the asymptotic trajectory valid in the vicinity of the periodic orbit. This method of attack provided valuable information on the general appearance and properties of asymptotic trajectories and gave one of us the incentive for the introduction of harmonic expansions such as those used later by himself[7] and by Bouckaert.[5] It suffers from the serious disadvantage that the trajectory is started from a region of instability particularly sensitive to small errors either of the machine or in the initial data. During the second period (spring of 1935) we preferred, for this reason, to start the trajectory outwards from a suitably chosen point on the equator and then to adjust the initial slope so that the trajectory would neither intersect nor fall short of the periodic orbit, which was already accurately known.[9] It was found possible to adjust the initial slope after a few runs with a precision usually around one-thousandth of a radian. When the initial slopes had been found for several points on the equator the initial data at intermediate points were determined by graphical interpolation and a score trajectories were started inwards. Later it became obvious that certain interesting trajectories would be missed in this way and so, instead of starting from the equator, appropriate

[10] The motion of the meridian plane is important in connection with the variation of intensity due to the rotation of the galaxy which has been discussed by A. H. Compton and I. A. Getting, Phys. Rev. **47**, 817 (1935). This point has been partially studied by L. A. van Wijk and H. Zanstra, Physica **3**, 75 (1936). See also C. Störmer, Astrophys. Norv. **1**, 157 (1935).

[11] For a full description of the differential analyzer and its operation see V. Bush, J. Frank. Inst. **212**, 447 (1931).

points were chosen on the line $\theta=0$ and trajectories were run from these points outwards. The initial slope was then adjusted so that the trajectory would be tangent to the envelope of the asymptotic family, which had been previously determined from those asymptotic trajectories already known. As an additional verification a few trajectories were run as far as the periodic orbit. After the initial data at intermediate points had been found by graphical interpolation as in the case of the equatorial runs, a score or more asymptotic trajectories were continued inwards. We have thus studied the following values of γ_1: 0.81, 0.83, 0.85, 0.87, 0.89, 0.91, 0.93, 0.95 and 0.99. Runs from equatorial points were made for the following intermediate even values of γ_1: 0.88, 0.90, 0.92, 0.94, 0.96, 0.98. In all some three hundred asymptotic trajectories were traced.

As mentioned in the introduction, a critical study of the precision of the results thus obtained must in the final analysis await the outcome of calculations now in progress. We should mention at the outset that fairly systematic checks based on the use of the energy Eq. (5) do not reveal serious systematic errors. Only in one instance did we find a small systematic error which was later traced to incorrect plotting of one of the known functions introduced in the machine. When this mistake was corrected and a part of the previous work was repeated, the observed changes in the trajectories were so small that it was not deemed necessary to repeat all of the previous runs, some twenty-five trajectories in all. One can, however, mostly judge of the accuracy of the present material from the point of view of its self-consistency. Asymptotic trajectories possess, as a matter of fact, a complicated system of envelopes to be more fully discussed below and even small accidental errors are immediately visible. It should be borne in mind that the final precision of a curve traced by the differential analyzer depends not only on the mechanical trustworthiness of the machine itself, but also on the accuracy of the laborious and often complicated numerical calculations required to introduce the initial conditions into each of the members of a coupled system of six integrating units and five input tables. It even depends on the care and faithfulness with which a crew of five assistants keep in step their respective cross hairs on the known functions plotted on metallic plates on the input tables. Our guiding principle for the reduction of the data obtained with the help of the differential analyzer has thus been to accept only such conclusions as are based on the study not of a single, but of a good many consistent trajectories.

4. General Description of Asymptotic Trajectories and Their Envelopes

After these considerations we pass on to a description of some general features of asymptotic trajectories. To begin with we should mention the trajectories calculated by Carl Störmer[12] by the method of numerical integration which reach the pole $r=0$ or $x=-\infty$. These trajectories are osculating to the line $\theta=0$ already mentioned above. Although most of them belong to a family different from the one we are concerned with here, there are a few which are members of both, in particular one for γ_1 between 0.9313 and 0.9314 and a few which are of importance for the study of the penumbra. Störmer has shown that for sufficiently small values of x all other trajectories oscillate about the nonoscillating orbit going to the pole. This is precisely the general character of the trajectories we have obtained. They oscillate about Störmer's nonoscillatory orbit; for decreasing values of x the loops come closer together and the trajectory oscillates outwards in the same manner as inwards. An example of a family of asymptotic trajectories is shown in Fig. 1, where for the sake of completeness the locus of the vertices of the family of periodic orbits and the line $\theta=0$ are also drawn.

A family of asymptotic trajectories possesses an extensive family of envelopes which we are now about to describe (Figs. 1 and 2). Beginning at the periodic orbit there is an envelope denoted by E_0 which first proceeds in a direction fairly parallel to the x axis and then rises rapidly towards a cusp C_0 where it meets a corresponding envelope proceeding upwards, which we denote by F_0. The system of envelopes continues in a similar manner; corresponding branches are

[12] C. Störmer, Terr. Mag. and Atmos. Elec. **37**, 375 (1932). Astrophys. Norv. **1**, 145 (1935).

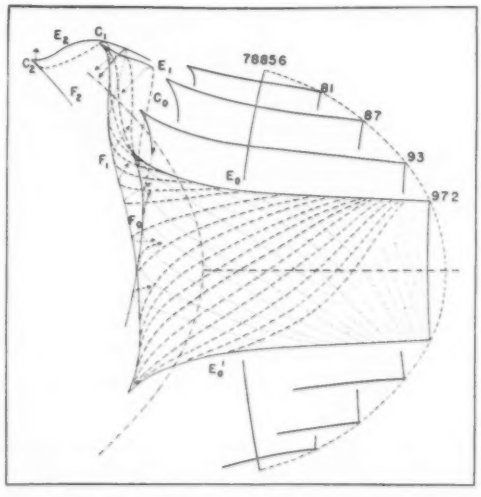

FIG. 1. The family of envelopes and periodic orbits, and a family of asymptotic trajectories ($\gamma_1 = 0.972$).

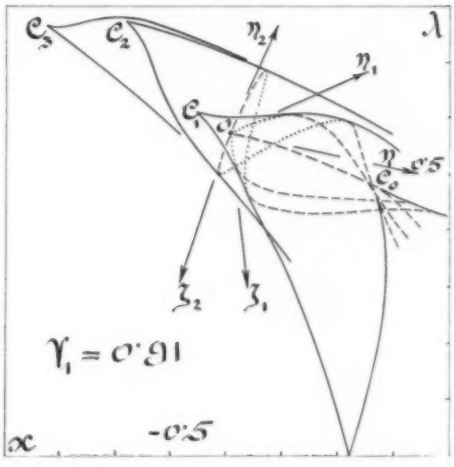

FIG. 2. Northern and southern sections of asymptotic trajectories.

denoted by C_1, C_2 $\cdots$, F_1, F_2, $\cdots$. These envelopes are tangent to the line $P=0$ (not drawn in the figure) at points which are denoted by S for the E envelopes and T for the F envelopes. At any S or T there is an asymptotic trajectory turning back on itself, i.e., a self-reversing doubly asymptotic trajectory. On either side of S or T an asymptotic trajectory touches the envelope and then proceeds in directions away from S or T. In particular the point S_0 is the vertex of the periodic orbit. The corresponding vertex for negative value of λ, and in general the corresponding points of tangency below the x axis will be denoted in the following by primed symbols.

The trajectories are divided by their points of contact with their envelopes into sections (Figs. 1 and 2). According to a known theorem in the theory of kinetic foci[13] any trajectory infinitely near an asymptotic orbit intersects each one of the sections once only in any finite domain of variation of σ. All asymptotic trajectories tend towards periodic orbits while performing an infinite number of oscillations between the envelope E_0 and its symmetrical counterpart E_0'. The trajectory in its infinitely close vicinity will therefore intersect each of the sections into which it is divided by its points of contact with its envelope. One may therefore choose the neighboring trajectory sufficiently close to the asymptotic orbit that the former may intersect the latter's sections as many times as desired but finally the former will pull away from the latter either by cutting the periodic orbit or by returning inwards. We thus have to distinguish between two kinds of sections (Figs. 1 and 2): northern sections (dashed) are those for which an infinitely close trajectory intersecting the asymptotic trajectory at an angle *smaller* than its own slope at that point finally cuts the periodic orbit. They form the northern boundary of the full light region or main cone. Southern sections (dotted) are such that an infinitely close trajectory intersecting the asymptotic trajectory at an angle *greater* than its own slope finally cuts through the periodic orbit. They form the southern boundary of the main cone. We have concluded from a study of the trajectories drawn by the differential analyzer that the sections coming from E_0 are northern sections, those coming from E_0' are southern sections. If we denote their slopes by η and ζ, respectively, we have the result that all trajectories included

[13] It is well known that the equation of the distance between trajectories infinitely close to some trajectory and this trajectory, as a function of the arc measured along the trajectory in question, is linear, homogeneous and of the second order, cf. E. T. Whittaker, *Analytical Dynamics* (Cambridge, 1904), p. 382. By a known result due to Sturm the zeros of such an equation separate one another, cf. M. Bocher, *Leçons sur les méthodes de Sturm* (Paris, 1917), p. 46. See also H. Poincaré, *Méthodes nouvelles de la mécanique céleste*, Vol. 3, p. 261.

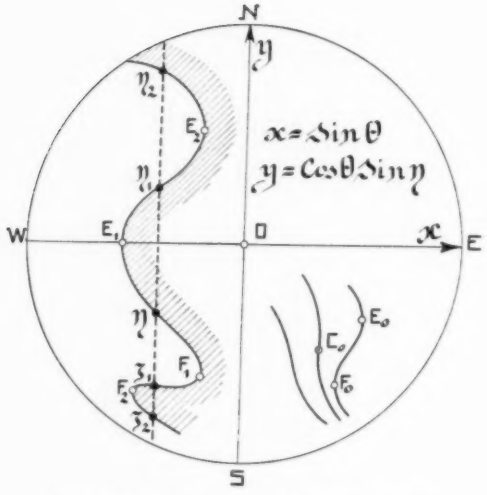

FIG. 3. Schematic representation of main cone.

between η and ζ come from infinity. The region between η and ζ lies within the main cone of which, in agreement with the results outlined in a preceding section, asymptotic trajectories are the generators. Each time that an asymptotic trajectory has a point of contact with its envelope the sections bounded by this point of contact are of different kinds. Sections of asymptotic trajectories diverging from the first cusp C_0 are therefore northern sections. After having touched the envelopes E_1 or F_1 they become southern sections and therefore the sections diverging from the cusp C_1 are southern sections. In the region between the two cusps C_0 and C_1 we may therefore have *three* asymptotic trajectories through the same point. We denote by η the slope of the trajectory coming from the cusp C_0, by η_1 the slope of the trajectory tangent to E_1 and by ζ_1 that of the curve tangent to F_1. At the next cusp C_1 all three slopes η, η_1 and ζ_1 become the same. Moreover, even before reaching C_1 our trajectories may have touched other envelopes E_2 or F_2 returning with slopes η_2 and ζ_2. What conclusions are to be drawn from these facts regarding the structure of the main cone?

Let us assume for instance that we have obtained, for a certain point x, λ and a given value of γ_1 the directions η, η_1, ζ_1, η_2, ζ_2. The latter belong to the given value of the latitude λ and are related to the energy r and the angle θ

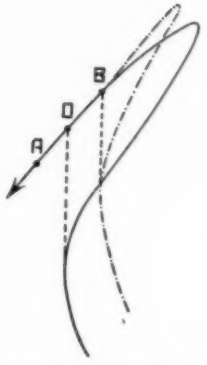

FIG. 4. Typical trajectories of second and third kinds.

by (2) and (1), respectively. For positive values of λ, i.e., in the northern hemisphere and for positive particles θ will be taken positive eastwards. We have adopted for our representation of the cone (Fig. 3) the orthogonal projection on the horizontal plane of its trace on the unit sphere centered at the point in question. In accordance with the conventions stated above we take the coordinates of our representative point, i.e., $\sin\theta$ and $\cos\theta \sin\eta$ as positive eastwards and northwards, respectively. Then the cone will have the general appearance shown *schematically* in Fig. 3, the full light region being to the west. Let us now see the significance of the envelopes and cusps. The envelope E_2 is such that on it η_1 and η_2 coincide. Generally envelopes are double points on the trace of the cone and there is a tangent parallel to the meridian plane. Cusps are triple points where the trace of the cone has a point of inflection with a tangent parallel to the meridian plane. These general principles suffice to interpret asymptotic trajectories in order to determine the main cone or region of full light.

It remains to show how the shadow of the earth limits a part of the main cone. In order that the preceding considerations remain valid it is necessary of course that all the asymptotic trajectories we have considered remain outside the earth. Hence if any of them has anywhere a tangent parallel to the λ axis it retains its previously discussed significance only for sufficiently small values of the energy, less than that which corresponds to the position of the tangent.

At a point such as A (Fig. 4) the η_1 direction gives a generator of the main cone, but at B the latter is already bounded by a trajectory of the second kind. At a point such as O the main cone is bounded by a trajectory which is at once of the first and of the second kinds. Such points indicate where the region of shadow, or region of the second kind, begins. A trajectory which is at once of the first and of the second kinds we shall briefly refer to as a trajectory of the third kind.

The complete main cones, as well as a fuller discussion of the azimuthal effect than has been hitherto possible, are reserved for a forthcoming companion paper.

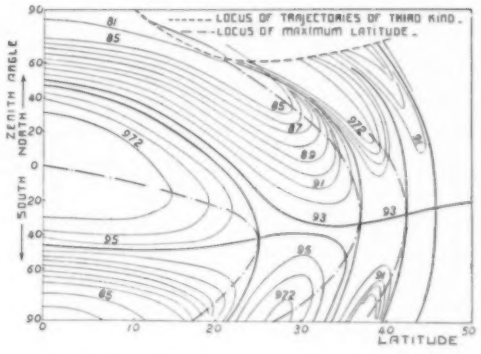

FIG. 5. The zenith angle in the meridian plane as a function of latitude.

5. Calculation of the North-South Asymmetry

Directions in the meridian plane correspond on the conformal map to the line $x=2\log\cos\lambda$ Eq. (6) for which $\theta=0$ by Störmer's formula (1). It is quite feasible to measure for each asymptotic trajectory cutting through this line the slope η and the corresponding value of the latitude λ. These values of η and λ can then be plotted on a diagram, for each value of γ_1, and a smooth curve drawn through the plotted points (Fig. 5). As is to be expected in accordance with our previous discussion a few of these points fall clearly outside the graph indicated by the other points, but in general the plotted curves are determined without ambiguity. For regions where sufficient data are missing it is easy to interpolate between neighboring well-determined curves. Particular attention should be paid in connection with this diagram to the significance of the envelopes and cusps. The intersection of an envelope with the line $\theta=0$ is shown as a point where the tangent to the plotted curve is parallel to the η axis. These are the "loci of maximum latitude" shown on the diagram. A point where a cusp lies on the line $\theta=0$ is a double point of the curves plotted. Its characteristic feature is that two branches of the locus $\gamma_1=$const. intersect, one of them having a tangent parallel to the η axis. This is clearly so because on one side of the cusp, as already discussed elsewhere, there are three asymptotic directions while on the other there is but one. The value of γ_1 for which the first cusp C_0 lies on the line $\theta=0$ is somewhere near $\gamma_1=0.94$. The following cusps C_1, C_2, etc., lie practically on it for $\gamma_1=0.93$. Further, Störmer's results quoted above show that these values form a progression the limiting value of which is 0.9313.

The trajectories of the third kind are important because they mark the point where the earth's shadow begins to appear. It is usually possible, after examination of the family of asymptotic trajectories drawn by the differential analyzer, to decide with good approximation where a trajectory of the third kind appears and to interpolate among neighboring curves to find the angle at which it intersects the line $\theta=0$. The locus of the values of zenith angle and latitude for which a trajectory of the third kind appears, for different values of γ_1, is shown in Fig. 5. It should be carefully borne in mind, in interpreting this locus, that a region may be in shadow for a given value of γ_1 and not for others. Thus for instance a point in shadow for $\gamma_1=0.93$ is still in the region of light for $\gamma_1=0.81$ at $\lambda=20°$.

The relation connecting γ_1 and the energy r for points on the meridian plane at a geomagnetic latitude λ is, from (1)

$$r=(\cos^2\lambda)/2\gamma_1. \tag{7}$$

By using this formula and the results of the previous analysis the least energies required for a particle to arrive at any given zenith angle in the meridian plane, at any point on the earth up to latitudes of 40°, may be readily found. It is simply necessary to read off the $\eta\lambda$ diagram

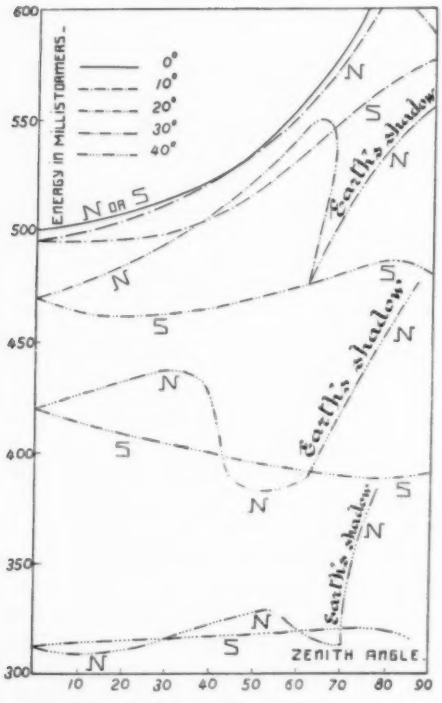

FIG. 6. North-south asymmetry.

(Fig. 5) the value of γ_1 corresponding to the given η and λ, interpolated if necessary. Typical curves relating the least energy of arrival with the zenith angle for latitudes 0°, 10°, 20°, 30° and 40° are reproduced in Fig. 6. It should be remembered that the energy (in millistörmer units) is measured with respect to the standard earth's radius (6370 km) and hence for observations at a given point on the earth account must be taken of the eccentricity of the earth's magnetic center.[14] Several important features are to be emphasized in connection with these curves. First it will be noted that, irrespective of the particles' sign, the energy region explored by the north-south asymmetry varies considerably with the latitude. The geomagnetic field thus provides for the separation of energies required for a spectral analysis of the corpuscular cosmic radiation. Experiments on this asymmetry thus furnish the most direct approach to the study of the energy spectrum. For this reason it is earnestly to be hoped that they will be continued particularly in the region between 35° and the geomagnetic equator, both at high and low altitudes above sea level. In this way valuable information will be obtained not only in view of the purpose mentioned above but also for the study of atmospheric absorption and scattering of particles of different energies.

Secondly it will be seen that the theory gives a full account of the minimum found by Johnson[1] in his Mexican experiments at a zenith angle of around 45°. It goes even further and, in a roughly quantitative way commensurate with present experimental precision, accounts for his whole result.

Lastly the effect of the earth's shadow should be carefully noted. It results in a large north-south asymmetry at high zenith angles for intermediate latitudes. For low latitudes the asymmetry near the horizon should therefore be reduced.

ACKNOWLEDGMENTS

A piece of work as extensive as that briefly reported here could not have been brought to a conclusion without the cooperation of many. It is a pleasure to acknowledge our indebtedness to Dean Vannevar Bush who made the differential analyzer at the Massachusetts Institute of Technology available to us on several occasions and placed the very complete resources of his laboratory at our disposal. Professor Samuel H. Caldwell, in charge of the Research Laboratory, not only helped us with his knowledge of the intricacies of the differential analyzer, but also contributed an ingenious method of setting up our problem on the machine. His assistants headed on different occasions by Messrs. E. W. Kimbark, J. J. Jager and R. D. Taylor were responsible for its efficient operation during long hours of tedious work. Dr. L. Bouckaert and Mr. E. J. Schremp helped us with the elaborate numerical computations required. Mr. L. de Borman carried out a good deal of the reduction of the data. One of us is indebted to the Massachusetts Institute of Technology and the C.R.B. Educational Foundation for the opportunity of continuing these researches at the University of Louvain.

[14] M. S. Vallarta, Phys. Rev. **47**, 647 (1935).

A Note on the Possible Effect of Screening in the Theory of Beta-Disintegration

M. E. Rose, *Institute for Advanced Study, Princeton, N. J.*

(Received March 23, 1936)

The present paper considers the possibility that screening by the atomic electrons has an appreciable effect on the energy distribution of β-particles emitted by heavy nuclei. A general formula is derived from which it is possible to conclude that the effect of screening is negligible. This result is also derived by another method. Finally, an explicit calculation based on the model of a charged sphere is shown to lead to the same conclusion.

1.

In a recent paper Konopinski and Uhlenbeck[1] have remarked that, on the basis of the Fermi theory of β-disintegration with their modified interaction, one finds for heavy elements such as Ra E an energy distribution which predicts too many slow electrons as compared with the experimental results.[2] An attempt by these authors to remove this difficulty by other modifications of the interaction between the heavy particle and the electron-neutrino field was not successful in diminishing the number of slow electrons without at the same time losing the degree of asymmetry in the distribution curve required by experiment.[3] Although there may be some question as to the existence of a real discrepancy between experiment and the theory, as modified by Konopinski and Uhlenbeck, it is of some interest to inquire whether there may be some influence hitherto not considered which could appreciably affect the energy distribution.

In this connection it is plausible to consider the possible effect of screening by the atomic electrons. It is evident, from a qualitative standpoint, that the screening will alter the distribution curve in the direction of the "free particle" distribution[4] which, incidentally, does fit the experimental curve for Ra E as given by Sargent. In the following we shall determine the effect of screening quantitatively.

By enclosing the system in a "sphere" (whose size is afterwards allowed to increase without limit) we may consider the wave function ψ of the β-particle to be of a discrete type. The screening can be represented by a Thomas-Fermi potential[5]

$$V=-(\alpha Z/r)\Phi(\gamma r), \quad \gamma=\alpha(128Z/9\pi^2)^{\frac{1}{3}}. \quad (1)$$

It is to be noted however, that the main argument given below depends on the use of the Thomas-Fermi potential only secondarily.

We now select a point r_0 such that for $r>r_0$ a solution of the wave equation of the W. K. B. type will be valid,[6] and for $r<r_0$ the argument of Φ in (1) is small enough to allow the approximation[7]

$$\Phi=1-\gamma r.$$

Then for $r<r_0$ the wave functions will be Coulombian with the energy W replaced by $W-V_0$ where the constant screening potential $V_0=\alpha Z\gamma$. The phase of the wave function at r_0 will be denoted by χ and the increase in phase from r_0 to the classical limit of motion (or to the boundary of the sphere) by θ. Further we label each state with an index n (radial quantum number). Then

$$\chi_{n+1}-\chi_n+\theta_{n+1}-\theta_n=\pi \quad \text{or} \quad d(\chi+\theta)/dn=\pi. \quad (2)$$

We then apply adiabatically an infinitesimal perturbation at small r producing an energy change

$$\delta W=\lambda\int F(r)\,|\psi|^2 d\tau_{\text{nuc.}}, \quad (3)$$

where $F(r)$ is an arbitrary function of r confined to nuclear dimensions and λ is very small. The integration in (3) is to be taken over the volume of the nucleus.

[1] E. J. Konopinski and G. E. Uhlenbeck, Phys. Rev. **48**, 7 (1935).

[2] B. W. Sargent, Proc. Camb. Phil. Soc. **28**, 538 (1932).

[3] This feature of the experimental results is apparently more reliable than the results for the low energy electrons. See also reference 11.

[4] That is, the distribution obtained by neglecting the Coulomb field of the nucleus.

[5] We use rational relativistic units, length being measured in $\hbar/mc$, energy in mc^2 and momentum in mc. In these units $e^2=\alpha$ (fine structure constant).

[6] Only differences in phase as given by Eq. (2) below rather than the exact values of the phases have to be given correctly by the W. K. B. formulas.

[7] For $Z\sim 80$, $\gamma=0.036$ while the singularity in the W. K. B. solution is at $r\lesssim 1$.

In general χ and θ could depend on λ and on W. Since the W. K. B. method is supposed to apply for $r>r_0$ and since $F=0$ in this region one may consider θ as depending only on W and not on λ while χ naturally depends on both λ and W. The perturbation formula (3) is supposed to apply to a constant n, i.e., to such changes of χ, θ that

$$\delta\chi+\delta\theta=0.$$

Since θ is a function only of W and not of λ this means that

$$(\partial\chi/\partial W+\partial\theta/\partial W)\delta W=-\lambda\partial\chi/\partial\lambda. \quad (4)$$

Substituting for δW and $\partial(\chi+\theta)/\partial W$ by means of (2) and (3) we have

$$(dn/dW)\int F(r)|\psi|^2 d\tau_{\text{nuc.}}=-(1/\pi)\partial\chi/\partial\lambda. \quad (5)$$

The right side of this equation is the same for a given F as long as the wave equation is the same. Thus it is the same for an electron of energy W in the field of a screened nucleus and an electron of energy $W-V_0$ in the field of an unscreened nucleus. Such states of screened and unscreened nuclei may be called corresponding states and the essence of the discussion lies in the possibility of establishing such a correspondence. The left side of the equation is the product of the number of states per unit energy range dn/dW and a weighted mean of the density $|\psi|^2$. Since F is arbitrary $(dn/dW)|\psi|^2$ at any point in the nucleus is the same for corresponding screened and unscreened states. This latter quantity we shall refer to as the electron density per unit energy range.

It should be noted that dn/dW and $|\psi|^2$ change by large factors if the standard normalization to the same value of $r^2|\psi|^2$ at infinity is used. Also the function F can be generalized to an operator which may involve the spin indices of the function ψ without altering the above proof. It thus follows that

$$(dn/dW)\Sigma\psi_\mu^* G_{\mu\nu}\psi_\nu \quad (5')$$

is the same for corresponding screened and unscreened states for any point inside the nucleus and for an arbitrary Hermitian $G_{\mu\nu}$.

The essential quantities which enter in the theories of β-decay are all of the form (5')[8] and the result of the above consideration can be expressed without formulas by saying that the electron distribution is always such as though the nucleus were not conscious of the screening and as though it emitted electrons into its immediate vicinity always in the same way; the only effect of the screening is then to accelerate the electrons by the Coulombian repulsion of the screening electrons and to change the kinetic energy $W-V_0$ into W by this acceleration. From this point of view the result has superficially an appearance of being self-evident. Actually it requires proof because it is possible to find examples in which it is not correct. One such example is given in section 3 of this note. In fact conclusions reached in (5) and (5') may be inexact because interference effects in the space between the nucleus and the screening charge can change the density $|\psi|^2$. These interference effects are neglected in the W. K. B. method used in obtaining (5). In the applications to β-decay it is reasonable to use such an approximation because the screening potential changes little within a wave-length of the electron.

Proceeding to the disintegration formula we write the Konopinski-Uhlenbeck result for the probability of emission of an electron with energy between W and $W+dW$ as

$$P_{KU}(W)dW=W(W_0-W)^4u(W)dW, \quad (6)$$

W_0 being the maximum emission energy. Then it follows from the above considerations that the effect of screening is to change this to

$$P(W)dW=(W-V_0)(W_0-W)^4u(W-V_0)dW. \quad (6')$$

Since for $Z\sim 80$, $V_0=0.02$, the change in P is of the order 3 percent or less. Hence one may conclude that the effect of screening is negligible.[9]

2.

It is possible to arrive at the conclusion expressed in (5) by another method in which explicit use of the W. K. B. solution is made. We denote by φ_1/r and φ_2/r the radial functions of the Dirac ψ which can be made to fulfill the normalization condition

$$\int_0^R(|\varphi_1|^2+|\varphi_2|^2)dr=1, \quad (7)$$

where R is the radius of a large sphere in which the system under consideration is enclosed. By

[8] Cf. E. Fermi, Zeits. f. Physik **88**, 161 (1934).

[9] I am indebted to Professor G. Breit who pointed out to me the derivation of this result.

the substitution

$$v_2=(1+W-V)^{\frac{1}{2}}\varphi_2$$

one finds that v_2 satisfies the differential equation[10]

$$d^2v_2/dr^2+f^2(r)v_2=0. \tag{8}$$

To (8) the W. K. B. method of solution may be applied. With

$$R[|\varphi_1(\infty)|^2+|\varphi_2(\infty)|^2]=1$$

we find

$$\varphi_2(\infty)=[(T+1)/2RT]^{\frac{1}{2}}\sin(kr+\text{phase}), \tag{9}$$

where $T=W-V$ and the wave number k is given by

$$T^2=k^2+1. \tag{10}$$

In a region where the W. K. B. solution just begins to be applicable we have

$$\varphi_2=\left[\frac{T'+1}{2RT}\frac{k}{k'}\right]^{\frac{1}{2}}\sin(k'r+\text{phase}), \tag{11}$$

where k' is the wave number and T' the kinetic energy in this region.

Since R can be made much larger than any other length entering the problem, the phase shift in the wave function is essentially given by

$$R\Delta k=\pi. \tag{12}$$

From (10), (11) and (12) we find that

$$|\varphi_2|^2/\Delta T=(1+T')/2\pi k', \tag{13}$$

which is independent of k and T. Hence keeping k' the same it follows that $|\psi|^2/\Delta T$ is independent of the screening. Since the screening has the effect of changing k' in accordance with the energy shift $W\rightarrow W-V_0$, it is evident that the electron density per unit energy range is given by the corresponding expression in the case of no screening with the energy W replaced by $W-V_0$.

3.

An alternative way in which we could represent the screening is to use a charged sphere potential.

$$V=-\alpha Z(1/r-1/r_s) \quad \text{for} \quad r<r_s,$$
$$V=0 \quad \text{for} \quad r>r_s; \quad r_s=1/\gamma.$$

With this model the calculation of the disintegration probability may be carried out with exact wave functions and thus it is possible to take into account the interference effects arising from the reflection of the electron waves by the charged sphere. The result one obtains is not the disintegration probability (6′) but a more complicated expression which contains (6′) as a first approximation.

For $r<r_s$ the wave function is again the Coulombian one with the energy displaced by an amount V_0 while for $r>r_s$ linear combinations of Bessel functions are used. The normalization constant entering in $|\psi|^2$ will depend on the wave functions at the point r_s. For large Z the "atomic radius" r_s is large compared to unity ($Z\sim 80$, $r_s=28$) so that we may use the asymptotic expansions of the wave functions. The disintegration probability thus obtained is

$$P_s(W)dW=P(W)[1+O(r_s^{-2})]dW, \tag{14}$$

where $P(W)$ is given in (6′). The correction term in (14) denoted by $O(r_s^{-2})$ arises from terms beyond the first in the asymptotic expansions of the wave functions. These higher terms are of an oscillatory nature and an average over a range of large values of the radius r_s has been carried out. Actually the term $O(r_s^{-2})$ contributes a correction much smaller than the relative difference between $P(W)$ and $P_{KU}(W)$ so that to a first approximation the screening is represented in the case of the present model in the same manner as before.[11]

I wish to express my sincere thanks to Professor G. Breit for his many courtesies to me.

[10] Cf. G. Breit, Phys. Rev. **38**, 463 (1931). The function $f^2(r)$ is defined on p. 470 of this paper.

[11] Since the completion of these calculations there has appeared a notice of a new investigation of the continuous β-ray spectrum of Ra E by A. I. Alichanow, A. I. Alichanian and B. S. Dzelepow, Nature **137**, 314 (1936). In these experiments particular attention has been given to the low energy portion of the distribution and it was found that a large number of slow electrons are emitted. These authors have made measurements starting at an energy (not including the rest energy) of 30 kv and have obtained a distribution curve which appears to be in agreement with the Konopinski-Uhlenbeck theory. The appearance of their curve suggests that the probability does not tend to zero at the origin, as is the case with the Sargent curves, but rather to a finite value comparable with the maximum probability. With these new measurements as a criterion in the case of heavy nuclei and with the results for light nuclei, see especially F. N. D. Kurie, J. R. Richardson and H. C. Paxton, Phys. Rev. **49**, 368 (1936), it seems that the Konopinski-Uhlenbeck theory is capable of accounting for all the features of the continuous β-ray spectrum.

The Spectra of Xenon in the Extreme Ultraviolet

J. C. BOYCE, *George Eastman Research Laboratory of Physics, Massachusetts Institute of Technology*

(Received March 23, 1936)

Increased dispersion and resolving power have made possible a revision and extension of the work of previous investigators on the spectra of xenon in the extreme ultraviolet. Lists of classified lines are given for Xe I, Xe II and Xe III in the range from λ2000 to λ600. No new lines were found for Xe I but the accuracy of the measurements is considerably improved. Revised identifications are suggested for Xe II in the light of new knowledge of the limits of that spectrum, the low states of Xe III. 128 lines of Xe III have been identified in collaboration with C. J. Humphreys, who will publish elsewhere with his analysis of the longer wave-length portion of the spectrum the consolidated term table for this spectrum.

THE extreme ultraviolet spectra of xenon have been investigated by using the two-meter normal incidence vacuum spectrograph[1] of the Carnegie Institution of Washington, which is located in the Spectroscopy Laboratory of the Massachusetts Institute of Technology. The method of reduction of the plates and the estimated precision of the data have been discussed with the results on neon[2] and the standards used have been published.[3] The lines newly or differently identified in the present investigation are denoted by an asterisk. The presence of a Roman numeral in the intensity column denotes that the line is a blend with a line of that spectrum. Previous measurements on xenon in this spectral range were made by Abbink and Dorgelo.[4] The gas used in the present investigation was purchased from the Air Reduction Company. Exposures were made of electrodeless discharges at different total pressures of a mixture of xenon with neon. Lines due to different stages of ionization were distinguished by the variation of their intensity with pressure.

Xe I

Classified lines are given in Table I. As this type of discharge does not favor the excitation of first spectra only a few lines were observed. The notation used for the upper levels from which these lines arise is that given by Humphreys and Meggers[5] in their term table. The ground term is now located at 97834.4 cm^{-1} as related to the other term values given in that table. This makes no appreciable change from the earlier results and the ionization potential, 12.078 volts, already published[6] remains the same.

Xe II

A partial term table for this spectrum has already been published by Humphreys, de Bruin and Meggers.[7] Present knowledge of the limits of this spectrum, the low states of Xe III, indicates that the previous assignment for the

TABLE I. *Xe I classified lines.*

λ	INT.	ν	CLASSIFICATION
1469.621	5	68044.7	$^1S_0 - 1s^\circ_4$
1295.560	8*d*	77186.7	$^1S_0 - 1s^\circ_2$
1250.199	2	79987.2	$^1S_0 - 3d^\circ_3$
1192.04	2	83890.2	$^1S_0 - 3d^\circ_2$

TABLE II. *Xe II classified lines.*

λ	INT.	ν	CLASSIFICATION
1244.756	5	80337.0	$5^2\,p^5\,^2P^\circ_{\frac{1}{2}} - s\,p^6\ \ ^2S_{\frac{1}{2}}$
1183.053	7 III	84527.1	$5^2\,p^5\,^2P^\circ_{\frac{1}{2}} - (^3P)\ 6s\ ^4P_{1\frac{1}{2}}$
1169.63	2	85469.9	$5^2\,p^5\,^2P^\circ_{\frac{1}{2}} - (^3P)\ 5d\ ^4D_{1\frac{1}{2}}$
1158.474	3	86320.5	$5^2\,p^5\,^2P^\circ_{\frac{1}{2}} - (^3P)\ 6s\ ^4P_{\frac{1}{2}}$
1100.432	10	90873.4	$5^2\,p^5\,^2P^\circ_{1\frac{1}{2}} - s\,p^6\ \ ^2S_{\frac{1}{2}}$
1083.860	5	92262.8	$5^2\,p^5\,^2P^\circ_{\frac{1}{2}} - (^3P)\ 6s\ ^2P_{1\frac{1}{2}}$
1074.476	15	93068.6	$5^2\,p^5\,^2P^\circ_{1\frac{1}{2}} - (^3P)\ 6s\ ^4P_{2\frac{1}{2}}$
1051.920	10	95064.3	$5^2\,p^5\,^2P^\circ_{1\frac{1}{2}} - (^3P)\ 6s\ ^4P_{1\frac{1}{2}}$
1048.272	8	95395.1	$5^2\,p^5\,^2P^\circ_{1\frac{1}{2}} - (^3P)\ 5d\ ^4D_{2\frac{1}{2}}$
1041.306	9	96033.3	$5^2\,p^5\,^2P^\circ_{1\frac{1}{2}} - (^3P)\ 5d\ ^4D_{1\frac{1}{2}}$
*1037.680	6	96368.8	$5^2\,p^5\,^2P^\circ_{\frac{1}{2}} - (^3P)\ 5d\ ^2D_{1\frac{1}{2}}$
1032.438	4	96858.1	$5^2\,p^5\,^2P^\circ_{1\frac{1}{2}} - (^3P)\ 6s\ ^4P_{\frac{1}{2}}$
*976.678	6	102388	$5^2\,p^5\,^2P^\circ_{\frac{1}{2}} - (^1D)\ 6s\ ^2D_{1\frac{1}{2}}$
972.769	7	102799	$5^2\,p^5\,^2P^\circ_{1\frac{1}{2}} - (^3P)\ 6s\ ^2P_{1\frac{1}{2}}$
*935.405	2	106906	$5^2\,p^5\,^2P^\circ_{1\frac{1}{2}} - (^3P)\ 5d\ ^2D_{1\frac{1}{2}}$
*925.866	5	108007	$5^2\,p^5\,^2P^\circ_{1\frac{1}{2}} - (^3P)\ 5d\ ^2D_{2\frac{1}{2}}$
*885.54	3	112925	$5^2\,p^5\,^2P^\circ_{1\frac{1}{2}} - (^1D)\ 6s\ ^2D_{1\frac{1}{2}}$
*880.802	5	113533	$5^2\,p^5\,^2P^\circ_{1\frac{1}{2}} - (^1D)\ 6s\ ^2D_{2\frac{1}{2}}$
803.066	3	124523	$5^2\,p^5\,^2P^\circ_{\frac{1}{2}} - (^1S)\ 6s\ ^2S_{\frac{1}{2}}$
740.406	3	135062	$5^2\,p^5\,^2P^\circ_{1\frac{1}{2}} - (^1S)\ 6s\ ^2S_{\frac{1}{2}}$

[1] K. T. Compton and J. C. Boyce, Rev. Sci. Inst. **5**, 218 (1934).
[2] J. C. Boyce, Phys. Rev. **46**, 378 (1934).
[3] J. C. Boyce and C. A. Rieke, Phys. Rev. **47**, 653 (1935).
[4] J. H. Abbink and H. B. Dorgelo, Zeits. f. Physik **47**, 221 (1928).
[5] C. J. Humphreys and W. F. Meggers, Bur. Standards J. Research **10**, 139 (1933).
[6] W. F. Meggers, T. L. de Bruin and C. J. Humphreys, Bur. Standards J. Research **3**, 731 (1929).
[7] C. J. Humphreys, T. L. de Bruin and W. F. Meggers, Bur. Standards J. Research **6**, 287 (1931).

TABLE III. *Xe III classified lines.*

λ	INT.	ν	CLASSIFICATION
*1978.702	3	50538.2	$(^4S)\ 5d\ ^3D^o_2 - (^3P)\ 6p\ ^3D_1$? (20_1)
*1921.630	2	52039.2	$s\ p^5\ ^3P^o_2 - (^4S)\ 6p\ ^3P_1$
*1896.904	5	52717.4	$(^4S)\ 5d\ ^3D^o_3 - (^3P)\ 6p\ ^3D_3$? (18_2)
*1874.907	5	53336.0	$(^4S)\ 5d\ ^3D^o_2 - 26$
*1854.365	6	53926.8	$(^4S)\ 5d\ ^3D^o_1 - 8_2$
*1834.254	4	54518.1	$(^4S)\ 5d\ ^3D^o_2 - 8_2$
*1826.477	7	54750.2	$(^4S)\ 5d\ ^3D^o_3 - (^3D)\ 6p\ ^1F_3$? (6_3)
*1825.858	3	54768.8	$(^4S)\ 5d\ ^3D^o_3 - 8_3$
*1819.845	6	54949.7	$(^4S)\ 5d\ ^3D^o_2 - (^3D)\ 6p\ ^3F_2$? (10_2)
*1817.381	2	55024.2	$(^4S)\ 5d\ ^3D^o_2 - 12_2$
*1804.109	2	55429.0	$s\ p^5\ \ ^3P^o_1 - (^3D)\ 6p\ ^3D_1$
*1750.749	2	57118.4	$s\ p^5\ \ ^3P^o_1 - (^3D)\ 6p\ ^3D_2$
*1579.498	5	63311.2	$s\ p^5\ \ ^3P^o_1 - 12_2$
*1562.563	4	63997.4	$s\ p^5\ \ ^3P^o_2 - (^3D)\ 6p\ ^3F_2$
*1554.438	1	64331.9	$s\ p^5\ \ ^3P^o_2 - (^3D)\ 6p\ ^3D_3$
*1549.975	2	64517.2	$s\ p^5\ \ ^3P^o_1 - (^3D)\ 6p\ ^3P_1$ (14_1)
*1511.121	3	66176.0	$s\ p^5\ \ ^3P^o_2 - 2_2$
*1509.454	2	66249.1	$s\ p^5\ \ ^3P^o_2 - (^3D)\ 6p\ ^1P_1$ (4_1)
*1468.180	4	68111.5	$s\ p^5\ \ ^3P^o_2 - 8_2$
*1457.356	3	68617.4	$s\ p^5\ \ ^3P^o_2 - 12_2$
*1432.204	4*bl*	69882.4	$s\ p^5\ \ ^3P^o_2 - (^3D)\ 6p\ ^3P_1$ (14_1)
*1393.496	1	71762.0	$s\ p^5\ \ ^3P^o_1 - (^3P)\ 6p\ ^3D_1$? (20_1)
*1356.364	3	73726.5	$s\ p^5\ \ ^3P^o_2 - (^3D)\ 6p\ ^1D_2$? (16_2)
*1253.645	2	79767.4	$s\ p^5\ \ ^3P^o_2 - 26$
*1232.074	25	81164.0	$s^2\ p^4\ \ ^1D_2 - s\ p^5\ \ ^3P^o_1$
*1225.089	3	81626.7	$s^2\ p^4\ \ ^1S_0 - s\ p^5\ \ ^1P^o_1$
*1183.053	8 II	84527.1	$s^2\ p^4\ \ ^1S_0 - (^4S)\ 5d\ ^3D^o_1$
*1156.480	9	86469.3	$s^2\ p^4\ \ ^1D_2 - s\ p^5\ \ ^3P^o_1$
*1130.344	30	88468.6	$s^2\ p^4\ \ ^3P_1 - s\ p^5\ \ ^3P^o_2$
*1066.391	12	93774.3	$s^2\ p^4\ \ ^3P_1 - s\ p^5\ \ ^3P^o_1$
*1058.128	2	94506.6	$s^2\ p^4\ \ ^1D_2 - (^4S)\ 5d\ ^3D^o_2$
*1055.328	5	94757.3	$s^2\ p^4\ \ ^1D_2 - (^4S)\ 5d\ ^3D^o_2$
*1048.754	3	95351.3	$s^2\ p^4\ \ ^1D_2 - (^4S)\ 5d\ ^3D^o_1$
*1047.801	10	95438.0	$s^2\ p^4\ \ ^3P_0 - s\ p^5\ \ ^1P^o_1$
*1017.680	35	98262.7	$s^2\ p^4\ \ ^3P_2 - s\ p^5\ \ ^3P^o_2$
*1010.376	3*bl* C II	98973.1	$s^2\ p^4\ \ ^1S_0 - (^3D)\ 5d\ ^1P^o_1$
*1003.370	35	99664.1	$s^2\ p^4\ \ ^3P_1 - s\ p^5\ \ ^3P^o_0$
*981.088	7	101928	$s^2\ p^4\ \ ^1D_2 - s\ p^5\ \ ^1P^o_1$
*974.124	8	102656	$s^2\ p^4\ \ ^3P_1 - (^4S)\ 5d\ ^3D^o_1$
*971.818	8	102900	$s^2\ p^4\ \ ^3P_1 - (^4S)\ 5d\ ^3D^o_0$
*965.540	10	103569	$s^2\ p^4\ \ ^3P_2 - s\ p^5\ \ ^3P^o_1$
*960.325	2	104131	$s^2\ p^4\ \ ^3P_2 - (^4S)\ 5d\ ^3D^o_3$
*958.585	4	104321	$s^2\ p^4\ \ ^3P_0 - (^4S)\ 5d\ ^3D^o_1$
*953.975	3	104825	$s^2\ p^4\ \ ^1D_2 - (^4S)\ 5d\ ^3D^o_1$
*917.257	4	109021	$s^2\ p^4\ \ ^1D_2 - (^3D)\ 5d\ ^3F^o_2$? (1^o_2)
*915.488	3	109231	$s^2\ p^4\ \ ^3P_1 - s\ p^5\ \ ^1P^o_1$
*901.746	7	110896	$s^2\ p^4\ \ ^3P_0 - s\ p^5\ \ ^1P^o_1$
*898.873	8	111250	$s^2\ p^4\ \ ^1D_2 - (^3D)\ 5d\ ^3F^o_2$? (5^o_2)
*896.003	20	111607	$s^2\ p^4\ \ ^3P_2 - (^4S)\ 5d\ ^3D^o_3$
*895.406	4	111681	$s^2\ p^4\ \ ^3P_1 - (^4S)\ 6s\ ^5S^o_2$
*893.989	20	111858	$s^2\ p^4\ \ ^3P_2 - (^4S)\ 5d\ ^3D^o_2$
*891.833	9	112129	$s^2\ p^4\ \ ^3P_1 - (^4S)\ 5d\ ^3D^o_1$
*889.276	15	112451	$s^2\ p^4\ \ ^3P_2 - (^4S)\ 5d\ ^3D^o_1$
*878.790	8	113793	$s^2\ p^4\ \ ^3P_0 - (^4S)\ 5d\ ^3D^o_1$
*870.346	6	114897	$s^2\ p^4\ \ ^3P_1 - (^4S)\ 5d\ ^3D^o_2$
*863.386	8	115823	$s^2\ p^4\ \ ^3P_1 - (^4S)\ 6s\ ^5S^o_2$
*861.071	5	116134	$s^2\ p^4\ \ ^1D_2 - (^3D)\ 6s\ ^3D^o_1$
*852.950	25	117240	$s^2\ p^4\ \ ^1S_0 - (^3P)\ 6s\ ^1P^o_1$
*851.147	8	117489	$s^2\ p^4\ \ ^3P_0 - (^4S)\ 6s\ ^5S^o_2$
*850.572	5	117568	$s^2\ p^4\ \ ^1D_2 - (^2D)\ 6s\ ^3D^o_2$
*840.162	7	119025	$s^2\ p^4\ \ ^3P_2 - s\ p^5\ \ ^1P^o_1$
*838.449	3	119268	$s^2\ p^4\ \ ^1D_2 - (^2D)\ 5d\ ^1P^o_1$
*826.134	4	121046	$s^2\ p^4\ \ ^1D_2 - (^2D)\ 5d\ ^3D^o_1$
*824.881	30	121230	$s^2\ p^4\ \ ^3P_2 - (^4S)\ 5d\ ^3D^o_2$
*823.210	25	121476	$s^2\ p^4\ \ ^3P_2 - (^4S)\ 6s\ ^5S^o_2$
*822.647	4	121550	$s^2\ p^4\ \ ^1D_2 - (^2D)\ 6s\ ^3D^o_2$
*820.166	4	121926	$s^2\ p^4\ \ ^3P_2 - (^4S)\ 5d\ ^3D^o_3$
*810.119	7	123430	$s^2\ p^4\ \ ^3P_1 - (^2D)\ 6s\ ^3D^o_1$
*808.860	3	123631	$s^2\ p^4\ \ ^1D_2 - (^2D)\ 5d\ ^3S^o_1$
*801.980	15	124691	$s^2\ p^4\ \ ^3P_2 - (^4S)\ 5d\ ^3D^o_2$
*800.819	3	124872	$s^2\ p^4\ \ ^3P_1 - (^2D)\ 6s\ ^3D^o_2$
*800.228	2	124964	$s^2\ p^4\ \ ^1D_2 - (^2D)\ 5d\ ^3D^o_2$
*799.338	8	125104	$s^2\ p^4\ \ ^3P_0 - (^2D)\ 6s\ ^3D^o_1$
*796.070	12	125617	$s^2\ p^4\ \ ^3P_2 - (^4S)\ 6s\ ^5S^o_2$
*793.977	8	125948	$s^2\ p^4\ \ ^1D_2 - (^2D)\ 6s\ ^1D^o_2$
*793.292	8	126057	$s^2\ p^4\ \ ^1D_2 - (^2D)\ 5d\ ^3D^o_3$
*792.896	15	126120	$s^2\ p^4\ \ ^3P_2 - (^2D)\ 5d\ ^3F^o_3$? (1^o_3)
*790.064	5	126572	$s^2\ p^4\ \ ^3P_1 - (^2D)\ 5d\ ^1P^o_1$
*780.030	7	128200	$s^2\ p^4\ \ ^1D_2 - (^2D)\ 5d\ ^1D^o_2$
*779.781	5	128241	$s^2\ p^4\ \ ^3P_0 - (^2D)\ 5d\ ^1P^o_1$
*779.126	25	128349	$s^2\ p^4\ \ ^3P_1 - (^2D)\ 5d\ ^3D^o_1$ $s^2\ p^4\ \ ^3P_2 - (^2D)\ 5d\ ^3F^o_2$? (5^o_2)
*769.143	10	130015	$s^2\ p^4\ \ ^3P_0 - (^2D)\ 5d\ ^3D^o_1$
*765.120	7*bl*	130698	$s^2\ p^4\ \ ^1D_2 - 13^o_2$
*763.736	7	130935	$s^2\ p^4\ \ ^3P_1 - (^2D)\ 5d\ ^3S^o_1$
*761.790	5	131270	$s^2\ p^4\ \ ^1D_2 - 15^o_2$
*761.540	10	131313	$s^2\ p^4\ \ ^1D_2 - 17^o_2$
*756.031	10	132270	$s^2\ p^4\ \ ^3P_1 - (^2D)\ 5d\ ^3D^o_2$
*754.144	5	132601	$s^2\ p^4\ \ ^3P_0 - (^2D)\ 5d\ ^3S^o_1$
*750.447	8	133255	$s^2\ p^4\ \ ^3P_1 - (^2D)\ 6s\ ^1D^o_2$
*750.155	8	133306	$s^2\ p^4\ \ ^1D_2 - 19^o_2$
*744.141	6	134383	$s^2\ p^4\ \ ^1D_2 - (^2P)\ 6s\ ^3P^o_1$ (21^o_1)
*742.566	15	134668	$s^2\ p^4\ \ ^3P_2 - (^2D)\ 6s\ ^3D^o_2$
*737.979	7	135505	$s^2\ p^4\ \ ^3P_1 - (^2D)\ 5d\ ^1D^o_2$
*733.314	10	136367	$s^2\ p^4\ \ ^3P_2 - (^2D)\ 5d\ ^1P^o_1$
*731.030	15	136793	$s^2\ p^4\ \ ^1D_2 - (^2P)\ 6s\ ^3P^o_2$
*727.058	9	137541	$s^2\ p^4\ \ ^1D_2 - (^2P)\ 6s\ ^1P^o_1$
*724.623	3	138003	$s^2\ p^4\ \ ^3P_1 - 13^o_1$
*723.873	5	138146	$s^2\ p^4\ \ ^3P_2 - (^2D)\ 5d\ ^3D^o_1$
*721.630	4*d*	138575	$s^2\ p^4\ \ ^3P_1 - 15^o_2$
*721.199	10	138658	$s^2\ p^4\ \ ^3P_2 - (^2D)\ 6s\ ^3D^o_2$
*715.986	4	139668	$s^2\ p^4\ \ ^3P_0 - 13^o_1$
*711.190	4	140609	$s^2\ p^4\ \ ^3P_1 - 19^o_2$
*710.677	5	140711	$s^2\ p^4\ \ ^3P_1 - (^2P)\ 6s\ ^3P^o_0$
*710.576	5	140731	$s^2\ p^4\ \ ^3P_2 - (^2D)\ 5d\ ^3S^o_1$
*705.783	5	141687	$s^2\ p^4\ \ ^3P_1 - (^2P)\ 6s\ ^3P^o_1$ (21^o_1)
*705.096	12	141825	$s^2\ p^4\ \ ^1D_2 - 23^o_2$
*703.906	9	142064	$s^2\ p^4\ \ ^3P_2 - (^2D)\ 5d\ ^3D^o_2$
*702.799	8	142288	$s^2\ p^4\ \ ^1D_2 - 25^o_1$
*699.070	5	143047	$s^2\ p^4\ \ ^3P_2 - (^2D)\ 6s\ ^1D^o_2$
*698.541	20	143156	$s^2\ p^4\ \ ^3P_2 - (^2D)\ 5d\ ^3D^o_1$
*697.526	8	143349	$s^2\ p^4\ \ ^3P_0 - (^2P)\ 6s\ ^3P^o_1$ (21^o_1)
*693.972	10	144098	$s^2\ p^4\ \ ^3P_1 - (^2P)\ 6s\ ^3P^o_2$
*691.036	7	144710	$s^2\ p^4\ \ ^1D_2 - 27^o_2$
*690.397	7	144844	$s^2\ p^4\ \ ^3P_1 - (^2P)\ 6s\ ^1P^o_1$
*688.231	4	145300	$s^2\ p^4\ \ ^3P_2 - (^2D)\ 5d\ ^1D^o_2$
*682.564	7	146506	$s^2\ p^4\ \ ^3P_0 - (^2P)\ 6s\ ^1P^o_1$
*676.606	9*bl*	147796	$s^2\ p^4\ \ ^3P_2 - 13^o_1$
*673.996	9	148369	$s^2\ p^4\ \ ^3P_2 - 15^o_2$
*673.813	9	148409	$s^2\ p^4\ \ ^3P_2 - 17^o_2$
*670.55	2	149132	$s^2\ p^4\ \ ^3P_1 - 23^o_2$
*668.473	4	149595	$s^2\ p^4\ \ ^3P_1 - 25^o_1$
*664.877	6	150404	$s^2\ p^4\ \ ^3P_2 - 19^o_2$
*661.124	4	151258	$s^2\ p^4\ \ ^3P_0 - 25^o_1$
*660.124	8	151487	$s^2\ p^4\ \ ^3P_2 - (^2P)\ 6s\ ^3P^o_1$ (21^o_1)
*657.828	8	152015	$s^2\ p^4\ \ ^3P_1 - 27^o_2$
*646.667	5	154639	$s^2\ p^4\ \ ^3P_2 - (^2P)\ 6s\ ^1P^o_1$
*629.217	7	158928	$s^2\ p^4\ \ ^3P_2 - 23^o_2$
*627.393	4	159390	$s^2\ p^4\ \ ^3P_2 - 25^o_1$

$(^1D)6s\ ^2D$ term was in error. It would now seem better to identify these terms as $(^3P)5d\ ^2D$. Another term has been found which is more satisfactory for the first level. Table II lists the 20 classified lines of Xe II which can be identified with some certainty. Publication of additional lines belonging to this particular spectrum of xenon, as well as of any revised term table, is reserved pending further investigation. There is no reason to alter the approximate value, 21.1 volts, given for the ionization potential by Humphreys, de Bruin and Meggers.

Xe III

The principal group of lines was located by analogy with the $s^2\ p^4\ ^3P - s\ p^5\ ^3P^o$ groups of Ne III, A III and Kr III. The ground P term is partially inverted as in tellurium I and iodine II.[8, 9] Other multiplets having differences characteristic of the ground state were then found to give connections with many odd terms, including two terms already found by de Bruin.[10] An

[8] O. Bartelt, Zeits. f. Physik **88**, 522 (1934).
[9] P. Lacroute, Ann. de physique **3**, 5 (1935).
[10] T. L. de Bruin, *Pieter Zeeman Jubilee Volume* (Martinus Nijhoff, The Hague 1935), p. 413.

analysis by C. J. Humphreys of the visible and near ultraviolet data, carried out simultaneously with the present investigation, made possible a rather complete identification of these odd terms. The exact description of many of the 128 lines classified in Table III was made possible by the very generous cooperation of Dr. Humphreys. All of the low terms of Xe III have been located and many intersystem combinations have been found. The consolidated term table for Xe III will be published by Humphreys elsewhere[11] together with his analysis of the longer wave-length portion of this spectrum. The ionization potential is 32.0 volts.

[11] C. J. Humphreys, Bur. Standards J. Research (in press).

The experimental part of this work was made possible by a grant to Dr. K. T. Compton from the Carnegie Institution of Washington. Some of the technical assistance necessary in plate measurement and reduction has been provided by a grant to the writer from the Permanent Science Fund of the American Academy of Arts and Sciences. The careful work of Dr. Carol A. Rieke in this capacity is gratefully acknowledged.

MAY 15, 1936 PHYSICAL REVIEW VOLUME 49

The Christiansen Filter Effect in the Infrared

R. Bowling Barnes and Lyman G. Bonner,* *Palmer Physical Laboratory, Princeton University*

(Received March 23, 1936)

A brief discussion is given of the history, construction, and applications of Christiansen light filters for use in the visible and ultraviolet regions of the spectrum. These filters, which consist of a powder of some crystalline or glassy substance suspended in a transparent medium, depend for their action upon the equality of refractive indices of powder and medium for some one wave-length of light. The theory of the effect in the infrared is briefly discussed, and methods are given for preparing and mounting the powders. The principal factors affecting the shape and size of the transmission peak, namely, the angle at which the two dispersion curves cross, the size of particle used, the thickness of the powder layer, and the solid angle included by the light striking and leaving the filter are discussed. Experimental results include transmission curves and wave-lengths of the transmission maxima for the following crystalline powders dispersed in air: quartz, MgO, calcite, marble, $CaSO_4$, eleven alkali halides, and three monovalent thallium halides. Curves are also given for quartz, MgO, and NaCl dispersed in organic liquids. The transmission peaks measured lie between 3μ and 90μ. In conclusion are discussed possible applications of the Christiansen effect in the infrared.

WITHIN the past few years, several papers have appeared in the literature in which various uses of Christiansen light filters have been discussed. One commercial company has advertised in the *Review of Scientific Instruments* that it can furnish various crystals in a powdered form suitable for use in the construction of these filters. In Germany the firm of Schott and Genossen-Jena offers for sale such filters under the name "monochromatic universal filters." Although the Christiansen filter effect has been known since 1884 it has lain dormant until the appearance of these papers except for brief descriptions which have appeared in each edition of Wood's *Physical Optics*. Even today the effect as such is not known to the average physicist. It is the purpose of the present paper to review the subject very briefly and then to describe the construction and several uses of such filters in the near and far-infrared. It will be shown that these filters may be used (1) to produce monochromatic beams of infrared radiation, (2) to eliminate the undesired short wave-length radiation in a grating spectrometer, (3) to determine the refractive indices of various fluids in the near-infrared.

If curve *a* of Fig. 1 represents the dispersion curve of a crystal, and curve *b* that of a given transparent medium, then a suspension of small

* National Research Fellow.

particles of this crystal in the medium should possess a maximum of transmission at the wave-length corresponding to the point of intersection of the two curves *a* and *b*. This wave-length we shall designate as λ_{Chr}. The reason for this transmission obviously lies in the fact that only at this wave-length is the sample optically homogeneous. Light of this wave-length passes through the cell unaffected, while light of all other wave-lengths suffers refraction at every particle-medium interface and is scattered strongly. In the case that λ_{Chr} lies in the visible region of the spectrum, directly transmitted light has the color corresponding to this wave-length. The direct image is surrounded by a haze having the color complimentary to λ_{Chr}.

C. Christiansen[1] first noticed this effect in 1884 while studying particle-liquid mixtures in an attempt to determine the refractive indices of various crystals. He explained the effect correctly and showed that light of practically any color could be obtained by varying the curve *b* of Fig. 1 so that it crossed *a* at the desired wave-length. He further pointed out that since the two curves *a* and *b* respond differently to changes in temperature, the point of intersection, would shift if the temperature of the cell were varied.

In 1885 Lord Rayleigh[2] published a paper entitled "On an Improved Apparatus for Christiansen's Experiment." From then until 1927 the filter effect was unused. At that time

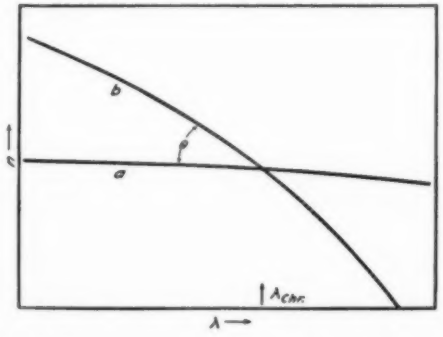

FIG. 1. Curve *a* represents the dispersion curve of a crystal, and *b* that of a transparent medium. The two intersect at an angle θ at the point $\lambda = \lambda_{Chr}$.

[1] C. Christiansen, Ann. d. Physik **23**, 298 (1884); **24**, 439 (1885).

[2] Lord Rayleigh, Phil. Mag. **20**, 358 (1885).

Weigert[3] and his co-workers published the first of a series of papers in which attention was directed to the fact that with proper temperature control and regulation such filters could be used quantitatively for the production of monochromatic light.

By correct choice of the substances involved, λ_{Chr} may be shifted from the visible to the ultraviolet or infrared regions of the spectrum. Christiansen, Staude, and others had previously suggested this possibility, and in 1932 Kohn and von Fragstein[4] published an account of the construction of a Christiansen filter for the ultraviolet. By using particles of fused quartz and a mixture of 56 percent benzol and 44 percent ethyl alcohol they obtained suitable filters having $\lambda_{Chr} = 3600$A at 20°C. With filters of this type they were able to isolate any desired region from 3000A on up into the visible. Individual lines of the mercury spectrum could be filtered successfully. These filters were also used by von Fragstein in his work on the determination of the reflection power of metals in the visible and ultraviolet regions.

In a still more recent paper, McAlister[5] has presented a rather thorough account of "The Christiansen Light Filter: Its Advantages and Limitations." Practical suggestions are given concerning the construction of a filter which may be used in an intense beam of light for the production of monochromatic light. The filters were made of borosilicate crown glass and a solution of carbon disulphide in benzene at 20°C. A series of filters covering the entire visible range, each having a half-width of about 100 to 200A were prepared. Fig. 2 is taken from McAlister's paper. Since a complete description is given by McAlister of the various choices of materials, particle size, etc., which are most advantageous for filters designed for use in this part of the spectrum, no further discussion of these points will be presented in this paper.

Other recent papers on the Christiansen effect include one by Abbot[6] on the applications of

[3] F. Weigert and H. Staude, Zeits. f. physik. Chemie **130**, 607 (1927); F. Weigert, H. Staude and E. Elvegard, ibid. **B2**, 149 (1929); F. Weigert and J. Shidei, ibid. **B9**, 329 (1930).

[4] H. Kohn and K. von Fragstein, Physik. Zeits. **33**, 929 (1932).

[5] E. D. McAlister, Smithsonian Misc. Collections, Vol. 93, No. 7 (1935).

[6] C. G. Abbot, J. Opt. Soc. Am. **25**, 42 (1935).

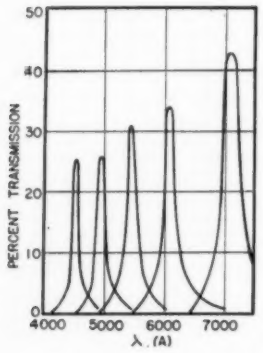

FIG. 2. Transmission curves of a series of five filters consisting of borosilicate crown glass particles immersed in mixtures of carbon disulphide and benzene (McAlister).

Christiansen filters to stellar energy spectra and one by Denmark and Cady[7] on the optimum grain size for these filters for use in the visible spectrum.

In order to demonstrate the principles involved in the construction of Christiansen filters the authors have found the following procedure both simple and expedient. A glass absorption cell having plane parallel windows is first filled with powdered fluorite (CaF_2) whose refractive index $n_D = 1.434$. Care should be taken to insure that the particles are clean and dry. Benzene, whose refractive index $n_D = 1.501$, is now poured into the cell until the latter is roughly half full. Again powdered fluorite is added to refill the cell. To this ethyl-alcohol $n_D = 1.362$ is added and the cell thoroughly shaken. This addition is continued until the light transmitted by the cell takes on a reddish hue. Each additional drop of alcohol decreases the refractive index of the liquid causing λ_{Chr} to shift towards shorter wave-lengths. Sufficient alcohol should be added to cause the transmitted image of a lamp filament to be clear yellow. The scattered light will be the complementary color to λ_{Chr}.

It is easy to see in the case of our fluorite-benzene-alcohol cell that the value of λ_{Chr} is a function of the temperature. If the cell be cooled in a stream of tap water, λ_{Chr} will shift to a deep red. Upon returning to room temperature λ_{Chr} will again be yellow. Placing the cell over a steam radiator will cause λ_{Chr} to be blue or violet. A temperature either too high or too low will cause the color to disappear λ_{Chr} being either in the ultraviolet or the infrared.

[7] H. S. Denmark and W. M. Cady, J. Opt. Soc. Am. **25**, 330 (1935).

THE CHRISTIANSEN FILTER EFFECT IN THE INFRARED

Many investigators[8] have studied the transmission of various powdered crystals mounted in such a way that the surrounding medium was air. These powders have invariably shown a rather high transmission peak on the short wave-length side of the characteristic frequency. No attention was paid to this abnormally high transmission although the curiosity of the investigators should have been stirred by the fact that a layer of powder shows a trend just opposite to that shown by a thin single crystal of the same material. Fig. 3 shows the general type of curve found in the literature. Pfund showed that, in case the average particle size was larger than λ_0, the wave-length of the characteristic absorption, this high transmission peak occurred at the wave-length at which the reflection of the crystal was a minimum, and explained the effect on this basis. The reflection power of a crystal is given, however, by the formula

$$R = [(n-1)^2 + n^2\kappa^2]/[(n+1)^2 + n^2\kappa^2].$$

At a wave-length well removed from λ_0, since κ is nearly equal to zero, $R = (n-1)^2/(n+1)^2$. We

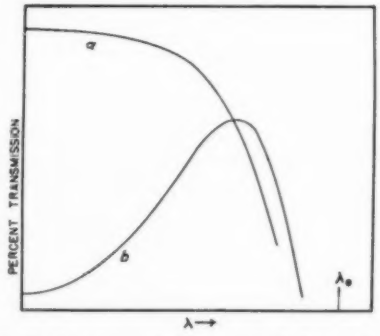

FIG. 3. Typical transmission curves of plate and powder. *a* is the transmission of a crystalline plate and *b* that of a powder of the same substance.

[8] A. H. Pfund, J. Opt. Soc. Am. **23**, 375 (1933); A. H. Pfund and S. Silverman, Phys. Rev. **39**, 64 (1932); S. Tolksdorf, Ber. Diss. 1928; O. Reinkober, Zeits. f. Physik **3**, 1 (1920).

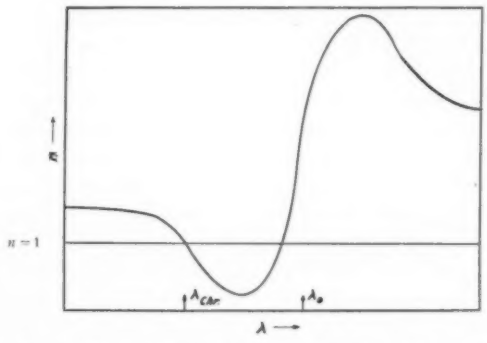

FIG. 4. Typical dispersion curve of a crystal for wave-lengths in the neighborhood of λ_0. At λ_{Chr} the index of the crystal is equal to that of air.

see then that this transmission peak also corresponds with the wave-length at which the refractive index of the crystal is unity, hence that at this point the dispersion curve of the crystal crosses that of air. It was pointed out by one of the authors[9] that this abnormal transmission is to be explained by a lack of refraction and not of reflection, and is in reality a true Christiansen filter effect. In Fig. 4 is shown a characteristic dispersion curve for a crystal in the neighborhood of λ_0. In the case of particles even a thin layer will be opaque due to refraction over most of the range. At some point, however, the indices of crystal and medium, which is air in this case, cross as is shown in the figure and a rather high transmission results.

PREPARATION OF FILTERS

The powder to be studied is usually dusted onto some material transparent in the desired wave-length region. Rocksalt plates may be used for the base material in the near infrared, while for wave-lengths $>30\mu$ thin sheets of paraffin ($\sim$0.5 mm in thickness) have been found quite satisfactory. Nitrocellulose films may be used over the whole infrared although some difficulties arise as a result of the characteristic absorption of the nitrocellulose, and trouble is frequently experienced in making the powder stick to the film. This last difficulty may sometimes be avoided by making a thick suspension of the powder in water, pouring this onto the film, and allowing the water to evaporate. In the near infrared a second rocksalt plate may be put over the particles if necessary, while in the case of paraffin as base material the powder may be pressed gently into the surface of the paraffin.

As will be shown later, the size and degree of separation of the powder is important in determining the characteristics of the Christiansen peak. For best results the particles should be all larger than λ_{Chr}, to increase the short wave opacity. On the other hand, if they are too large the true absorption of the crystal will cut down the size of the transmission peak. The particles should therefore be only slightly larger than λ_{Chr} in diameter, and the separation should be sharp. In the experience of the authors, this separation may be most easily performed in one of two ways.

If the particles are insoluble in water they may be separated by allowing them to fall through a known height of water. Stoke's law, assuming spherical particles, may be used to calculate the velocity of fall for the various particle sizes desired. The procedure is simple. The material is ground to as fine a powder as possible in an agate mortar and then placed in a cylinder of water high enough to give a convenient time of fall. After a thorough shaking they are allowed to settle for a time equal to that calculated for particles slightly larger than those desired to fall the full height of the vessel. At the end of this time the water and smaller particles are quickly decanted and the process repeated several times on the remaining powder. The particles that have been poured off are now taken and the time of fall increased to that for particles slightly smaller than those desired. The decantation process is continued until a sharp line of demarkation is seen between powder and clear liquid during the time of fall. A check with a microscope has shown in several cases that the diameter calculated, even with the assumption of spherical particles, was not far different from that obtained. Samples have been prepared in which the diameter ranged from 10μ to 12μ, 12μ to 15μ, etc. For quartz particles in water the times to fall one inch for 1μ and 100μ particles are 28,200 and 2.82 seconds, respectively.

[9] R. B. Barnes, R. R. Brattain and R. S. Firestone, Phys. Rev. **47**, 792 (1935). Since in regions removed from the characteristic frequency the reflection power of the crystals studied is usually about five percent, reflection losses alone could not account for the opacity found for powder layers only two or three particles thick.

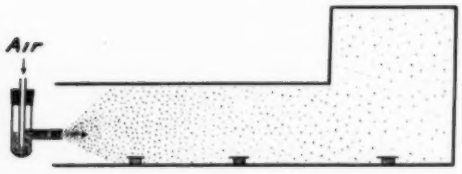

FIG. 5. An apparatus for separating powders according to particle size by an air stream method.

Particles soluble in water may be separated by the same method if a suitable liquid can be found. Otherwise the separation may be effected by allowing them to settle out of an air blast under suitable conditions. In Fig. 5 is diagrammed a method which we have found convenient in separating some of the alkali halides. A steady stream of air is blown into the tube through the nozzle. Particles are carried out of the jet by the air stream and enter the box, which serves to reduce cross currents. Receptacles placed at various points catch particles of different sizes, the smallest landing the greatest distance from the jet. The separation may, of course, be regulated also by the strength of the air blast. The separation here is not as sharp as that obtained by the other method, and the necessary conditions must be determined empirically for each size and variety of particle, but even so separations satisfactory for most purposes may be made.

FACTORS DETERMINING THE CHARACTERISTICS OF THE PEAKS

There are, in all probability, three principal factors regulating the sharpness and height of these Christiansen transmission peaks and these will be taken up in order.

(1) The width of the peak will obviously be some function of the angle (θ of Fig. 1) at which the dispersion curve of the crystal crosses that of the medium. If the angle is small refraction at the surface becomes small for a wave-length appreciably removed from λ_{Chr} and the peak is broad, while for a large angle the peak will tend to be sharper.

(2) Particle size, as was mentioned above, and the thickness of the powder layer play quite important parts in determining the characteristics of the transmission peak. In case any large fraction of the particles are of diameter $\rho \ll \lambda_{Chr}$, the layer will not be completely opaque for $\lambda < \lambda_{Chr}$ due to a simple powder effect.[10] On the other hand since, for the case of particles in air, λ_{Chr} is always in the neighborhood of and on the short wave side of λ_0, the true absorption of the crystal is appreciable. If, then, any large fraction of the particles are of diameter $\rho \gg \lambda_{Chr}$ this true absorption may reduce the percentage transmission at the center of the peak considerably. For the same reason the thickness of the powder layer is important. Microphotographs of filters which we have used have shown that a layer only 2 or 3 particles deep will be quite opaque in the region $\lambda < \lambda_{Chr}$.

(3) Since the action of these filters depends, not on absorption of the undesired light, but simply on scattering, the efficacy of the filter will be in part determined by the angle at which the light strikes the powder layer, and by the solid angle included in the observation method. The maximum efficiency will of course be obtained if only light emerging perpendicular to the face of the filter is used. We have found the filters to be quite satisfactory, however, even when used at the focus of an optical system of aperture $f : 2$. Some improvement may be obtained in such a case by using two filters spaced such a distance apart that the light scattered by the first is well removed from the light beam before it strikes the second.

EXPERIMENTAL RESULTS

Apparatus

Two types of apparatus were used in performing the experiments reported in this paper. For the region 1–15μ a rocksalt prism spectrometer was used. In this region were investigated principally the Christiansen peaks resulting from anomalous dispersion in the neighborhood of the inner vibration frequencies of complex crystals, and also the peaks for crystals embedded in media other than air. For investigation between 30 and 130μ a wire grating spectrometer of the type described by Barnes[11] was used. The spacing constant of the grating was 0.4 mm, but

[10] A. H. Pfund, Phys. Rev. **36**, 71 (1930).
[11] R. B. Barnes, Rev. Sci. Inst. **5**, 237 (1934).

since in order to facilitate measurements wide slits were used the full resolution of the spectrometer was never obtained. In this long wave region were found principally the peaks due to lattice vibrations of the alkali halide crystals. In all cases percentage transmission curves were obtained by taking readings, at each wave-length, of the energy with the sample in, and out of, the light beam. The samples were placed at the focus of a strongly converging beam.

Results

(1) *NaCl.* Of the systems investigated in the present work, the one about which the most data from other sources have accumulated, and which gives complete confirmation of the theory of the Christiansen effect is that of NaCl powder immersed in CS_2. The peak for rocksalt in air should occur at 32μ, as is shown both by the dispersion and reflection curves, but because of experimental difficulties we were unable to verify this. The peak for the NaCl-CS_2 system, however, falls in a readily accessible region, and in one in which the dispersion curves of both crystal and medium are well known. The dispersion of CS_2 has recently been determined by Pfund,[12] while the values for rocksalt have long been known from Paschen's work on the dispersion of a prism of the material. The cell for this investigation was made by putting a thin layer of finely powdered NaCl between rocksalt plates, sealing three of the edges with water glass, and flowing CS_2 into the space between. Fig. 6 shows the curve obtained. *a* is for the dry NaCl powder, *b* for the powder wet with CS_2, and *c* is the transmission curve of pure CS_2, taken from Pfund. At the top are shown the dispersion curves for the two materials, and it may be seen that they cross exactly at the wave-length, 5.45μ, at which the Christiansen peak occurs.

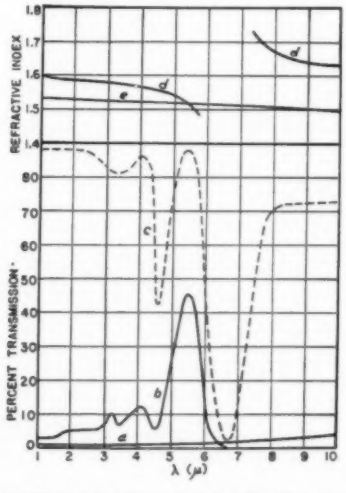

FIG. 6. NaCl powder immersed in CS_2. The transmission curves are *a*, the dry powder; *b*, the powder wet with CS_2; *c*, pure CS_2. At the top are shown the dispersion curves of *d*, CS_2, and *e*, NaCl, showing that they intersect at $\lambda = \lambda_{Chr}$.

[12] A. H. Pfund, J. Opt. Soc. Am. **25**, 351 (1935).

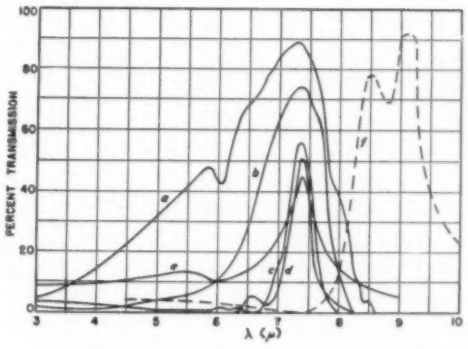

FIG. 7. Effect of particle size on the quartz Christiansen peak. The curves are for the following sizes: *a*, 5–10μ; *b*, 10–20μ; *c*, 30–40μ; *d*, 50–60μ; *e*, unseparated powder. Curve *f* shows the reflection power of a quartz plate.

(2) *Quartz.* Powdered quartz was available in great quantity, and since the material is quite insoluble in water and so could be readily separated by the rate of fall method, most of the experiments on the effect of particle size have been made on this crystal. One of the fundamental vibrations of quartz, which is probably an inner vibration of the SiO_4 tetrahedron occurring in the structure, lies at about 9μ. The Christiansen peak, expected just on the short wave side of this falls experimentally, for the powder in air, at about 7.35μ. Fig. 7 shows the transmission curves for approximately equal layers of quartz particles of various thicknesses, mounted on nitrocellulose films. The small irregularities on the sides of the curves, which become particularly marked for the $5–10\mu$ particles, result from the true absorption of the nitrocellulose. The effect of particle size in narrowing and decreasing the height of the peak

is quite well shown by these curves. A curve is also shown for quartz particles which had undergone no separation whatsoever, and it may be seen from this that even a random selection of particles shows the Christiansen effect quite markedly. The dotted reflection curve shows that the wave-length of the Christiansen peak agrees with that of the reflection minimum. In Fig. 8 the effect of immersion in CCl_4 and in a 50 percent by volume mixture of CCl_4 and CS_2 on the quartz peak is shown. The positions of these peaks agree well with the known dispersion curves for the substances involved.

(3) *MgO.* Fig. 9 shows the positions of the Christiansen peaks for unseparated MgO powder in air and in CCl_4. The dispersion curve of CCl_4 was also obtained by Pfund,[12] and so the establishment of these two values, $n=1$ at 12.2μ, 1.43 at 9.0μ, together with previously known values at shorter wave-lengths, permit a rough dispersion curve to be drawn for MgO. This curve also is shown in the figure.

(4) *Carbonates.* From reflection measurements it is known that all crystalline carbonates have three fundamental frequencies, characteristic of the $CO_3^=$ radical, in the near infrared. Experiments were performed both on powdered calcite and on marble and the results, though not conclusive, indicated the presence of two peaks of 6.2 and 11.1μ with possibly a third at about 9μ.

(5) *Sulfates.* Only one sulfate was investigated, namely, plaster of paris ($CaSO_4 \cdot 1/2H_2O$). A small but definite transmission peak, characteristic of the sulfate radical, was located at 7.9μ.

(6) *Alkali- and thallium-halides.* The Christiansen peaks in air were located for a total of

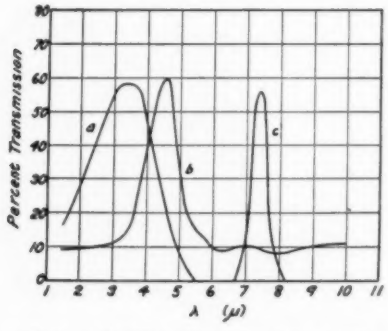

FIG. 8. Shift of the Christiansen peak for quartz powder in liquids. *a*, quartz in a 50 percent by volume mixture of CS_2 and CCl_4; *b*, quartz in pure CCl_4; *c*, quartz in air.

TABLE I. *Positions of the Christiansen peaks for various crystals.*

CRYSTAL	WAVE-LENGTH (in μ) CHRISTIANSEN	RESTRAHLEN	FUNDAMENTAL
LiF	11.2	26	32.6
NaCl	(32)	52.0	61.1
NaBr	37		74.7
NaI	49		85.5
KCl	37	63.4	70.7
KBr	52	81.5	88.3
KI	64	94	102.0
RbCl	45	73.8	84.8
RbBr	65		114.0
RbI	73		129.5
CsCl	50		102.0
CsBr	60		134.0
TlCl	45	91.9	117.0
TlBr	64	117	
TlI	90	151.8	

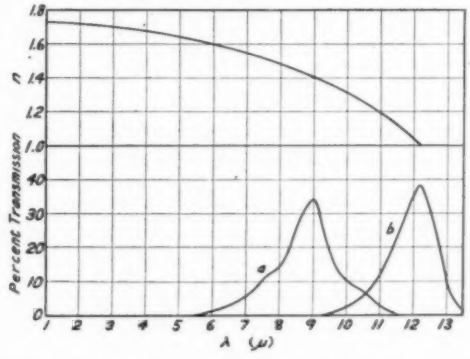

FIG. 9. *a*, MgO powder in CCl_4, *b*, MgO powder in air. At the top is shown a rough dispersion curve for MgO as determined by these two points and by measurements in the visible spectrum.

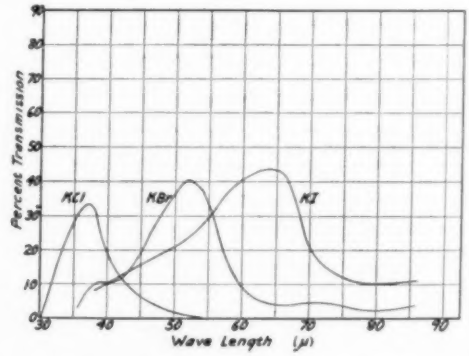

FIG. 10. Curves showing the Christiansen transmission peaks for powdered KCl, KBr, and KI. These curves are typical of those obtained for the alkali halides.

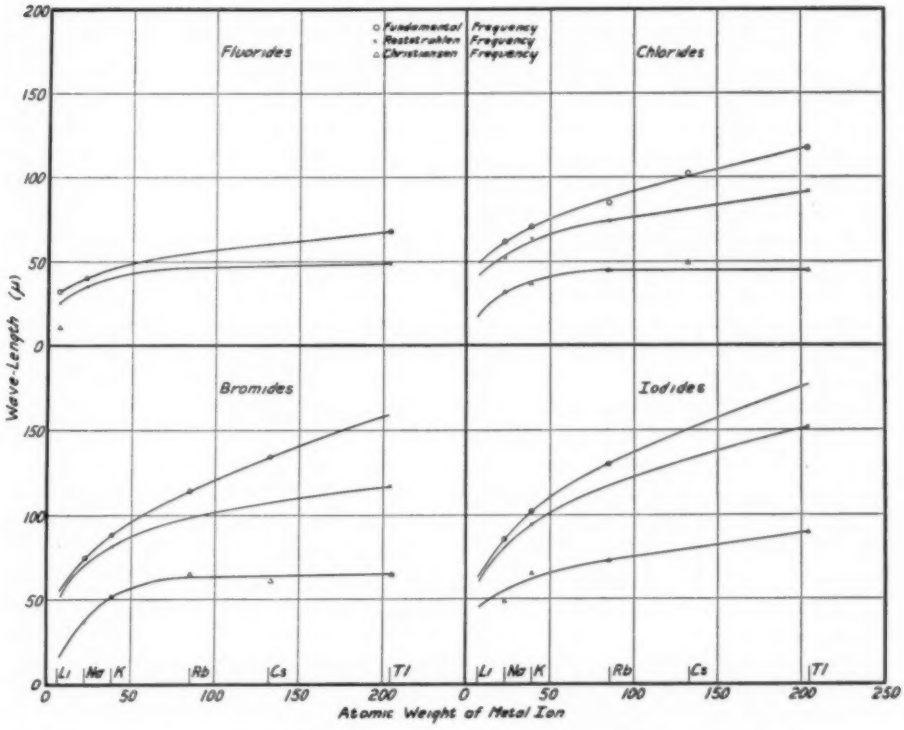

FIG. 11. Here the wave-lengths of the Christiansen, reststrahlen, and fundamental frequencies are plotted, for each halogen separately, as a function of the atomic weight of the metal ion.

eleven alkali halides, and also for three monovalent thallium halides, which also crystallize in a cubic lattice. With the exception of that for LiF these peaks all fell in the region of the grating spectrometer and so were investigated as unseparated powders mounted on 0.5 mm paraffin. Paraffin of this thickness has quite a high transmission in the infrared beyond 30μ. Crystals of this type possess only one characteristic frequency, and hence only one Christiansen peak. Table I gives the positions of the peaks for all the crystals of this type investigated. Included in the table for purposes of comparison, are the wave-lengths of the fundamental frequencies and reststrahlen frequencies for the same crystals, as given by Barnes.[13] Fig. 10 gives the actual measured transmissions for the powders of KCl, KBr, and KI, while in Fig. 11 the three types of frequency, Christiansen, reststrahlen, and fundamental are plotted, for each halogen separately, as a function of the atomic weight of the metal ion.

[13] R. B. Barnes, Zeits. f. Physik **75**, 723 (1932).

USES OF THE CHRISTIANSEN EFFECT IN THE INFRARED

Below we shall discuss briefly several interesting and important applications of the Christiansen effect in connection with infrared spectroscopy.

(1) In the use of grating spectrometers one of the most difficult problems that arises is that of the elimination of overlapping orders. With most gratings, in order to make measurements at a wave-length λ all energy of wave-length less than $\lambda/2$ must be removed. Many devices such as selective sources and receivers, filters, prism monochromators, etc., have been used. In a good many cases the desired effect may be attained more simply by the use of a suitable Christiansen

filter. In the near infrared powders of quartz, LiF, MgO, and doubtless many other crystals have sharp and conveniently located peaks. In the far infrared the alkali halides form a series, together with the monovalent thallium halides, covering quite a range of wave-lengths. By proper choice of particle size these filters may be made quite opaque in the short wave regions but will still possess a high transmission in the neighborhood of the peak.

(2) The production of comparatively monochromatic beams of light by means of these filters immediately suggests their possible use in the construction of a survey spectrometer for the far infrared, similar to the reststrahlen method introduced by Rubens. Since only a source, two mirrors, and a receiver would be required the apparatus would be simple. Whereas the reststrahlen method requires one or more good sized crystals of each material, which are often difficult or impossible to obtain, only a small amount of the crystal powder is needed to make one of these filters. Using only the substances investigated in the present work, some fifteen or twenty different wave-lengths are available between 6μ and 90μ, and it is very likely that this list will be extended by further work in the field.

(3) Since the very existence of the Christiansen effect depends upon the equality of the refractive indices of particle and medium for some wave-length, we have here a method for determining dispersion curves in the infrared. In case the dispersion of either crystal or medium is known, the measurement of the Christiansen peak gives one point on the dispersion curve of the other. Since it is usually easier to obtain the dispersion curves of crystals in the infrared than of liquids, a series of such crystal powders could be used to establish points on the dispersion curves of liquids. In the inverse case, the dispersions of some liquids are known, and in the previous section were shown curves of the transmissions of MgO, NaCl, and quartz immersed in CS_2 and CCl_4.

(4) It has recently been pointed out to us by Professor E. U. Condon, that since the measurement of the Christiansen peak in air gives one point on the dispersion curve of the crystal, namely, that at which $n=1$, this value may be used in the classical dispersion equation, together with values from the visible and ultraviolet regions of the spectrum to determine the intensity constant characterizing the infrared absorption band of the crystal. This problem will be discussed in a later paper.

MAY 15, 1936 PHYSICAL REVIEW VOLUME 49

The Band Spectrum of Boron Fluoride

HERBERT M. STRONG AND HAROLD P. KNAUSS, *Mendenhall Laboratory of Physics, Ohio State University*

(Received March 16, 1936)

The spectrum of boron fluoride as excited by the electrodeless discharge has been photographed at both high and low dispersion. Sixteen new bands were observed in the region between λλ3712 and 2580A. These bands degrade to the violet; have five head-forming branches, and resemble very closely the third positive bands of CO, a result to be anticipated from the fact that CO and BF both possess ten extranuclear electrons and should therefore have similar electronic configurations. Two systems were found with a common lower electronic level: an A system ($\nu^{(0,0)}=32{,}020.5$ cm^{-1}) of 12 bands and one isotope band, and a B system ($\nu^{(0,0)}=37{,}991$ cm^{-1}) of three bands. The constants obtained from the vibrational analysis are: ω_e', 1631.40 cm^{-1}; ω_e'', 1323.64 cm^{-1}; $x_e'\omega_e'$, 23.10 cm^{-1}; $x_e''\omega_e''$, 9.40 cm^{-1}.

INTRODUCTION

THE BF molecule is isoelectronic with N_2 and CO, hence considerable interest attaches to its band spectrum. Largely because of difficulties in exciting and isolating the band spectrum of BF, it has been inadequately investigated. The chemically stable compound of boron and fluorine, BF_3, is a gas at room temperature, and a Geissler discharge in BF_3 has been used by several investigators in searching for BF

bands. Johnson and Jenkins[1] attempted to excite the BF spectrum in BF_3 gas but were troubled with the appearance of SiF bands. Under better conditions of purity, Tawde and Johnson[2] obtained bands in the visible region of the spectrum which they ascribed to BF. However, the bands did not show the expected resemblance to CO bands.

Experience with the electrodeless discharge in this laboratory[3] showed that the band spectrum of a diatomic fragment of a polyatomic molecule is brought out strongly in this source, hence the project was undertaken of subjecting BF_3 to this type of discharge for the purpose of obtaining BF bands. This technique also offered to simplify the problem of eliminating impurities.

While this investigation was in progress, Dull[4] reported obtaining three bands of BF in the ultraviolet, showing a marked similarity in structure to bands of the third positive group of CO. We have observed the same bands, and sixteen others of the same type. This report deals with the vibrational analysis of the observed bands.

Experimental

Preliminary experiments were made with gas generated by the method of Germann and Booth.[5] The generator was sealed to an electrodeless discharge tube and a pumping system. A Féry type quartz spectrograph was used to photograph the spectrum, and many bands were obtained, including those of CO, BO, SiF, OH, N_2, and some which could not be fitted into any known band system. Visual observation with a spectroscope showed the presence of the bands of Tawde and Johnson.[2] Upon seeking conditions for the maximum intensity of the latter, it was found that the presence of a liquid-air trap in the pumping system weakened the intensity of these bands very rapidly. Lowering the liquid-air bath on the trap resulted in releasing BF_3 back into the discharge tube. In a very short time, however, the bands of Tawde and Johnson again disappeared, and CO bands became very intense. This always occurred with a tube that was not baked out, suggesting that the CO was released from the walls of the tube, while the BF or BF_3 apparently was "cleaned up" under the influence of the discharge.

Through the kindness of Professor H. S. Booth, and Mr. Karl Willson at Western Reserve University, we obtained some samples of BF_3 gas which they had dried and purified very carefully. The technique adopted in transporting and exciting the gas was as follows. A discharge tube of about 30 cm length and 5 cm diameter was fitted with a window transparent to the ultraviolet, either of quartz attached by a quartz-to-Pyrex graded seal, or of glass blown into a very thin re-entrant bubble. The other end of the discharge tube was provided with a side arm, and an exhaust tube. A short section of the exhaust tube was constricted, and contained a pellet of Wood's metal. The tube was baked for several hours at 500°C while exhausting, and then sealed off from the pumps. The Wood's metal was melted into the constriction in the exhaust tube, closing the latter so that it could be attached to the BF_3 generator without readmitting air to the discharge tube. The Wood's metal was then melted out of the constriction, and pure BF_3 gas was admitted at a pressure of about half an atmosphere. Thereupon the tube was sealed off once more, and was ready to be transported to this laboratory. The precautions described were found to be essential in order to eliminate impurities, of which the most persistent was CO. With the technique described, the only remaining bands appearing besides those of BF were the SiF bands. Undoubtedly, some SiF_4 is formed by reaction of BF_3 with the hot glass when sealing off, as well as with the walls of the tube duringthe discharge.

The discharge tube was placed within the helix of a high-frequency oscillator, and the pressure of the gas within the tube was brought down to a suitable value by refrigerating the side arm with liquid air. It was found that with a Dewar flask placed to bring the liquid-air level about one cm below the tip of the arm, the pressure could be maintained indefinitely by occasional adjustments as the liquid air evaporated. In this way,

[1] R. C. Johnson and H. G. Jenkins, Proc. Roy. Soc. A116, 327 (1927).
[2] N. R. Tawde and R. C. Johnson, Phil. Mag. 13, 501 (1932).
[3] H. M. Strong, Thesis (M. S., Ohio State University, 1933).
[4] R. B. Dull, Phys. Rev. 47, 458 (1935).
[5] A. F. O. Germann and H. S. Booth, J. Phys. Chem. 30, 369 (1926).

the vapor pressure in the discharge was substantially constant in spite of "clean-up" produced by the discharge.[6]

The 100-watt oscillator previously described[7] was used for some of the preliminary work. The three-meter oscillator of the Central Scientific Company was also used at moderate dispersion. For exposures at higher dispersion, a more powerful oscillator was constructed. This consisted of an 852 triode in a Hartley circuit, the output of which was condenser coupled to a tuned circuit using an 849 triode biased for class *C* amplification. The plates of the tubes were supplied with direct current at 1200 volts by means of a motor-generator. A frequency of approximately 3000 kilocycles per second was obtained with the circuit elements employed.

A Hilger E_1 Littrow mounted quartz spectrograph was used to photograph the region from 4000 to 2300A. This instrument has a dispersion of 14A/mm at 4200A, and 5A/mm at 2300A. Suitable exposures were obtained in $1\frac{1}{2}$ hours. Longer exposures brought out more general blackening, rather than more band features.

A 21-foot grating was also used, the region 6000 to 2500A being covered in the first order. The grating has 30,000 lines to the inch, giving a dispersion of 1.2A/mm, and is mounted on a Paschen-Runge mounting. The maximum exposure time attempted was 36 hours.

The spectrum of the iron arc was superimposed on the band spectrum for comparison. A Geneva Society comparator was used to make wavelength measurements.

[6] H. M. Strong and H. P. Knauss, Phys. Rev. **47**, 642A (1935).
[7] H. P. Knauss and J. C. Cotton, Phys. Rev. **38**, 1190 (1931).

Results

Nineteen bands, degraded to the ultraviolet, which were observed in the region 4000 to 2300A on plates taken with the Hilger E_1 spectrograph have been ascribed to BF. Of these, six were sufficiently intense to appear on the 21-foot grating plates in the first order, including three bands reported by Dull.[4]

The probable error of measurements made on the 21-foot grating plates is 0.05 cm^{-1}. The other measurements, on Hilger E_1 plates, have a probable error varying from 1 to 6 cm^{-1} in going from higher to lower frequencies in the region occupied by the observed bands.

In Fig. 1 the band at 3122A is reproduced together with a comparable band of CO at 2833A. The scale of enlargement for the latter is only about 0.6 as large as that for the former, chosen in order to match similar features of the

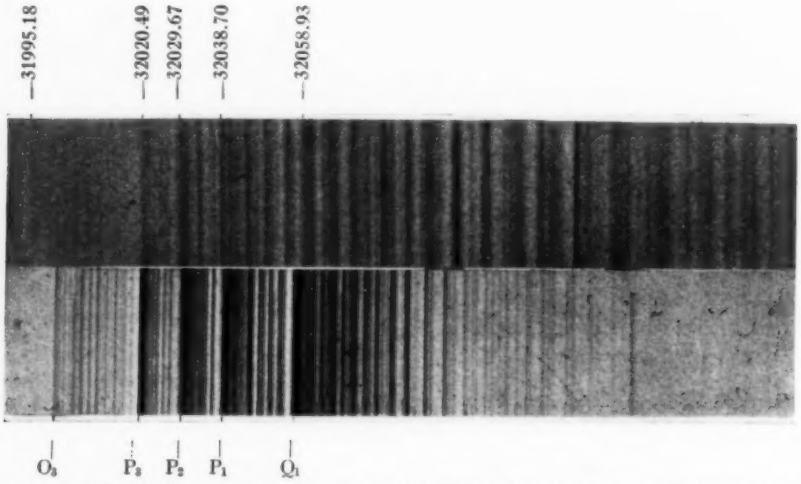

FIG. 1. *Above.* (0,0) Band of the *A* system of BF at 3122A, with frequencies of heads shown in cm^{-1}. *Below.* (0,0) Band of the third positive system of CO at 2833A. Designation of heads from rotational analysis of Dieke and Mauchly.[8] The lower strip is enlarged about 0.6 as much as the upper one in order to illustrate similarities of band structure.

two bands. The designations for the sub-heads of the CO band are taken from the rotational analysis of Dieke and Mauchly.[8] The features of the BF band are not sufficiently clear-cut for purposes of rotational analysis. Three strong subheads could be distinguished in most of the bands, corresponding to the P_3, P_2 and P_1 heads of CO. Weaker heads, observable in some of the bands, appear to correspond to O and Q branch heads of the CO bands, and have been designated accordingly. The edge of the Q branch, while not strictly a head, is listed wherever it appears as a distinct feature of the band.

Twelve of the observed bands belong to the same system, designated as the A system. One band at 3560A is the isotope band of $B^{10}F^{19}$, corresponding with the (0,3) band of $B^{11}F^{19}$ at 3548A. The intensities and frequencies of the heads of the A system bands are listed in Table I. Three other bands have final levels in common with the A system, but an initial level which is different; these are designated as members of a B system, and are tabulated in Table II. In Table III are listed three bands not assigned to either system.

The vibrational spacing of bands of the A system is represented by the equation:

$$\nu_h = 31{,}869.98 + 1631.40(v'+\tfrac{1}{2}) - 23.10(v'+\tfrac{1}{2})^2 - 1323.64(v''+\tfrac{1}{2}) + 9.40(v''+\tfrac{1}{2})^2$$

where ν_h represents the frequency in cm^{-1} of the sub-head assumed to be nearest the band origin, the one corresponding to the P_3 sub-head of the CO band, Fig. 1. The frequency separation of the sub-heads varies from one band to the next, and in the absence of a rotational analysis of the bands, no attempt is made to show this in the equation. The B system bands are represented by:

$$\nu_h = 38{,}651.4 - 1323.64(v''+\tfrac{1}{2}) + 9.40(v''+\tfrac{1}{2})^2$$

where ν_h again refers to the P_2 head.

The constants in the above equations are based on the high dispersion plates. The residuals (obs.-calc.) thus obtained for the heads measured at low dispersion are preponderantly positive, which may indicate a slight displacement of the iron comparison lines relative to the bands. Since the residuals are not large in comparison with the probable error, no adjustment of the data seemed necessary.

[8] G. H. Dieke and J. W. Mauchly, Phys. Rev. **43**, 12 (1933).

TABLE I. *A system bands of BF.*

v'	v''	Int.	ν Obs. (cm^{-1})		Obs.–Calc. (cm^{-1})
		9	32058.93	Q_1	
		9	*32038.70	P_1	
0	0	9	*32029.67	P_2	
		7	*32020.49	P_3	+0.06
		2	*31995.18	O	
		5	30751.6	Q_1	
		7	*30734.70	P_1	
0	1	5	*30724.80	P_2	
		5	*30715.41	P_3	−0.18
		4	30696.82	O	
		5	29467.5	Q_1	
		6	*29449.30	P_1	
0	2	5	*29438.67	P_2	
		3	*29429.70	P_3	+0.15
		4	29413.2	O	
		4	28199.2	Q_1	
		5	*28182.66	P_1	
0	3	5	*28172.23	P_2	
		4	*28162.20	P_3	−0.11
		3	*28144.07	O	
0	3**	0	28087.5	Q_1	
		0	28072.1	P_1	
		1	28057.4	P_2	
		0	28039.3	P_3	−4.3
		0	26952.4	Q_1	
		0	26938.4	P_1	
0	4	0	26922.3	P_2	+8.4
		0	26898.4	O	
		3	33640.7	Q_1	
		4	*33623.59	P_1	
1	0	4	*33613.86	P_2	
		4	*33605.69	P_3	+0.06
		2	33580.0	O	
		0	32334.6	P_1	
		0	32320.1	P_2	
1	1	0	32301.7	P_3	+0.9
		1	32287.2	O	
		1	31052.1	P_1	
		1	31029.6	P_2	
1	2	1	31019.5	P_3	+4.7
		3	29782.1	P_1	
		4	29765.4	P_2	
1	3	2	29756.2	P_3	+8.7
		2	28534.8	Q_1	
		1	*28518.60	P_1	
		0	*28509.07	P_2	
1	4	0	*28499.36	P_3	+0.29
		1	28482.3	O	
		0	27305.6	P_1	
		0	27290.4	P_2	
1	5	0	27278.0	P_3	+8.6
		0	27255.9	O	
2	0	0	35181.7	Q_1	
		2	35162.6	P_1	
		3	35153.8	P_2	
		2	35145.2	P_3	+0.6
		1	35124.8	O	

* Frequencies computed from wave-length measurements made on 21-foot grating plates are marked by an asterisk. Other wave-length measurements and all intensity estimates are based on E_1 plates.
** Isotope band, $B^{10}F^{19}$.

DISCUSSION

With the aid of constants of the A system of the $B^{11}F^{19}$ molecule, positions were calculated for possible bands of what we may call the A^i system of the less abundant molecule $B^{10}F^{19}$. Only one measured band could be assigned to the A^i system. In all other cases, the failure to observe the A^i bands could be accounted for either by the low intensity to be expected or by confusion with an A band. The excellent agree-

TABLE II. *B system bands of BF.*

v'	v''	INT.	ν OBS.	OBS.–CALC.
		6	38028.3 Q_1	
		7	38009.7 P_1	
0	0	8	37999.1 P_2	
		7	37991.4 P_3	−0.5
		6	36722.1 Q_1	
		4	36704.7 P_1	
0	1	6	36700.5 P_2	
		4	36687.9 P_3	+0.8
		2	36660.3 O	
		4	35435.8 Q	
		3	35418.4 P_1	
0	2	4	35409.4 P_2	
		3	35400.8 P_3	−0.3
		2	35390.7 O	

TABLE III. *Unassigned bands.*

INT.	ν OBS.	INT	ν OBS.	INT.	ν OBS.
0	38833.1	0	38544.5	0	37224.8
1	38801.4	0	38518.3	0	37207.1
2	38787.3	1	38505.4	1	37196.0
1	38775.1	0	38493.7	0	37187.1
				0	37118.6

TABLE IV. *Comparison of lower level of BF bands with a* $^3\Pi$ *level of CO.*

	$\omega_e(H)$ (cm^{-1})	$x_e\omega_e(H)$ (cm^{-1})	D (volts)	r_0 (A)	B_e (cm^{-1})
CO	1739.3	14.5	4.0	1.204	1.686
BF	1323.64	9.40	?	1.33*	1.36*

* Computed from empirical relationship of Allen and Longair.[9]

ment between the observed and calculated position of the isotope band removes any doubt which otherwise might attach to the identification of the emitter of the bands.

An estimate of the interatomic distance, r_e, can be made with the aid of the relationship proposed by Allen and Longair:[9]

$$r_e^3\omega_e\mu^{\frac{1}{2}} = 10.6\times10^{-33},$$

where μ is the reduced mass, and ω_e is the frequency (in wave numbers) for vibrations of small amplitude about the equilibrium position, obtained from the spectrum. On this basis, the value of r_e for the common (lower) state of the A and B systems of BF is 1.33A; that for the upper state of the A system is 1.24A.

On the basis of the predicted similarity between BF and CO spectra, and the observed resemblance illustrated in Fig. 1, it is natural to suppose that the A system bands correspond to the third positive bands of CO, and the B system to the $3A$ bands of CO. If this is correct, the lower level of the bands is itself an excited state, and the molecular constants obtained for it do not apply to the unexcited state of the molecule. As suggested by Dull,[4] the lower state may be either $^3\Pi$ or $^3\Sigma$ depending on whether the transition is $^3\Pi-{}^3\Sigma$ or $^3\Sigma-{}^3\Pi$. In Table IV a comparison is made with the a $^3\Pi$ level of CO, on the basis of the assumed correspondence.

[9] H. S. Allen and A. K. Longair, Phil. Mag. **19**, 1032 (1935).

ACKNOWLEDGMENTS

The authors express thanks to Professor H. S. Booth, and Mr. Karl S. Willson for preparing the pure samples of BF_3, and for suggesting effective means of avoiding contaminations of the samples. They are grateful also to Professor Alpheus W. Smith for critical assistance in the preparation of this report.

The Band Spectra of the Hydrides of Lithium

Part III. Potential Curves and Isotope Relations

F. H. CRAWFORD AND T. JORGENSEN, JR., *Physics Research Laboratory, Harvard University*

(Received April 2, 1936)

The empirical band spectrum rho-values, ρ^*, as computed from the constants of LiH and LiD depart markedly from the ratio of the reduced masses, $\rho=(\mu/\mu')^{\frac{1}{2}}$. The isotope discrepancy, $(\rho^*-\rho)$ is *positive* for the 11 band constants measured for the ground state and *negative* for 10 of the 13 in the upper state. By using Dunham's equations, the *anharmonicity* constants a_1, $a_2\cdots a_6$ are computed for the ground state and the effect of anharmonicity on the isotope ratio calculated. In only 2 cases out of 5 does this reduce the isotope discrepancy and then by amounts from 6 to 22 percent. In the *upper state* the anharmonicity constants must be got by a laborious approximation process. It is shown that the resulting set of a values accounts quite satisfactorily for both the *sign* and *value* of the 9 band constants, which have been previously reported as *abnormal*. This well-known abnormality can therefore not be ascribed in any significant measure to L uncoupling. The Dunham corrections further *reduce* the isotope discrepancy in 4 out of 5 cases by an average of about 25 percent. The dissociation energies (Morse) are found to be for LiD, $D_0''=2.53$, $D_0'=1.15$ volts and for LiH $D_0''=2.54$ and $D_0'=1.18$ volts (all ± 0.2 volt and measured from the $v=0$ level).

INTRODUCTION

THE $^1\Sigma\rightarrow{}^1\Sigma$ band spectra of LiH and LiD are of particular interest for testing the finer points of the theory of molecular spectra for two reasons. In the first place the molecules are relatively light and therefore the isotope shifts to be expected are larger than for any known molecules except H_2 and HD. In the second place the upper electronic state is quite abnormal in that the molecules appear to *shrink* in size as well as to vibrate more rapidly as the amount of vibrational energy increases. Similar effects are present in the case of the hydrides of Na and K though they are there less pronounced in magnitude than in the present case. In addition the simplicity of the structure of $^1\Sigma\rightarrow{}^1\Sigma$ bands is of great assistance in the measurement of those molecular constants on the precise determination of which the present discussion so largely depends.

Preliminary accounts of results and the data on which the present paper depends have been given earlier.[1]

It is now well known experimentally that the molecular constants of hydrides and deuterides (MH and MD) are not in general related precisely by powers of the reduced mass ratio $\rho\equiv(\mu/\mu')^{\frac{1}{2}}$, where $\mu=MH/(M+H)$ and $\mu'=MD/(M+D)$, of the simple isotope theory. As here defined $\rho=0.750486$ and is therefore <1 and we find in the *ground state* that the eleven constants which can be measured with reasonable certainty all give ratios (say ρ^*) which are slightly *nearer* unity.

Thus $(\rho^*-\rho)$ which we may call the *isotope discrepancy* is in every case *positive*. In the *first excited* state, on the other hand, we find $(\rho^*-\rho)$ is positive for only three of the constants and *negative* for the other ten. It seems probable—although sufficient data are not at hand for certainty—that the first result, i.e., $(\rho^*-\rho)>0$, is the normal behavior for the ground states of most molecules.

As in Part II we shall write the complete energy expression (in cm^{-1}) for a rotating-vibrating diatomic molecule in a singlet state as

$$\frac{W}{hc}=\frac{W_0}{hc}+\sum_{l=0,\,1\cdots}\ \sum_{j=0,\,1\cdots}\times Y_{lj}^*(v+\tfrac{1}{2})^l[J(J+1)]^j. \quad (1)$$

The empirically determined "rho-value," ρ_{lj}^* referred to in the paragraph above, is then given by $(Y_{lj}{}^i{}^*/Y_{lj}{}^*)^{(1/l+2j)}$ and in general varies with *both* l and j. Since the elementary isotope theory[2]

[1] Crawford and Jorgensen, Phys. Rev. **45**, 737 (1934); Part I, Phys. Rev. **47**, 358 (1935); Part II, Phys. Rev. **47**, 932 (1935); Phys. Rev. **48**, 475 (1935). In Parts I and II complete references to the earlier literature are given.

[2] See, for example, Jevons, *Report on the Spectra of Diatomic Molecules*, p. 212.

predicts that $(\rho_{1j}^*-\rho)=0$ the departure of this difference from zero may be taken as an indication that the empirical molecular band constants Y_{1j}* and Y_{1j}* have lost their (assumed) precise mechanical significance. This implies for example that Y_{10}* (identical with the vibration constant ω_e*, where the asterisk is used to emphasize its empirical nature) does not give *exactly* the rate of vibration for small amplitude motions about the equilibrium position. This latter mechanically simple constant we shall designate by ω_e. Likewise $Y_{01}^*\equiv B_e^*\neq B_e$, where $B_e=h/8\pi^2cI_e$, and therefore the actual moment of inertia at the equilibrium position, I_e, cannot be computed directly from $h/8\pi^2cB_e^*$.

Now although various approximations in the solution of the wave equation for a rotating-vibrating diatomic molecule have been pointed out as partly responsible for these differences, it seems desirable to call attention to the classification of neglected effects given by Van Vleck[3] in a recent careful reexamination of the whole problem. The neglected energy terms, although not all capable of specific evaluation in forms suitable for immediate comparison with experiment can be considered as due to four effects:

1. *Anharmonicity* terms due to the interaction of *rotation* and *vibration*. This question has been considered in great detail by Dunham[4] who, writing the molecular potential energy function in the general form:

$$V=a_0\xi^2[1+a_1\xi+a_2\xi^2+a_3\xi^4+a_4\xi^5+\cdots] \quad (2)$$

obtained small correction terms to the usual energy expression. These correction terms (actually only five were evaluated, see Eqs. (7) to (11) below) involve the potential coefficients a_1, a_2, etc., and a factor $p^2=(B_e/\omega_e)^2$ and in general may be positive or negative depending on the precise form of Eq. (2). Since their values depend on p^2, these terms will be very small for heavy molecules and of importance only for hydrides. Here p^2 varies from $\approx 10^{-4}$ for certain states of H_2, LiH, etc., to 10^{-5} and 10^{-6} for a large number of the electronic states of molecules formed from the first two rows of the periodic table.

2. Terms due to the *interaction* of *electronic* and *nuclear* motions (neglecting the interaction of neighboring electronic levels). The use of a potential function of the type of Eq. (2) is equivalent to considering the frequencies of electronic motions so high that the nuclei in a nonvibrating molecule are essentially fixed. To this approximation, terms in the original complete wave equation for a diatomic molecule[5] which vanish when averaged over the frequencies connected with the electronic motions, are neglected. In higher order approximations of the energy of the system these neglected terms do, however, make contributions. The form of these contributions has been considered by Kronig,[6] Dieke[7] and Van Vleck[8] where simple approximations for a few of these terms are given, suitable for electronic states of symmetrical molecules with $L=0$ or for those states (with $L\neq 0$) which can be satisfactorily approximated by considering the nuclei coalesced. The precise evaluation of these terms in the general case requires more detailed knowledge of the molecular wave-functions concerned. They do, however, contain p^2 as a factor and probably tend to *increase* both $(\rho_{10}^*-\rho)$ and $(\rho_{01}^*-\rho)$. The remaining corrections arise from the interaction of other electronic states with the one under consideration and are of two sorts.

3. L uncoupling terms.[8] These are due to the interaction of electronic states whose Λ values differ by ± 1, are zero for $\sigma^1\Sigma$ states and have no appreciable effect on vibrational constants, i.e., the coefficients Y_{10}*. Their sign is + or − according as the perturbing state is *above* or *below* the one in question. They vary as b_e/ν, where $\nu\approx$ the electronic separation of the states involved.

4. Terms arising from the interaction of states of the *same* Λ *value*.[3] These terms are of a distinctly *new* type and do not affect the rotational constants Y_{0j}*. They also are of the order of B_e/ν and may be + or −.

[3] Van Vleck, Phys. Rev. **49**, 417A (1936); J. Chem. Phys. (in press). Note that the energy expressions used by Van Vleck are in absolute energy units while ours are in cm^{-1}.

[4] Dunham, Phys. Rev. **41**, 721 (1932).

[5] Van Vleck, Phys. Rev. **33**, 467 (1929), Eq. (11).

[6] Kronig, Physica **1**, 618 (1934).

[7] Dieke, Phys. Rev. **47**, 661 (1935).

[8] Hill and Van Vleck, Phys. Rev. **32**, 269 (1928).

A detailed evaluation of the effects (3) and (4) requires of course a fairly complete knowledge of the electronic states of the molecule in question. Since the corrections of these four types (unless an actual large scale "perturbation" is present) are usually small, we can treat them as independently additive. Consequently we can write:

$$Y_{lj}^* = Y_{lj}[1+(\Delta_1)_{lj}+(\Delta_2)_{lj}+(\Delta_2)_{lj}+(\Delta_4)_{lj}] \quad (3)$$

where Y_l is the mechanically significant value Y_{lj}^* would assume if the contributions $(\Delta_1)_{lj}$, etc., of the above effects were zero or experimentally undetectable. Here then

$$Y_{lj}^{i*}/Y_{lj}^* = (\rho^*)^{l+2j}, \quad (4)$$

and since ρ is usually near unity we may write to the same degree of approximation:

$$(\rho_{lj}^* - \rho) = \Delta_1\rho_{lj}+\Delta_2\rho_{lj}+\Delta_3\rho_{lj}+\Delta_4\rho_{lj}, \quad (5)$$

where in general $\Delta_4\rho_{l0}$ and $\Delta_4\rho_{0j}$ will be zero.

From the above it is apparent that only the corrections due to anharmonicity $[(\Delta_1)_{lj}$ and $\Delta_1\rho_{lj}]$ can be computed in a detailed manner at the present time. We therefore propose in this paper to deal primarily with these.

Effects of Vibration and Rotation Interaction

Dunham's calculations of the explicit form of the Y_{lj}'s in terms of the anharmonicity constants a_1 to a_6 of Eq. (2) indicate that each coefficient of Eq. (1) is of the form:

$$Y_{lj}^* = f_{lj}(\omega_e, B_e)[A_{lj}(a_1, a_2\cdots) + p^2C_{lj}(a_1, a_2\cdots)] \quad (6)$$

and that therefore by neglecting the last three terms of Eq. (3), $Y_{lj}=f_{lj}/A_{lj}$ and $(\Delta_1)_{lj} = p^2C_{lj}/A_{lj}$. Here A_{lj} and C_{lj} are functions of the anharmonicity constants $a_1, a_2\cdots$ and are therefore the same for each isotope, while f_{lj} and p both contain factors dependent on mass and are different in the two cases. In general f_{lj} decreases rapidly with both l and j. Dunham's calculations were carried far enough to obtain five of the C_{lj} terms. Since it will be necessary to refer repeatedly to these equations we shall give them here in a form slightly more suitable for numerical reckoning.[8a]

[8a] For convenience fractions have been divided out and given uniformly to four decimals. This is quite accurate enough for any experimental data.

$$Y_{10}^* = \omega_e^* = \omega_e[1+p^2C_{10}], \quad (7)$$

$$Y_{01}^* = B_e^* = B_e[1+p^2C_{01}], \quad (8)$$

$$Y_{02}^* = D_e^* = -4B_ep^2[1+p^2C_{02}], \quad (9)$$

$$Y_{11}^* = \alpha_1^* = B_ep[6(1+a_1)+p^2C_{11}], \quad (10)$$

$$Y_{20}^* = x_1^* = B_e/2[3(a_2-1.25a_1^2)+p^2C_{20}], \quad (11)$$

$$Y_{00}^* = B_e/8[3a_2-1.75a_1^2], \quad (12)$$

$$Y_{30}^* = x_2 = B_ep/2[10a_4-35a_1a_2 + (56.25a_1^2-8.5a_2)a_2-22.0313a_1^4], \quad (13)$$

$$Y_{40}^* = x_2 = 5B_ep^2[3.5a_6-15.75a_1a_2 + (33.9375a_1^2-8.125a_2)a_4 - (61.0313a_1^3-60.375a_1a_2+7.875a_3)a_3 + (90.8791a_1^4-77.9531a_1^2a_2 + 4.6875a_2^2)a_2-22.6084a_1^6], \quad (14)$$

$$Y_{21}^* = \alpha_2 = 6B_ep^2[5a_3-(3+13a_1)a_2 + (10+7.5a_1+7.5a_1^2)a_1+5], \quad (15)$$

$$Y_{31}^* = \alpha_3 = 20B_ep^2[7a_5-(4.5+25.5a_1)a_4 + (14+26.25a_1-22.5a_2+54.375a_1^2)a_3 - (8.5+45a_1-6.375a_2+59.0625a_1^2 - 51.375a_1a_2+94.3125a_1^3)a_2 + (21+28.125a_1+35.25a_1^2 + 29.7422a_1^3+29.7422a_1^4)a_1+7], \quad (16)$$

$$Y_{12}^* = \beta_1 = 12B_ep^3[4a_2-(9+4.5a_1)a_1-9.5], \quad (17)$$

$$Y_{22} = \beta_2 = 24B_ep^4[15a_4-(30+47.5a_1)a_2 + (61+117a_1+103.5a_1^2-26a_2)a_2 - (125+123.75a_1+90a_1^2+45a_1^3)a_1-65], \quad (18)$$

$$Y_{03}^* = H_e^* = 16B_ep^4(a_1+3), \quad (19)$$

$$Y_{13}^* = \gamma_1 = 12B_ep^5[26.6667a_3-(120+88a_1)a_2 + (279+189a_1+63a_1^2)a_1+233], \quad (20)$$

$$Y_{04}^* = 64B_ep^6[a_2-(9+2.25a_1)a_1-13], \quad (21)$$

where the C_{lj}'s are given by

$$C_{10} = \tfrac{1}{4}[25a_4^*-47.5a_1a_3+(57.375a_1^2 - 16.75a_2)a_2-18.0469a_1^4], \quad (22)$$

$$C_{01} = \tfrac{1}{2}[15a_3-(9+23a_1)a_2 + (14+10.5a_1+10.5a_1^2)a_1+15], \quad (23)$$

$$C_{02} = \tfrac{1}{2}[-45a_4+(90+102.5a_1)a_3 - (119+207a_1+166.5a_1^2-46a_2)a_2 + (199+173.25a_1+126a_1^2 + 62a_1^3)a_1+163], \quad (24)$$

$$C_{11}=[175a_5-(112.5+397.5)a_4 +(190+356.25a_1-357.5a_2 +643.125a_1^2)a_3-(167.5+459a_1 -125.625a_2+602.4375a_1^2-584.625a_1a_2 +891.1875a_1^3)a_2+(285+286.875a_1 +288.75a_1^2+243.6328a_1^3 +243.6328a_1^4)a_1+175], \quad (25)$$

$$C_{20}=\tfrac{1}{2}[256a_6-682.5a_1a_5+(1066.875a_1^2 -442.5a_2)a_4-(1491.5625a_1^3 -1833.75a_1a_2+271.25a_3)a_3 +(1873.3203a_1^4-1940.1563a_1^2a_2 +213.375a_2^2)a_2-408.3106a_1^6]. \quad (26)$$

From the equations it is at once apparent that if all of the Y^*'s could be determined with comparable precision most of the a's could be determined in two or more ways. Actually Y_{00}^* is not measurable directly, Y_{04}^* is seldom obtained and only an extremely complete and careful analysis gives the α's, β's or γ's with enough accuracy to be of much value. The detailed procedure to be employed therefore depends on the data available and in any event the uncertainty in a given a increases with its subscript.

Ground State

In the ground state of both LiH and LiD the quantities ω_v, B_v, D_v and H_v change so regularly with v that relatively good values of most of the smaller constants are obtainable. It is desirable therefore to compute the a's from the smaller constants and to use these for determining independently the correction factors C_{1j} of Eqs. (22) to (26). This is open to the objection that the corresponding correction terms are not known for Eqs. (13) to (21) and may be relatively important. Since their contributions to the total energy expression will be small if not experimentally undetectable this means merely that to represent data of a given precision we need the a's very much less accurately.

A glance at Eqs. (13) to (21) shows that a_1 can be obtained from (19) and thence a_2 from (17). Then a_3 can be obtained from either (15) or (20) and a_4 from (13) or (18). Finally a_5 and a_6 can be obtained from (16) and (14), respectively. The results of these calculations are given in Table I for both LiH and LiD where because of the larger number of bands observed in the latter case the results for LiD are more trustworthy. When a given a is obtained in two ways, one usually can be recognized as the more reliable. Thus x_2 contributes 26 percent of the final value 5.79 of a_4 in Eq. (13) while β_2 contributes 23 percent towards 6.53 in Eq. (18). Since x_2 is probably more certain than the very small β_2 the first value is the more dependable. Such values are indicated by a dagger. It should be further remarked that since $\alpha_3(\equiv Y_{31}^*)$ was too small to be measured for either isotope, theoretically a_5 could not be determined. Actually, however, solution of Eq. (16) for a_5 shows that unless $|\alpha_3|$ exceeds considerably its rough theoretical value of 1.3 percent $|\alpha_2|$, a reasonably good value should result from setting $\alpha_3=0$. Likewise in the case of a_6 determined from Eq. (14) we require $x_3(\equiv Y_{40}^*)$ which could be measured only for LiD. Since this occurs only in the practically dimensionless ratio $x_3/5B_e\rho^2$ in the solution for a_6, the LiD value of this term was employed in finding a_6 for LiH. The coefficients are seen to alternate regularly in sign and to increase almost *linearly* in absolute value with the subscript. This as Dr. H. M. James, in this laboratory, has found, is apparently a characteristic of normal electronic levels.

TABLE I. *Potential coefficients for ground state.*

Eq.	a_n	LiH	LiD
(19)	a_1	−1.84	−1.858
(17)	a_2	+2.33	+2.580
(15)	a_3	−2.69	−3.446
(20)		−2.98†	−3.456
(13)	a_4	+5.51†	+5.79†
(18)		+4.35	+6.53
(16)	a_5	−14.0	−12.2
(14)	a_6	≈+33	+20.7

† Values so marked are the more reliable of a pair.

With a reasonably good set of a values we are now in a position to do several things. We may first determine from Eqs. (7) and (8) better approximations to the mechanically significant constants ω_e and B_e. These then enable us to determine what we might call the Dunham approximation to D_e^*, x_1^* and α_1^*, and finally to determine $\Delta_1\rho_{1j}$ the Dunham contributions to the isotope discrepancy. The first step gives us

$$Y_{10}{}^{i*}=\omega_e{}^i[1+1/10{,}042], \quad Y_{10}^*=\omega_e[1+1/5660],$$

$$Y_{01}{}^{i*}=B_e{}^i[1-1/7376], \quad Y_{01}^*=B_e[1-1/4157].$$

TABLE II.

(lj)	C_{lj}	Values of Y_{lj}^{ii*} (for LiD) Observed	Dunham	Kratzer	Pekeris	Values of Y_{lj}^{*} (for LiH) Observed	Dunham	Kratzer	Pekeris
02	−35.69	$-2.856\cdot10^{-4}$	-2.72510^{-4}	−2.727	—	$-8.62\cdot10^{-4}$	-8.58510^{-4}	$-8.594\cdot10^{-4}$	—
11	−235.6	0.09198	−0.0875	−0.1060	−0.0780	−0.2132	−0.2070	−0.2480	−0.1823
20	−837	−13.23	−11.046	12.70	—	−23.20	−19.64	22.54	—

TABLE III. *Ground state isotope effects.*

Band Constant	(lj)	A_{lj}	C_{lj}	ρ_{lj}^{*}	$(\rho_{lj}^{*}-\rho)$	$\Delta_1\rho_{lj}$	$\Delta_1\rho_{lj}/(\rho_{lj}^{*}-\rho)$
ω_e^{*}	10	1	+6.18	0.750628	$+0.00014_2$	−0.00006	−42%
B_e^{*}	01	1	−8.42	.750685	+ .00020	+ .00004	+22%
D_e^{*}	02	1	−35.69	.7520	+ .0015	+ .000084	+ 6%
α_1^{*}	11	$6(1+a_1)<1$	−235.6	.7556	+ .0051	− .000143	−3%
x_1^{*}	20	$3(a_2-1.25a_1^2)<1$	−837	.7551	+ .0046	− .000754	−16%

(+ sign in the last column indicates that the Dunham correction *decreases* the isotope discrepancy.)

TABLE IV. *Upper state isotope effects.*

Band Constant	(lj)	A_{lj}	ρ_{lj}	ρ_{lj}^{*}	$(\rho_{lj}^{*}-\rho)$	$\Delta_1\rho_{lj}$	$\Delta_1\rho_{lj}/(\rho_{lj}^{*}-\rho)$
ω_e^{*}	10	1	−53.25	0.770918	+0.02043	+0.002618	+13%
B_e^{*}	01	1	−46.22	.754561	+ .004075	+ .001136	+28%
D_e^{*}	02	1	+214.4	.7424	− .008	− .00264	+30%
α_1^{*}	11	+0.83538	+3550	.2036	− .1622	− .06963	+43%
x_1^{*}	20	+18.064	−8840	$.6951_2$	$-.0553_7$	+ .01203	−22%

These results give $p^{ii}=2.859\times10^{-5}$ and $p^{2}=1.611\times10^{-5}$ and enable the observed values of $D_e^{*}x_1^{*}$ and α_1 to be compared with the Dunham approximations as well as those of Kratzer[9] and in the case of α_1^{*}, of Pekeris.[10] The numerical values are collected in Table II, where it appears that the difference between Kratzer's and Dunham's values for D_e^{*} are inappreciable and fairly close to the observations. In the case of α_1^{*} Dunham's values are the best, though differing by more than the experimental uncertainty, with Kratzer's too high and Pekeris' as much too low. The agreement in the case of x_1^{*} is not as good and Kratzer's expression in this case lies closer to the observations.

Isotope Ratios

Turning to the isotope relations a little manipulation of Eq. (6) shows that we can write

$$\Delta_1\rho_{lj}=-[\rho(p^2-p'^2)/(l+2j)A_{lj}]C_{lj}, \quad (27)$$

where $\rho=0.750486$. We find also that $\rho_{10}^{*}=0.750628$ and $\rho_{01}^{*}=0.750685$. Hence $(\rho_{10}^{*}-\rho)=+0.00014_2$ and $(\rho_{01}^{*}-\rho)=+0.00020$. But from Eq. (27) we have $\Delta_1\rho_{10}=-0.00006$ and $\Delta_1\rho_{01}=+0.00004$. Therefore the residual discrepancy $(\rho_{lj}^{*}-\rho-\Delta_1\rho_{lj})$, in the first case is increased to +0.00020 and in the second decreased to +0.00016. Since L uncoupling is ruled out for the ground $\sigma^1\Sigma$ state the first discrepancy is presumably due to effects (2) and (4) while the second must be due to effect (2) (the Kronig effect) alone, since effect (4) does not influence rotational constants (and particularly B_e^{*}) appreciably. Similar calculations have been carried out for ρ_{02}^{*}, ρ_{11}^{*} and ρ_{20}^{*} and the results are collected in Table III where it is seen that the Dunham effect is inappreciable in the case of α_1^{*} and varies from 16 to 42 percent of the total discrepancy in the other cases. In only two cases does it decrease the discrepancy.

Excited State (Calculation of a Values)

The attempt to determine the a values for the excited state in the same way as for the ground

[9] Kratzer, Zeits. f. Physik **3**, 289 (1920).
[10] Pekeris, Phys. Rev. **45**, 98 (1934), also Jevons, reference 1, p. 27, and Birge, Bull. Nat. Res. Council (1926), p. 237.

state immediately leads to quite discrepant values. Thus Eq. (19) gives for a_1 roughly -2 whereas Eq. (10) (neglecting p^2C_{11}) gives -0.814. Now the discrepancy may be due to the uncertainty in H_e^* as measured, or to the neglect of p^2C_{03} in Eq. (19), of p^2C_{11} in Eq. (10) as well as of effects (2), (3) and (4) above. Whatever the difficulty, a reasonable value for a_1 cannot be obtained by averaging such divergent values—and since the value of a_2 depends to such an extent on the value of a_1, using Eqs. (11) and (17) we have four widely different values for a_2 with no basis for preferring any particular one of them. As a result, beyond a_2 even the sign of the higher a's is in doubt. After following down all the possibilities it soon became probable that the neglect of the Dunham correction terms was not the primary difficulty—but that the real trouble arose from the difficulty in extrapolating the measured values of D_v and H_v, respectively, to obtain D_e^* and H_e^*. This uncertainty was such as to produce even greater errors in β_1, γ_1, β_2, etc., and consequently to render the values of a_1, a_2, a_3 and a_4 as obtained respectively from Eqs. (19), (17), (15) and (13) quite untrustworthy. It seemed accordingly necessary to resort to a method of successive approximation, using only those experimental constants which could be determined fairly reliably from least squares representation of the remaining data, *viz.*, the values of ω_v and B_v. Since the variation with vibration of ω_v and B_v was much smaller for LiD than for LiH, the calculations were carried out for the LiD data (actually the LiH data gave comparable results—though the actual numerical values depended uncomfortably on the precise number of observations used in the least-square reckonings). The necessary expressions for LiD are:

$$\omega_v = 180.711 + 13.987u - 1.1784u^2 + 0.07932u^3 - 0.00353u^4 + 0.00006940u^5 \text{ (7 points)}$$

and

$$B_v = 1.6048_1 + 0.015940u - 0.0023732u^2 + 0.00012783u^3 - 0.00000417u^4 \text{ (6 points)}.$$

An examination of the equations from (10) to (17) then shows that the a's of odd subscript can be obtained from the *rotational* constants α_1, α_2, and α_3 while the a's of even subscript can be obtained from the *vibrational* constants x_1, x_2 and x_3. The general procedure was to determine a first approximation to a_1, say a_{11}, from Eq. (10) by neglecting p^2C_{11}. With this a first approximation to a_2, say a_{21}, was then obtained from Eq. (11) neglecting p^2C_2O. Then by using Eqs. (15), (13), (16) and (17) in order, a_{31}, a_{41}, a_{51} and a_{61} were obtained. It was then possible to compute C_{11} and C_{20} approximately to get the second approximation of a_1 and a_2, say a_{12} and a_{22}, respectively. This led then to better values for the higher a's, to more reliable values for C_{11} and C_{20}, etc. The process is unfortunately very tedious and while not converging very rapidly soon gives results which do not oscillate very much in successive stages of the calculations.

The results are given in Table V for a_{n2} and a_{n5} together with the values of C_{ij} resulting.[11]

TABLE V. *Potential coefficients for upper state.*

Eq.	Band Constant	A_n	A_{n2}	A_{n5}		Value of C_{ij}
10	$Y_{11}^* = \alpha_1^*$	a_1	-0.8604	-0.8608	C_{10}	-53.45
11	$Y_{20}^* = x_1^*$	a_2	$+6.884$	$+6.948$	C_{01}	-46.22
15	$Y_{21}^* = \alpha_2$	a_3	-11.33	-11.44	C_{02}	$+214.40$
13	$Y_{30}^* = x_2$	a_4	$+30.40$	$+31.11$	C_{11}	$+3550$
16	$Y_{31}^* = \alpha_3$	a_5	-66.57	-67.77	C_{20}	-8840
17	$Y_{40}^* = x_3$	a_6	$+67.32$	$+68.48$		

The striking fact is the rapidity with which the coefficients increase in absolute magnitude as compared with the more normal ground state, and in particular the fact that a_2 is over 12 times as large as $|a_1|$. This will be discussed in more detail below.

The next step was to determine whether this set of a values was satisfactorily consistent with the predictions of the remaining equations. For this purpose Eq. (7) was used to determine from $Y_{10}^* = \omega_0^*$ the true value, ω_e, of the rate of oscillation for zero amplitude, and from Eq. (8), $Y_{01}^* = B_e^*$, the true value of $h/8\pi^2 I$. These then gave $p^2 = (B_e/\omega_e)^2$ and from Eqs. (9) and (19) theoretical values of $Y_{02}^* = D_e^*$ and $Y_{03}^* = H_e^*$, respectively, could be obtained. The results were $Y_{02}^{i*}(\text{calc.}) = -5.162 \times 10^{-4}$, $Y_{03}^{i*}(\text{calc.}) = +34.22 \times 10^{-8}$, $Y_{02}^*(\text{calc.}) = -16.88 \times 10^{-4}$ and $Y_{03}^*(\text{calc.}) = 202.18 \times 10^{-8}$. It was next necessary in each case to obtain least-square curves which

[11] The values of C_{11} and C_{20} are the fourth approximations since these were the values determining the corrections in Eqs. (10) and (11) for the fifth approximations to a_1 and a_2, respectively.

passed through the observed data and these calculated values for $v=-\frac{1}{2}$. Since measurements could not be made for $v=1$ on LiD (and were uncertain on LiH) it was necessary to assign a probable value to say D_1, compute a least-square expression for D_1 to D_5 and calculate a D_e^* by setting $v=-\frac{1}{2}$. After a few trials a value of D_1 could be chosen such that this extrapolated D_e^* coincided with the one calculated theoretically. This gave for LiD

$$\beta_1^i=+2.64\times10^{-4}, \qquad \beta_2^i=-0.8907\times10^{-5},$$

$$\beta_1=+11.23\times10^{-4} \quad \text{and} \quad \beta_2=-4.7353\times10^{-5}.$$

A similar procedure in the case of the H_v values gave for LiD $\gamma_1^i=-39.54\times10^{-8}$, $\gamma_2^i=+18.420$ and for LiH, $\gamma_1=-250.01\times10^{-8}$ and $\gamma_2=+122.44\times10^{-8}$. Now it is to be admitted at once that great reliance cannot be placed on the actual values obtained from such an attempt to represent by least squares functions changing as rapidly as are D_v and H_v. The results, however, do represent a considerable improvement over those obtained empirically in Parts I and II. Thus in the case of LiD using Eq. (17) and the old value of $\beta_1^i=1.32\times10^{-4}$ we find $a_2=+3.56$ which is about *half* the value given in Table V. If we use the *new* value of β_1^i given above we find $a_2=+5.90$ a result differing by only 15 percent. Likewise for LiH from the *old* $\beta_1(=10.1\times10^{-4})$ we have $a_2=5.30$ while from the *new* β_1, $a_2=5.80$, likewise a shift in the right direction. Again using Eq. (20) and the values of γ_1^i and γ_1 we have for LiD a_3 (old) $=+3.9$, a_3 (new) $=-5.9$ and for LiH, a_3 (old) $=+3.7$, a_3 (new) $=-3.0$. Here the new values are both too small but have been altered 200 percent in the right direction and actually changed in sign by our process. Finally, using Eq. (18) and the values of β_2^i and β_2 we have for LiD: a_4 (old) $=+69.0$ and a_4 (new) $=+51.2$, while for LiH: a_4 (old) $=+56.5$ and a_4 (new) $=+53$, again a shift in each case in the right direction.

We therefore conclude that to the extent that (1) the undetermined Dunham corrections p^2C_{1j} and (2) the omitted Kronig and Van Vleck terms may be neglected—the anomalous behavior of the upper states of LiD and LiH can be accounted for semi-quantitatively in terms of a potential curve which departs in a characteristic way from the usual shape. It is thus apparent that the anomalies of the upper state involving some 9 small coefficients which differ in sign or magnitude from the usual case, are pictured in a very satisfactory way in terms of a single potential curve and that this same curve accounts for a sizable fraction of the observed isotope discrepancy.

Upper State Isotope Relations

We are now in a position to compute the Dunham contributions, $\Delta_1\rho_{1j}$, to the isotope discrepancies just as in the case of the ground state. The results of this with $\rho(p^2-p^{i2})$ of Eq. (27) $=0.4917\times10^{-4}$ are given in Table III where the striking fact is apparent that the isotope discrepancies are *reduced* in four out of five cases, the Dunham term varying from 13 to 43 percent of the total discrepancy $(\rho_{1j}^*-\rho)$.

Potential Curves

With the a values determined we may now write approximations to the potential curves (convergent near the equilibrium positions only) of the ground $^1\Sigma$ and upper $^1\Sigma$ states of LiH and LiD. These are for the ground state:

$$V=a_0'\xi^2(1-1.858\xi+2.580\xi^2-3.45\xi^3 +5.79\xi^4-12.2\xi^5+20.7\xi^6+\cdots, \quad (28)$$

where for LiH $a_0'=6.57078\times10^4$ and for LiD $a_0'=6.5715\times10^4$ and for the upper state:

$$V=a_0''\xi^2(1-0.8608\xi+6.948\xi^2-11.44\xi^3 +31.11\xi^4-67.77\xi^5+68.48\xi^6+\cdots, \quad (29)$$

where for LiH $a_0''=4.91646\times10^3$ and for LiD $a_0''=5.11154\times10^3$.

The ground states for the two molecules are thus very closely alike and follow the usual type lying *above* the osculating parabola for $\xi<0$ and *below* for $\xi>0$. On the other hand, the curves for the upper states differ somewhat more from one another and are distinctly anomalous in that although they rise above the corresponding parabolas for $\xi<0$ they quickly cross over and pass *above* again for small positive values of ξ. This behavior is more readily seen in Fig. 1 where the dotted curve is given by $a_0''\xi^2$ and the heavy curve represents Eq. (28). It is this peculiar form of anharmonicity in the upper state which

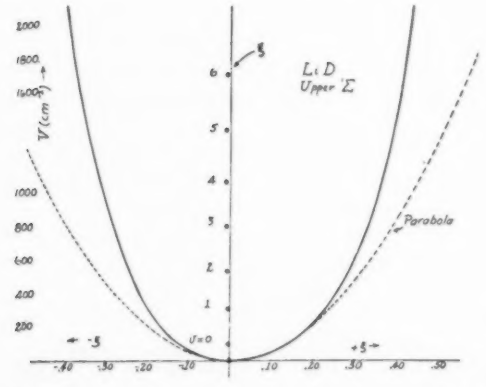

FIG. 1. The heavy line represents Eq. (29) while the parabola is $a_0\xi^2$. The rapid rise of the curve above the parabola on the right is to be noted. It is this which causes the molecule to travel more rapidly than usual along the right branch and hence to have an average ξ, $\bar{\xi}$, which is *less* than ξ_0. The corresponding average values for $v=0$, 1, etc., are indicated by circles at the appropriate height. It is this peculiar shape which likewise causes the observed vibrational rate ω_v to *increase* with v to a maximum value before decreasing thereafter in the normal way. The heavy curve of course must eventually fall away and cross the parabola as the molecule goes toward dissociation, though that point is far out of the range of validity of Eq. (29).

accounts in detail for the anomalies to which attention has been called so often in the literature. We therefore assume that although some L uncoupling may be present in this state it probably does not have much effect on the potential curve and is reflected only in the residual isotope discrepancies $(\rho_{1j}^* - \rho - \Delta_1\rho_{1j})$.

For purposes of reference the values of B_e^* and ω_e^* as well as the values corrected for the Dunham effect for both states of the two molecules are given as follows:

$$\text{LiD}\begin{cases} B_e^{i*\prime} = 1.6048 & B_e^{i\prime} = 1.6107 & r_e^{i\prime} = 2.5795\text{A} \\ \omega_e^{i*\prime} = 180.711 & \omega_e^{i\prime} = 181.472 & \\ B_e^{i*\prime\prime} = 4.2338 & B_e^{i\prime\prime} = 4.2344 & r_e^{i\prime\prime} = 1.5909_1\text{A} \\ \omega_e^{i*\prime\prime} = 1055.12 & \omega_e^{i\prime\prime} = 1055.015 & \end{cases}$$

$$\text{LiH}\begin{cases} B_e^{*\prime} = 2.8186 & B_e^{\prime} = 2.8375 & r_e^{\prime} = 2.5896\text{A} \\ \omega_e^{*\prime} = 234.41 & \omega_e^{\prime} = 236.225 & \\ B_e^{*\prime\prime} = 7.5131 & B_e^{\prime\prime} = 7.5149 & r_e^{\prime\prime} = 1.5915\text{A}. \\ \omega_e^{*\prime\prime} = 1405.649 & \omega_e^{\prime\prime} = 1405.401 & \end{cases}$$

From these the equilibrium separations are found where $(r_e' - r_e^{i\prime}) = +0.0101\text{A}$ and $(r_e'' - r_e^{i\prime\prime}) = +0.00055\text{A}$.

Further from Eq. (12) we see that the *height* of the potential curves at the minima should be different for the two isotopes. Thus for the ground state $Y_{00}^* = 15.93\ \text{cm}^{-1}$ and $Y_{00}^{i*} = 8.98$, a difference of $6.95\ \text{cm}^{-1}$, while for the upper state $Y_{00}^* = 7.39\ \text{cm}^{-1}$ and $Y_{00}^{i*} = 0.26\ \text{cm}^{-1}$, a difference of $7.13\ \text{cm}^{-1}$. Consequently we see that the electronic origin of the LiH bands should lie $0.18\ \text{cm}^{-1}$ towards the violet of the LiD bands—an effect unfortunately too small to detect in this case.

These facts together with the data accompanying Eqs. (28) and (29) then enable us to draw three conclusions, *viz.*, (1) the *heavier* isotopic molecule is the *smaller*, its potential curve (2) has the greater convexity at the minimum and (3) lies below that of the lighter isotope. These differences it will be recalled are in the same direction as those predicted by Kronig[6] from the interaction of nuclear and electronic motions (effect (2) above).

By using Morse's expression for the dissociation energy, $D = \omega_e^2/4x$, we have after correcting for the zero-point vibrational energy $\mathbf{D}_0'' = 2.53$ volts for LiD and 2.54 volts for LiH where the difference is not significant. If then the upper state dissociates into a normal H atom and a 2^2P Li atom we have $\mathbf{D}_0' = 1.15$ volts for LiD and $\mathbf{D}_0' = 1.18$ volts for LiH. These results due to the small number of vibrational levels in the ground state can hardly be depended on to more than ± 0.2 volt.

Effect of Electron Pressure on Plasma Electron Oscillations

ERNEST G. LINDER, *RCA Manufacturing Co., Inc., Camden, N. J.*

(Received March 18, 1936)

A general equation for electron motion in a plasma is developed which includes a term arising from electron gas pressure. The resulting expression is

$$\partial^2\xi/\partial t^2+(4\pi ne^2/m)\xi=(kT/m)\nabla^2\xi,$$

where ξ is electron displacement, n electron density, and T electron gas temperature. From this it is found that the possible frequencies of free vibration form a series given by $f_i=(kT/\lambda_i^2m+ne^2/\pi m)^{\frac{1}{2}}$. The lower limit corresponds to the Tonks-Langmuir value $(ne^2/\pi m)^{\frac{1}{2}}$, while the other frequencies depend upon the possible standing waves which may exist. The theory explains the observed variation of frequency with electron gas temperature.

IN their investigation of electron oscillations in ionized gases, Tonks and Langmuir[1] did not take into consideration forces arising from electron gas pressure. The writer has found that if this force is included the previously not understood variation of resonance frequency with electron temperature may be explained.

In order to determine the effect of electron pressure, consider the equation of motion,

$$m\ddot{\xi}=-eE+\partial p/n\partial x, \tag{1}$$

where the last term represents the force arising from pressure. The electron displacement is denoted by ξ. The electric field E arises from electron displacements. In an undisturbed plasma the electron and positive ion densities are uniform and equal, and the net charge in any element of volume is zero, hence the plasma is field free. However, if electron displacements occur, the net charge in a volume element is no longer zero, in general, and electric forces are set up. The expression for this force, is[1]

$$E=4\pi ne\xi. \tag{2}$$

Departures from a uniform distribution will give rise also to pressure gradients. It will be shown that the forces thus arising may be of the same order of magnitude as the force E, and that their inclusion in the theory gives a variation of frequency with electron gas temperature.

If the undisturbed electron density is taken to be n_0, the change due to any displacement $\xi(x)$ is

$$\delta n=n_0\partial\xi/\partial x, \tag{3}$$

so that

$$n=n_0(1+\partial\xi/\partial x). \tag{4}$$

Now

$$p=nkT,$$

hence

$$\frac{\partial p}{\partial x}=kT\frac{\partial n}{\partial x}=n_0kT\frac{\partial^2\xi}{\partial x^2}. \tag{5}$$

Substituting (5) and (2) in (1) yields

$$\frac{\partial^2\xi}{\partial t^2}+\frac{4\pi ne^2}{m}\xi=\frac{kT}{m}\frac{\partial^2\xi}{\partial x^2}. \tag{6}$$

A more general equation can be derived from Maxwell's equations, and a force equation similar to (1), wherein $\partial p/\partial x$ is replaced by grad p. The procedure is the same as that given by Tonks and Langmuir,[1] except that the term involving pressure is carried through. The resulting equation is the same as (6) if $\partial^2\xi/\partial x^2$ be replaced by $\nabla^2\xi$.

For a plane wave the possible frequencies are given by,

$$f_i=(kT/\lambda_i^2m+ne^2/\pi m)^{\frac{1}{2}}, \tag{7}$$

where the λ_i's are the possible wave-lengths determined by the standing wave systems which may exist. For a given n and T, there is therefore a series of possible frequencies, the lower limit of which is the Tonks-Langmuir frequency $(ne^2/\pi m)^{\frac{1}{2}}$. This series, however, appears experimentally as a single broad band due to the breadth of the individual resonances and the closeness of spacing.

It is assumed that the possible range of wave-lengths lies between a length comparable to the size of the containing vessel, and a length comparable to the Debye distance for the plasma. It will be shown that the experimental data can be fitted by choosing a wave-length within this region.

[1] L. Tonks and I. Langmuir, Phys. Rev. **33**, 195 (1929).

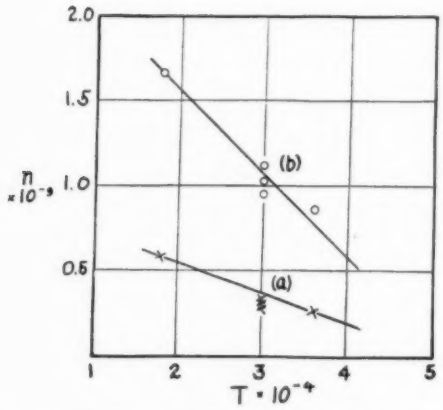

FIG. 1. Showing combinations of n, the number of electrons per cc, and T, the electron gas temperature, which give resonance under applied frequency of 1.6×10^8.

In Fig. 1 are plotted data, some of which were taken from Tonks' paper,[2] and some of which, previously unpublished, were kindly supplied to the writer by him. These represent combinations of n and T, which gave resonance when the plasma was placed between condenser plates to which a fixed frequency (1.6×10^8) was applied. The linear relation is represented by (7) if both sides are squared, and f is regarded as a constant. The two lines, (a) and (b), correspond to two resonances which were observed, but for which there is no explanation. They apparently represent two modes of oscillation, and may be related to plasma shape.[3] It will be noted that there is a very definite effect due to electron temperature, the values of n required for resonance varying by as much as 2 : 1, over the temperature range investigated.

The slopes of these lines should be, according to (7),

$$dn/dT=-\pi k/e^2\lambda^2 \qquad (8)$$

To fit the data it is found that the effective wave-lengths must be $\lambda_a=0.36$ cm, and $\lambda_b=0.22$ cm. The plasma diameters in the two cases were about 1.9 cm and 2.5 cm, respectively. The discharge did not fill the entire cross section of the tube, which was 3 cm in diameter. The Debye distances, $\lambda_D=(kT/4\pi ne^2)^{\frac{1}{2}}$, are 0.064 and 0.038 cm, respectively. It is evident that the necessary λ's lie within the required range in both cases.

The width of the resonance band may be estimated as follows: Assume the small wave-length limit to be given by $\alpha\lambda_D$, where α is a small numerical constant, found by Langmuir[4] to be 3.31. Since $\lambda_D=(kT/4\pi ne^2)^{\frac{1}{2}}$ we may make use of (7) and write the limiting frequency as

$$f_m=\left(\frac{4\pi^2}{\alpha^2}+1\right)^{\frac{1}{2}}\left(\frac{ne^2}{\pi m}\right)^{\frac{1}{2}}=2.14\left(\frac{ne^2}{\pi m}\right)^{\frac{1}{2}}.$$

Hence the maximum frequency is 2.14 times the lowest frequency, giving a band width of about one octave, which is in agreement with experiment.

The contribution of the pressure term to the frequency may be computed by using the above-determined values of λ. It is found that the frequencies predicted for the (a) and (b) resonances are 50 percent and 45 percent greater, respectively, for a given electron density, than when pressure is not considered. The available data do not permit a decisive check of this because of the unexplained fact that several resonances are observed. The agreement is better with the (a) type but worse with the (b).

It should be noted that Eq. (8) for the slope is independent of any constant factor multiplying f in (7), for example, to correct for plasma configuration as was done by Tonks.[2] The expression for slope would be unchanged by any such factor.

[2] L. Tonks, Phys. Rev. **37**, 1458 (1931).
[3] L. Tonks, Phys. Rev. **38**, 1219 (1931).
[4] I. Langmuir, Proc. Nat. Acad. Sci. **14**, 633 (1928).

An Interpretation of Page's "New Relativity"

H. P. ROBERTSON, *Princeton University*

(Received March 4, 1936)

Page's proposed extension of the theory of relativity is examined from the standpoint of the general kinematical theory developed by the present author, of which it is found to be a special case. The contention that this extension renders Einstein's theory untenable would seem to be without real foundation; for although such an attempt to treat of observers in motions other than those contemplated in the special theory of relativity must lead to a theory transcending this latter, Page's theory is shown to be readily understandable in terms of a simple, though somewhat artificial, space time of a type met in the general theory of relativity.

IN a recent issue of this *Review* L. Page[1] has developed a relativistic kinematics suitable for observers suffering constant relative accelerations, and has announced his intention of setting up a corresponding theory of the electromagnetic field. We here examine this program, in the light of previous related work, in order to determine whether or to what extent its results are incompatible with the existing relativistic theories. As a result of this examination we are led to the conclusion that Page's kinematics is included as a special case in the general kinematical theory formulated some months ago by the present author[2] for a different purpose, and that as such, although outside the frame of the special theory of relativity, it may readily be understood from the standpoint of the general theory. It is further pointed out that an electrodynamical theory, based on transformations of the kind employed by Page, has been developed by H. Bateman[3] and by E. Cunningham.[4] For the sake of conciseness and completeness the terminology of the theory of groups is at times invoked, but it is to be emphasized that all results are obtained by a straight-forward analysis, for an understanding of which a knowledge of the theory of groups is not required.

1. KINEMATICAL PRELIMINARIES

We begin, then, with a brief statement of the results of our kinematical analysis, referred to above,[2] which will be of service in the following. It is there assumed that, for the purposes in mind, the space-time region in question admits a three-parameter family of possible equivalent observers, in the sense that through each event there passes the world-line of one (and in general only one) such observer A, and that his view of the development of the whole, as obtained with the aid of a proper clock, light signals and a theodolite, is intrinsically indistinguishable from that of any other observer A′ in the family. It is then shown that under these conditions A can define operationally a set of coordinates $\eta^\mu \equiv (\tau\eta\theta\psi)$, and can introduce a Riemannian metric

$$\begin{aligned} ds^2 &\equiv d\tau^2 - \xi^2(\tau)du^2, \\ du^2 &\equiv d\eta^2 + \sigma^2(\eta)[d\theta^2 + \sin^2\theta d\psi^2], \end{aligned} \tag{1.1}$$

in which

$$\sigma(\eta) \equiv \sinh\eta, \quad \eta \quad \text{or} \quad \sin\eta \tag{1.2}$$

according as the Riemannian curvature k of the auxiliary three-space with metric du^2 is -1, 0 or $+1$, respectively; the function $\xi(\tau) \geq 0$ characterizes the type of relative motion between any two equivalent observers of the family, and is so far arbitrary. This metric ds^2 possesses the important properties:

(a) The world-line of each of the fundamental particle-observers A′ is a geodesic $\eta^\alpha = \text{const.}$ ($\alpha = 1, 2, 3$) of ds^2, along which the interval s measures the clock time τ of A′.

(b) The world-lines of all light paths are the null-geodesics of the metric.

The coordinates η^μ of any event E in the region are determined operationally by A as follows. Let t_1 be the time at which A must send out a light signal in order that it pass through

[1] Page, Phys. Rev. **49**, 254 (1936).
[2] Robertson, Astrophys. J. **82**, 284 (1935).
[3] Bateman, Proc. Lond. Math. Soc. **7**, 70 (1908); **8**, 223 (1909).
[4] Cunningham, Proc. Lond. Math. Soc. **8**, 77 (1909). It is of interest to note that this paper bears the title "The Principle of Relativity in Electrodynamics and an Extension Thereof."

E, and let t_2 be the time at which a signal sent out from E reaches the world-line of A. Then the coordinates τ, η assigned the event E by A are obtained from his clock readings t_1, t_2 by means of the equations

$$2F(\tau)=F(t_2)+F(t_1), \qquad 2\eta=F(t_2)-F(t_1), \quad (1.3)$$

where $$F(\tau)\equiv\int d\tau/\xi(\tau) \quad (1.4)$$

is any primitive of $1/\xi(\tau)$. The angles θ and ψ are those made by the direction of either light signal with the zenith and meridian, respectively, of A's theodolite. The transformation $\eta^\mu\rightarrow\eta'^\mu$ from the coordinates employed by A to those employed by any other fundamental observer A′ is given by $\tau'=\tau$ and a transformation $\eta^\alpha\rightarrow\eta'^\alpha$ of the spatial coordinates which leaves du^2, and therefore ds^2, invariant in form as well as in fact; that this latter transformation is a member of a *six*-parameter group G_6 of motions is accounted for by the fact that each of the ∞^3 particle-observers may orient his theodolite in any one of ∞^3 ways. For the case $k=0$, of greatest interest for our present purposes, this group G_6 is the group of Euclidean motions, consisting of the three-parameter group T_3 of Euclidean translations and the group R_3 of rotations; we may then for most purposes ignore the latter, and confine ourselves to the group T_3 of translations between observers with similarly oriented theodolites.

2. Constancy of Light Velocity

The kinematical theory given in résumé above is clearly the general solution of the equivalence problem stated by Page in Part 1 of his paper. However he, following E. A. Milne, would have the theory expressed in terms of a time t and a distance r assigned to the event E *as in the special theory of relativity*, i.e. he would replace our τ, η or t_1, t_2 by their expressions in terms of the variables

$$t\equiv\tfrac{1}{2}(t_1+t_2), \qquad r\equiv\tfrac{1}{2}c(t_2-t_1). \quad (2.1)$$

This in itself is of course no restriction on the generality of the solution, although it leads to the more cumbersome expression

$$ds^2=[\xi^2(\tau)/\xi(t_1)\xi(t_2)]\{dt^2 - [dr^2+R^2(d\theta^2+\sin^2\theta\, d\psi^2)]/c^2\} \quad (2.2)$$

for the line element (1.1), where

$$R^2(t,r)\equiv c^2\xi(t_1)\xi(t_2)\sigma^2(\eta) \quad (2.3)$$

and τ, η, t_1, t_2 are to be expressed in terms of t, r with the aid of (1.3), (2.1).

Now the path of any light signal which intersects the world-line of A is given by

$$r=\pm c(t-t_0), \qquad \theta=\text{const.}, \qquad \psi=\text{const.},$$

and may therefore be interpreted as a radial straight in the Euclidean (xyz)-map constructed from the Cartesian coordinates (xyz) obtained from the polar coordinates $(r\theta\psi)$ in the usual way; hence any light signal sent by A or received directly by A is propagated rectilinearly in the (xyz)-map with the constant *coordinate* velocity $dr/dt=\pm c$. However, it is readily seen from (2.2) that other light paths do not in general possess this property, and that to follow Milne and Page in requiring that they do, places a severe restriction on the function $\xi(\tau)$ characterizing the relative motions of the fundamental particle-observers. We remark in passing that this result in no way contradicts that obtained in section 3 of the paper referred to above,[2] where it is shown that, at least in the open models $k=-1, 0$, coordinates $(TXYZ)$ may always be introduced in which light is propagated rectilinearly with constant coordinate velocity c; these latter are defined in quite another way than the $(txyz)$ here employed, and are such that the transformations from one particle-observer to another constitute a six-parameter subgroup of the general Lorentz group.

In order to interpret Page's work in terms of the kinematics outlined above, we must first investigate the restriction imposed by his requirement that *all* light signals, and not only those which A is in position to observe directly, are propagated rectilinearly with constant coordinate velocity c in the Euclidean map constructed from the coordinates (xyz). It is seen immediately from (2.2) that, in order for all null elements $ds=0$ to be null elements in the Minkowskian $(txyz)$-map, the function $R(t,r)$ defined by (2.3) must be identically equal to r; that this condition is also sufficient follows from the fact that the null geodesics of a conformally-flat manifold are at the same time null geodesics of the associated flat. On replacing $\xi(\tau)$ by its

value $1/F'(\tau)$ in terms of the derivative F' of F, the condition $R \equiv r$ yields the differential equations

$$F'(a)F'(\tau)(\tau-a)^2=\{2\sigma[(F(\tau)-F(a))/2]\}^2 \quad (2.4)$$

for $F(\tau)$, where we have expressed all variables in terms of t_1, t_2 and have then set $t_1=a$, $t=\tau$. The solution $F(\tau)$ is given, to within an additive constant, by a quadrature, and the corresponding forms of $\xi(\tau)$ by differentiation. The results of this computation may be expressed in terms of the general linear fractional function

$$f(\tau)\equiv(A\tau+B)/(C\tau+D),\ \Delta\equiv AD-BC>0, \quad (2.5)$$

in the various cases k as follows:

$$F=f, \qquad \xi=(C\tau+D)^2/\Delta, \qquad (k=0); \quad (2.6)$$

$$F=\log f, \qquad \xi=(A\tau+B)(C\tau+D)/\Delta, \qquad (k=-1); \quad (2.6')$$

$$F=2\tan^{-1} f,$$

$$\xi=[(A\tau+B)^2+(C\tau+D)^2]/2\Delta, \ (k=+1). \quad (2.6'')$$

Now in a certain sense

$$\lambda\equiv c\xi(\tau)\sigma(u) \quad (2.7)$$

may be considered as a significant measure of the "distance" at "time" τ between two particle-observers with the fixed u-interval u, and we define

$$v\equiv d\lambda/d\tau, \qquad \alpha\equiv d^2\lambda/d\tau^2, \quad (2.8)$$

as the corresponding measures of the relative "velocity" and "acceleration," respectively. It now follows from the results of the preceding paragraph that the requirement of constant coordinate-velocity of light in the (xyz)-map implies that *the relative motion of any two fundamental particle-observers must be such that their relative α-acceleration is constant.*

An examination of the three sets of equations (2.6) shows that the only case in which the relative velocity v can be zero for all τ is that in which $k=0$, $C=0$; we then have

$$\xi=D/A; \qquad t=\tau, \qquad r=Dc\eta/A, \quad (2.9)$$

and the original line element (1.1) is itself Minkowskian on change of spatial scale. The only other case in which the acceleration α vanishes throughout the motion is that in which $k=-1$, $C=0$, whence

$$\xi=\tau; \qquad t=\tau\cosh\eta, \qquad r=c\tau\sinh\eta, \quad (2.10)$$

and the new line element (2.2) is the Minkowskian form on which the special theory of relativity is based; the original metric (1.1) is in this case the "polar" form implied in the work of Milne.

Finally, to come to the case adopted by Page, we note that he requires (pp. 260, 263) that the relative motion of two particle-observers be such that at some instant they coincide spatially and are then momentarily at relative rest. The first of these conditions allows us to reject the case (2.6''), for in it the distance function $\xi(\tau)$ has only complex roots; the second condition then throws out the hyperbolic case (2.6'), in which the two roots of $\xi(\tau)$ are real but distinct. Thus we find, as *the only case in which two particle-observers are at some time momentarily in coincidence and at relative rest*, the parabolic case (2.6), in which $\xi(\tau)$ has a double root and the spaces $\tau=$const. are Euclidean. The remainder of our investigation will be devoted to a discussion of this case.

3. Transformation Theory

On taking as the origin of τ that event at which all ∞^3 particle-observers momentarily coincide, the invariant metric (1.1) defined by (2.6) may be written

$$ds^2=d\tau^2-(\varphi\tau^2/2c)^2[d\eta_1^2+d\eta_2^2+d\eta_3^2], \quad (3.1)$$

where the η_a $(a=1, 2, 3)$ are the Cartesian coordinates associated with the polar coordinates $(\eta\theta\psi)$ in the usual way, and φ is the (constant) acceleration between two particle-observers whose (constant) u-distance is unity. Our first task is that of discovering the transformation $(\tau\eta_a)\rightarrow(tx_a)$ which throws (3.1) into the conformally-Minkowskian form (2.2), where the x_a are the Cartesian coordinates associated with $(r\theta\psi)$. We may now take

$$F(\tau)=-2c/\varphi\tau, \quad (3.2)$$

and the Eqs. (1.3), (2.1) yield as the required transformation

$$\tau=(t^2-r^2/c^2)/t, \qquad \eta_a=2x_a/(t^2-r^2/c^2)\varphi; \quad (3.3)$$

the form (2.2) of the metric is then found to be

$$ds^2=(\tau/t)^2[dt^2-(dx_1^2+dx_2^2+dx_3^2)/c^2]. \quad (3.4)$$

The transformation (3.3) has merely the effect of allowing the given observer A at $\eta=0$ to introduce a new coordinate mesh, of the kind demanded by Page, in which A is at the origin $r=0$ of the new spatial coordinates x_a, and in which the new temporal variable t is also a direct measure of proper-time along his world-line. In order to find the relations between the coordinates (tx_a) employed by A and the coordinates $(t'x_a')$ similarly introduced by another particle-observer A' at $\eta_a=\beta_a$, we must consider the group of motions admitted by the metric (3.1); as indicated above, we may here confine ourselves to the subgroup T_3 of translations between observers with similarly oriented theodolites. Hence the transformation A→A' is given by

$$\tau'=\tau, \qquad \eta_a'=\eta_a-\beta_a, \tag{3.5}$$

and the transformation which it induces on the corresponding Minkowskian coordinates is defined implicitly by

$$\begin{aligned}(t'^2-r'^2/c^2)/t'&=(t^2-r^2/c^2)/t\ (=\tau)\\ x_a'/t'&=x_a/t-\varphi\tau\beta_a/2.\end{aligned} \tag{3.6}$$

Now this transformation must leave (3.4) invariant in form as well as in fact, and it must therefore be a member of the general conformal group in four dimensions; hence it must be compounded of at most dilatations, translations, rotations (including reflections), and inversions. The explicit form, as found directly from (3.6), is

$$\begin{aligned}t'&=b^2t/R^2,\\ x_a'-b_a&=b^2[x_a-(1+2\Sigma b_ex_e/b^2)b_a]/R^2,\end{aligned} \tag{3.7}$$

where

$$\begin{aligned}&R^2(tx_a;b_a)\equiv\Sigma(x_a+b_a)^2-c^2t^2,\\ &b_a\equiv 2c^2\beta_a/\beta^2\varphi, \qquad \beta^2\equiv\Sigma\beta_a^2, \qquad b^2\equiv\Sigma b_a^2;\end{aligned} \tag{3.8}$$

this transformation may in fact be broken down into the reflection

$$\bar{x}_a=x_a-2(1+\Sigma b_ex_e/b^2)b_a \tag{3.9}$$

in the plane through $x_a=-b_a$ orthogonal to the vector b_a, followed by the space-time inversion

$$t'=b^2t/R^2, \qquad x_a'-b_a=b^2(\bar{x}_a+b_a)/R^2 \tag{3.10}$$

in the pseudo-sphere

$$R^2(t\bar{x}_a;b_a)\equiv R^2(tx_a;b_a)=b^2 \tag{3.11}$$

of radius b and center at the event $(0,-b_a)$. Thus the group I_3 induced by T_3 is that subgroup of the general conformal group which consists of the ∞^3 transformations $t(b_a)$ of the form (3.7), and which possesses the differential invariant (3.4); the law of composition of this (Abelian) group I_3 is given by

$$t(b_a)t(c_a)=t(b_a+c_a). \tag{3.12}$$

That (3.7) is indeed the explicit form of the transformation derived by Page can be seen by comparing it with his Eqs. (46), (47), (68), on going over to the variables there employed. The particle-observer A' at $x_a'=0$ moves radially away from A in the direction of the vector b_a with a coordinate-velocity v which satisfies the equation

$$v(1-v^2/c^2)^{-\frac{1}{2}}=\beta\varphi t, \tag{3.13}$$

as can be found directly from (3.7); hence the t rate of change of the left-hand side of (3.13), which Page calls the "relativity acceleration" of A' relative to A, is the constant $\beta\varphi$—and is the same as their relative α-acceleration, as defined by (2.8). The geometrical theorems derived by Page in Part 4 of his paper are consequences of general theorems on inversions, as applied to the spatial inversion defined by (3.10) at time $t=t'=0$.

We also see, in retrospect, that the transformation $(\tau\eta_a)\rightarrow(tx_a)$, defined by (3.3) for a given observer A, is itself interpretable as an inversion of the variables

$$b_0^2/c^2\tau, \qquad b_0\eta_a \qquad (b_0\equiv 2c^2/\varphi)$$

in the pseudo-sphere of imaginary "radius" ib_0 about the origin.

Our approach has been based on the existence of an invariant interval ds^2 which satisfies the conditions (a), (b) stated in section 1 above, and which therefore offers an invariantive description of the only elements so far involved in the theory—namely, the equivalent particle-observers, their proper clocks and theodolites, and all light signals. In the light of this, and considering the rather arbitrary definition of t and r, it is difficult to see why Page's "physical interval" $c^2dt^2-dx^2$ should be expected to appear as an invariant. It is to be noted, in this connection, that the *content* of Page's Eq. (32) is equivalent to the fact that our ds^2 is invariant in the two-dimensional case $\theta=$ const., $\psi=$ const.; his expressions (31), (32) are not, however,

invariants of the transformation $(tr)\rightarrow(t'r')$ in the technical sense, for they depend on the parameter φ of the transformation. On the other hand, the differential expression (69) which he writes down for the full four-dimensional case is not at all equivalent to our differential invariant (3.4); even if it be modified by the same treatment as that accorded (32) in bringing it into invariant form, it could at best be expected to be invariant under a one-parameter subgroup of I_3, and not under the full group.

4. Associated Particle-Observers

It remains to clarify the role of the ∞^3 possible particle-observers which Page associates with each given particle-observer A of the type dealt with above. These auxiliary observers have as their world-lines the curves $x_a=$const.; in order to avoid confusion with the primary particle-observer A we shall refer to the former as test-particles. Computation shows that the world-lines $x_a=$const. are not geodesics of the metric ds^2, unless $x_a=0$—hence, in Page's terminology, the reference systems employed by two observers A and A′, while *equivalent*, are not *homogeneous*. Now we have examined,[5] in connection with the general kinematical theory described in section 1 above, the possible modes of motion of such a six-parameter family of test particles in a space time possessing the uniformity properties here implied, and have found that they must satisfy differential equations of the form

$$\frac{d^2\eta^\mu}{ds^2}+\left\{\begin{matrix}\mu\\ \nu\sigma\end{matrix}\right\}\frac{d\eta^\nu}{ds}\frac{d\eta^\sigma}{ds}=\Gamma\left(\tau,\frac{d\tau}{ds}\right)\left[\delta_0^\mu-\frac{d\tau}{ds}\frac{d\eta^\mu}{ds}\right], \quad (4.1)$$

where $\eta^0\equiv\tau$, the Christoffel symbols are computed from the coefficients $g_{\mu\nu}$ of (1.1), and Γ is some function of at most τ and $d\tau/ds$. On evaluating these expressions for the metric (3.1) and taking η^a as defined by (3.3), in which the x_a are constants, these equations of motion reduce to

$$dt/ds=t/\tau, \qquad (\Gamma+1/\tau)x_a d\tau/ds=0; \quad (4.2)$$

hence the ∞^3 world-lines $x_a=$const. associated with *each* of the particle-observers A are solutions of (4.1) provided we set

$$\Gamma(\tau, d\tau/ds)\equiv -1/\tau. \quad (4.3)$$

These results allow us to conclude, in accordance with the general theory developed in section 5 of the paper cited above,[5] that the ∞^6 solutions of (4.1) fall into classes characterized by a parameter $d\geq 0$. The class $d=0$ consists of the ∞^3 world-lines of the fundamental particle-observers, the class $d=\infty$ of the ∞^5 light paths in space time, and each class $d(\neq 0, \infty)$ of the ∞^5 test particles which are at the fixed x distance d from the particle-observer with which each of them is associated. Further, the motion of each member of such a class d is such that its λ distance, as defined by (2.7), from the observer A with which it is associated, approaches asymptotically the value d.

Finally, these considerations unearth a surprising formal connection between Page's work and the transformation theory of the de Sitter universe in the general theory of relativity. To exhibit this connection, we first note that in any case in which Γ is a function of τ alone, the equations (4.1) may be interpreted as the equations of the ∞^6 geodesics of the metric

$$dS^2\equiv e^{2\int\Gamma d\tau}ds^2 \quad (4.4)$$

conformal to the original metric (1.1). For the case (3.4) of interest here, this new metric may, on subjecting t to the transformation

$$t\equiv(b_0/c)e^{cz/b_0}, \qquad (b_0\equiv 2c^2/\varphi) \quad (4.5)$$

be taken in the form

$$dS^2=dz^2-e^{-2cz/b_0}(dx_1^2+dx_2^2+dx_3^2). \quad (4.6)$$

This invariant metric satisfies the conditions (a) and (b) of section 1 above, except that it is no longer a direct measure of clock time along the geodesic paths of the fundamental particle-observers. It is, on the other hand, *the stationary form of a contracting de Sitter universe* of constant Riemannian curvature $-c^2/b_0^2$; the relation between a particle-observer A and an associated test particle $x_a=$const. in the space time (3.4) of interest here is, to within the time transformation (4.5) above, formally the same as that between two associated free observers in the de Sitter universe (4.6), and the relation between

[5] Robertson, Astrophys. J. **83**, 187 (1936); in particular, sections 4 and 5.

[6] Cf. the discussion of the de Sitter universe by the present author in Phil. Mag. **5**, 835 (1928). Eq. (11) of this discussion are in fact equivalent to those defining Page's transformation (68) between equivalent particle-observers.

two equivalent observers A, A′ here is formally the same as that between two free observers in general relative motion in the de Sitter universe.[6]

5. Summary and Conclusion

This examination of Page's work, from the standpoint of our general kinematics, has shown that it deals with one of the three possible cases in which there exists a set of ∞^3 equivalent particle-observers with respect to whom light is propagated rectilinearly with a constant coordinate velocity c in a coordinate system (tx_a) defined as in the special theory of relativity. In each of these cases there exists a significant Riemannian metric, of the type employed in the cosmological applications of the general theory of relativity, which is invariant under the group G_6 of motions which describe the equivalence; it is apparent *a priori* that this group is a six-parameter subgroup of the general conformally-Minkowskian group of transformations on the variables (tx_a), and that it is the direct product of the group R_3 of Euclidean rotations on the spatial variables x_a and a three-parameter group I_3 which has as its minimal invariant varieties the spaces $\tau=\text{const}$. We have in particular examined this group I_3 in the case adopted by Page, and have shown how it may be generated from translations, reflections and simple inversions.

The three cases thus found are characterized by the fact that in them the fundamental particle-observers undergo a constant relative α-acceleration, which in Page's case agrees with the t rate of change of the "relativistic" velocity defined by the left-hand side of (3.13); we must regard this agreement as a happy coincidence, however, for it is difficult to see what significance is to be attributed to Page's procedure outside the special relativistic theory of electrodynamics, where it leads to the usual classical expression for the ponderomotive force (and not to the relativistic four-vector by which it should even there be replaced). It would seem that, insofar as the present line of attack is concerned, this leaves little justification for Page's "hope of finding a rational detailed description of atomic structure" by an investigation of "equivalent reference systems having other types of motion [than with constant acceleration], particularly relative rotation"; indeed, it has long since been pointed out by E. Cunningham[7] that "no such relation [as that defined by the conformal group] can express anything corresponding to a rotational motion of the space-frame of reference." It would further seem, particularly in view of the severe restrictions which their introduction implies, that the quasi-Minkowskian coordinates $(txyz)$ are of no very great intrinsic significance, although possibly of convenience for some purposes. But, above all, it is to be remembered that we are here on the *kinematical* level of description, and that the question of whether or not two observers are *dynamically* equivalent can be decided only in terms of the more complete physical theory of which the kinematics is but a noncommittal tool; thus, while we are willing to entertain the view that a general kinematical theory such as that outlined in section 1 above may play a useful role in comological speculations, we should not be disposed to attempt to reconcile it with the obvious dynamical inequivalence of observers in general relative motions in terrestial or atomic problems. Otherwise stated, either these more general types do represent possible motions of dynamically equivalent observers, in which case we should expect to have recourse to methods and concepts of the type met in the general theory of relativity, or their dynamical inequivalence should be expected to set serious limitations to the usefulness of the kinematics.

Insofar as electrodynamics is concerned, we confine ourselves to the remark that the problem of transforming the electromagnetic field under the general conformal group has been given a detailed solution by Bateman and by Cunningham in the papers cited above[3,4]; we do not here go into the question of whether or to what extent their theory is equivalent to the phenomenological theory of electrodynamics based on the line element (3.4) as in the general theory of relativity.

Finally, I should like to thank Princeton University for granting me sabbatical leave during the present academic year, and to express my appreciation to the California Institute of Technology for the facilities for work which it has placed at my disposal during this time.

[7] Cunningham, *The Principle of Relativity* (Cambridge, 1914), p. 89. Cf. also p. 79 of reference 4 above.

The Design, Operation, and Performance of the Round Hill Electrostatic Generator

L. C. Van Atta, D. L. Northrup, C. M. Van Atta* and R. J. Van de Graaff, *Massachusetts Institute of Technology*
(Received March 25, 1936)

The design, technique of operation, and performance of the Round Hill electrostatic generator are presented in some detail. The problems of operating wide paper belts, of eliminating vibration, and of controlling humidity are discussed. The original belt charging system, with the belts operated at saturation charge density, is described and its range of usefulness is indicated. A consideration of the problems of voltage control and voltage steadiness at reduced charging currents leads to two modified designs of the belt charging system. The measurement of voltage by means of the generating voltmeter is discussed with special emphasis on the precautions necessary to eliminate or to correct for sources of systematic error. Under the conditions realizable with the Round Hill generator the probable error in voltage measurements is less than one percent on a relative scale and about two percent on an absolute scale. The magnitude of voltage fluctuations is less than 0.1 percent. The generator performance data for the positive and negative terminals are given in graphical form. The maximum charging current is 2.1 ma and is practically independent of voltage. The highest voltage obtained consistently without sparking is 2.4 megavolts positive and 2.7 megavolts negative, giving 5.1 megavolts between the terminals. At this voltage there is 1.1 ma of current available for application to an accelerating tube.

IN 1933, there appeared a general discussion[1] of the principles involved in the electrostatic production of high voltage by means of belt generators operating at atmospheric pressure. There was included a brief description of the external structure of the Round Hill electrostatic generator. During the intervening period a belt-charging system has been designed, constructed, and improved, so that a very steady, controllable voltage is now available for nuclear research. Complete generator performance data have been obtained through the utilization of the generating voltmeter which, with proper precautions, has proved to be a convenient and reliable instrument for voltage measurement.

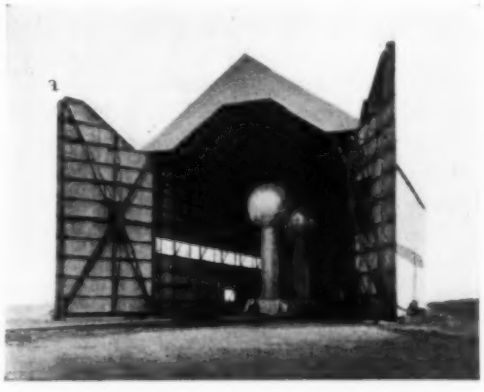

FIG. 1. Electrostatic generator and housing.

External Structure

The generator structure consists essentially of two spherical terminals supported by cylindrical insulating columns on steel trucks. The spheres are made of aluminum alloy 15 feet in diameter with walls $\frac{1}{4}$ inch thick. The insulating columns are cylinders of Textolite 22 feet in length of free insulation, 6 feet in diameter, and of $\frac{5}{8}$ inch wall thickness. The steel trucks act as heavy bases for the generator units and house the driving and accessory equipment. An electrically-driven winch, with an endless cable passing under the trucks, is used to transport the generator units along a 14-foot gauge railroad track. As shown in Fig. 1, a steel building 140 feet long, 75 feet wide, and 75 feet high houses the generator and the laboratory and shop rooms. Structural girders supporting the roof limit the unobstructed ceiling height to 60 feet. Further details relating to the external structure have been given previously.[1]

Belts and Pulleys

In each generator unit electrical charge is conveyed to the spherical terminal by means of two simple belts running inside the supporting

* National Research Fellow, July, 1933 to March, 1935.
[1] R. J. Van de Graaff, K. T. Compton and L. C. Van Atta, Phys. Rev. **43**, 149 (1933).

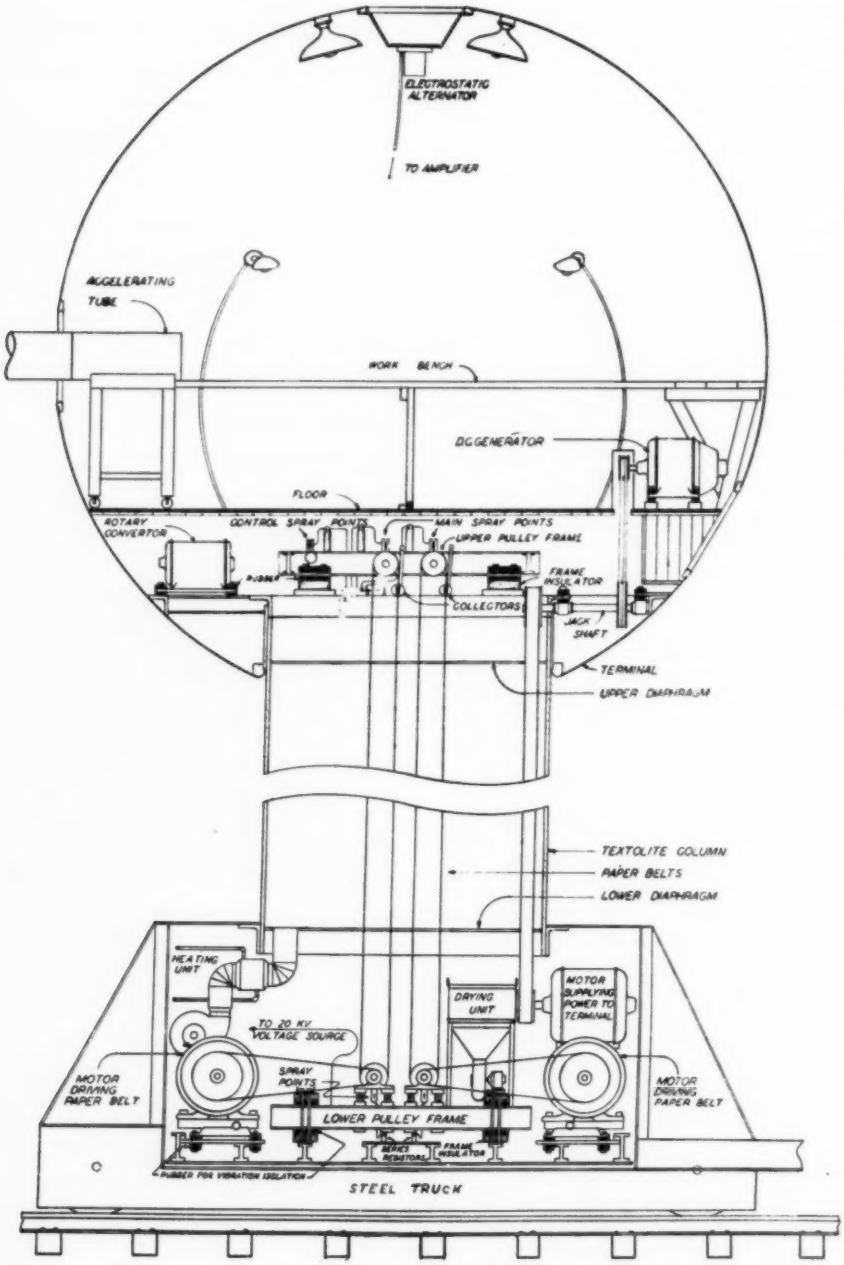

FIG. 2. Sectionalized view of the interior of one generator unit showing the belt-charging system and auxiliary equipment in terminal and truck.

column as shown in Fig. 2. The belt material is electrical insulation paper[2] 0.017 inch thick and 47 inches wide. This material satisfies very well the electrical and mechanical requirements and has the advantage of being inexpensive as compared with silk or rubberized fabric. The seams are made on a 45-degree bias for greater strength and smoother operation. The edges to be joined are tapered to bring all laminations of the paper into the joint and to preserve a uniform belt thickness. A celluloid-base belt cement[3] is used for the joints instead of glue because of its superior electrical properties and its flexibility at low humidity.

Proper initial conditioning is essential to the successful operation of such a wide paper belt. After being mounted between pulleys in the generator column the belt first undergoes a two-day period of stretching under a tension of about 1000 pounds between pulleys at a relative humidity greater than 75 percent. The belt is then dried over a period of about three days while the humidity is gradually reduced to approximately 25 percent. The belt lengthens by about 0.3 percent of its length during the stretching period and contracts by about 0.2 percent upon drying. The pulley is not allowed to turn until the belt is dry since a damp belt tends to crease as it runs over the pulley.

The belts are carried on steel pulleys 6 inches in diameter and 50 inches long, the lower pair acting as drivers and the upper pair as idlers. The pulleys are of seamless steel tubing having chrome-vanadium forged end plugs which extend with reduced diameter to provide substantial shafts. Self-aligning ball bearings are shrunk onto the shafts and are housed in solid pillow-blocks. One shaft of each of the lower pulleys extends through the bearing for a belt drive to a 10 hp induction motor. An endless rubberized fabric flat belt and a constant-tension motor base[4] are employed to obtain a quiet and efficient drive. Each pair of pulleys is mounted on a heavy square frame of channel iron so that the pulleys and frame can be isolated as a unit, mechanically and electrically.

[2] John A. Manning Paper Co., Troy, N. Y.
[3] Sea Lion Waterproof Belt Cement, Chicago Belting Co., 113 North Green Street, Chicago, Ill.
[4] The Rockwood Mfg. Co., Indianapolis, Ind.

Because of the small stretch in dry paper belts, the pulleys require little crowning. The crowning actually employed is $\frac{1}{32}$ inch in the 6 inches diameter, applied as a uniform taper on the last 4 inches of pulley at each end. Since the pulley is 3 inches wider than the belt only part of this crowning is effective when the belt is centered. The pillow-blocks of each lower pulley are mounted on heavy threaded studs in the supporting frame to provide a sensitive means for adjusting the level of the pulley, since the centering of the belt, as well as its tension, depends critically upon this adjustment.

Two pulley speeds are provided, 3600 r.p.m. and 2880 r.p.m., corresponding to belt speeds of 5650 f.p.m. and 4520 f.p.m. At the higher speed the two belts enter the sphere at the rate of 44,200 sq. ft. per minute. The windage loss per belt is approximately 4 kw at the higher speed and 2 kw at the lower speed. The no-load power consumed by both units of the generator in operation at the higher belt speed is then 16 kw, while the full-load power consumed is 26 kw.

Vibration Isolation

Because of the necessity of using sensitive measuring instruments in the terminal, mechanical vibration and noise must be reduced to a minimum. This has been accomplished by mechanically isolating all moving parts, as indicated in Fig. 2, and by absorbing inside the terminal such noise as is transmitted to it. In addition the heavy pulleys for the paper belts were dynamically balanced until the amplitude of their vibration when rotating at 3600 r.p.m. in free support was less than 0.002 inch.

For isolating the upper and lower pulley frames and all the heavy machinery a soft rubber[5] was used. In the case of lighter equipment and machinery a sponge rubber[5] proved more satisfactory. In addition, all the equipment within the truck is mounted on a heavy false floor, which is supported at the corners on soft rubber. In all cases a one-inch thickness of rubber was used with the proper area to obtain a ten percent deformation in the rubber under the isolated load. The maximum load per square inch is about 100 lbs. for the soft rubber and 10 lbs. for the

[5] United States Rubber Co., Passaic, N. J.

sponge rubber. Because of the marked improvement in quietness of operation gained by such efforts, vibration isolation has been extended to include every piece of machinery associated with the generator.

The interiors of the metal terminals would have extremely poor acoustical properties if a large area of sound absorbing material were not provided. This is partly accomplished by a $\frac{5}{16}$-inch sponge rubber flooring. Additional absorbing area may be obtained by "quilting" $\frac{1}{4}$-inch flameproof felt[6] to the metal wall.

Humidity Control

In the case of any high-voltage, low-current generator, insulation requirements are severe. The unusually high average relative humidity and the fact that the hangar is not completely weather-tight, make this problem exceptionally serious at Round Hill. The average relative humidity is approximately 84 percent during the summer months and 74 percent during the winter months. Normally the hangar is about 300 yards from the sea, but during extreme high tides has been entirely surrounded by water.

The space inside the column and truck is carefully enclosed to make humidity control practicable. Both heating and drying are employed to reduce the humidity. The heating system consists of an automatically operated kerosene water heater mounted on the outside of the truck, a water circulation system which includes a gear pump, an automobile radiator inside the truck, and a blower for circulating the air of the truck through the radiator and into the column. A heater output equivalent to 4 kw is sufficient to maintain the truck and column 10°C above the surroundings, but ten kilowatts are available for emergency use.

The drying system consists of three trays each containing 30 pounds of Silica Gel.[7] Two trays are mounted over small blowers in the truck. The third tray is reactivated outside the truck over a combination blower and heater which circulates air at 160°C through the tray. The trays in the truck are replaced alternately at 12-hour intervals. Water is removed from the air at the average rate of one-quarter pound per hour.

The combined heating and drying systems described above and indicated in Fig. 2, maintain the inside humidity below 35 percent with an outside humidity of 100 percent. Experience has shown that this renders the maximum working voltage of the generator independent of weather conditions.

The resistance of the Textolite column supporting each of the terminals has been maintained above 10^{10} ohms by coating the outer surface with ceresin wax and by keeping the interior of the column warm and dry. The insulation requirements for the charging belts are especially stringent because of the high gradients imposed upon them in the region of the charging mechanism and at the entrance to the high voltage terminal. For this reason the belts are of electrical insulation paper and are maintained thoroughly dry.

Power Supply in the Terminals

Both a.c. and d.c. power are supplied to the laboratories in the high voltage terminals. For reasons of economy, 6 kw of d.c. power are initially developed to care for the major heating and lighting demands, while a 1 kw inverted rotary converter supplies a.c. where this is essential. The long vertical drive from a motor in the truck to the d.c. generator in the terminal was accomplished, as shown in Fig. 2, by the use of a large-diameter, flanged paper pulley at the top, a rubberized fabric endless belt, and a motor base[4]

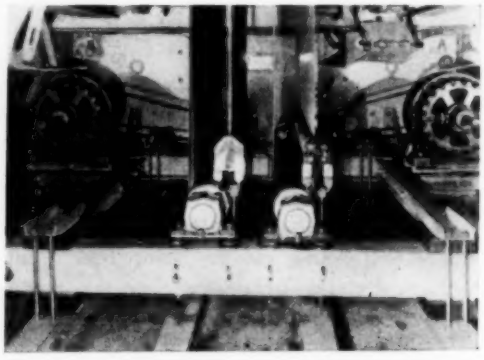

FIG. 3. View of the interior of one of the generator trucks showing the lower pulley frame.

[6] Merchandise No. 3565, American Felt Co., 211 Congress St., Boston, Mass.

[7] Silica Gel Corporation, Baltimore, Md.

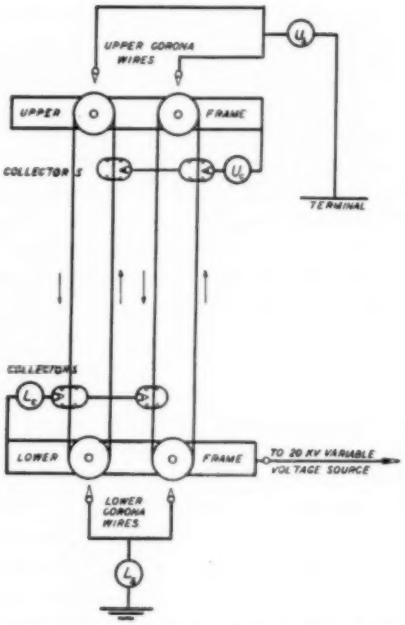

FIG. 4. Schematic diagram of the original belt-charging system.

designed to maintain constant tension on the belt.

From a centralized power panel in each terminal, the a.c. voltage and frequency and the d.c. voltage can be controlled and measured. Convenience outlets make these voltages available at the work benches.

ORIGINAL BELT-CHARGING SYSTEM

The original belt-charging system employed for this generator, shown schematically in Fig. 4, is equivalent in principle to that indicated in Figs. 2 and 3 of a former publication.[1] The structural frames carrying the upper and lower pulley systems are insulated from the terminal and truck, respectively. Voltage is applied to the lower pulley system from a filtered 20-kv rectified a.c. voltage source. Whereas there are two charging belts in each generator unit the following discussion can be simplified by considering the system as comprised of only a single belt. The charging current is supplied at each end of the belt by fine wires[8] stretched across the face of the belt at a distance of about $\frac{5}{8}$ inch from the upper and lower pulleys as shown in Fig. 5 and connected, respectively, to the terminal and to ground.

The charge sprayed on the belt by the lower spray wire under the excitation of the frame voltage is removed from the ascending belt inside the terminal by a collector connected to the insulated upper frame. The collector consists of a 0.003-inch wire inside a 3-inch diameter cylindrical shield connected electrically to the wire and slotted for the passage of the belt. The shield around the collector wire is almost essential for reliable operation since the collector current is then independent of the upper frame voltage and dependent only on the charge density on the belt.

As the upper frame voltage increases due to the collector current, corona is produced at the upper spray wire and charge is deposited on the descending belt. The equilibrium voltage of the

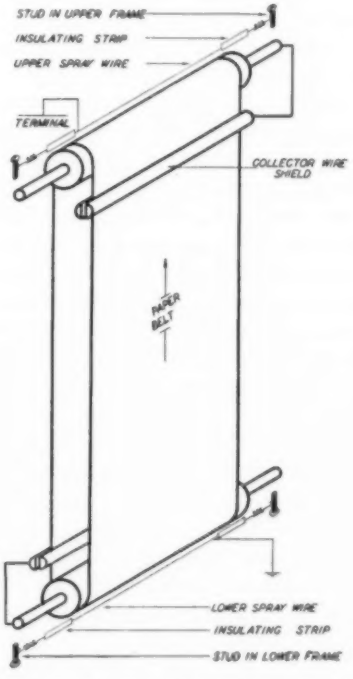

FIG. 5. Isometric drawing of belt showing the location of spray wires and collector shields.

[8] 0.003-inch bright, hard drawn, high carbon steel wire, John A. Roebling's Sons, 107 Liberty St., New York City.

[1] Fine wires as corona sources for belt charging were first used on the Carnegie electrostatic generator at the Department of Terrestrial Magnetism, Washington, D. C.

upper frame is reached when the leakage through the belt of charge deposited by the upper spray wire equals the collector current. In effect, both upper and lower spray wires must neutralize the charge brought to them on the belt before producing a net charge of the opposite sign. Unless the lower wire is spraying more than enough charge to saturate the belt, each spray wire current is approximately equal to the generator charging current delivered by the belt.

The collectors on the lower frame enable the generator to operate by self-excitation due to the priming action of frictional charge produced on the paper belts in running over the pulleys. Because of the air conditioning inside the column, the generator consistently delivers its full current under self-excitation. In fact, when the lower collectors are removed the generator still develops half its full current with negative polarity. However, the self-excitation feature is not particularly useful in the present case because of the desirability of definitely fixing the polarity and of controlling the charging current.

Under normal conditions the system just described is operated with saturation charge density on both ascending and descending belts. This condition is realized by the proper choice of the lower frame voltage and spray wire spacing, and the upper spray wire spacing. The adjustment is not critical since excess charge deposited on the belt discharges to the pulley at the point of departure of the belt from the pulley. This charging system has been used considerably and has proved quite satisfactory so long as the belts are operated at saturation charge density.

Control of Generator Voltage

In order to realize the maximum usefulness of the generator, it is necessary to have a convenient method for precise voltage control over a considerable range of voltage. In many cases it would be feasible to operate the belts at saturation charge density and to obtain voltage control by varying the belt speed or by imposing a controllable corona current drain on the terminal. In the present case it would not be practicable to control the speed of the four 10-hp induction motors. A corona device for limiting the voltage has been tested and found to be fairly satisfactory electrically for controlling the voltage of the positive terminal. It is not satisfactory when used with the negative terminal because of persistent sparking to the corona device and is not convenient to use because of the dimensions of the apparatus and the precision required.

The generator voltage may be controlled most conveniently by varying the charge density on the belts. For a given drain on the terminal the equilibrium voltage assumed by the generator will depend on the charging current. If the current drawn from the terminal is altered the charging current must be correspondingly altered to maintain a constant voltage. This adjustment may be made manually, or may be accomplished automatically by employing the output from a generating voltmeter to control the exciting voltage applied to the lower frame.

To test this method of voltage control the exciting voltage applied to the lower frame was made continuously variable. As the charge density on the belts was reduced below saturation, the charging current and the equilibrium terminal voltage decreased in the expected manner. At reduced charge densities, however, there were present violent fluctuations in the charging current having the period of the belt, 1.6 c.p.s., and an amplitude too large to be tolerated. The typical curve in Fig. 6 shows the variation of charging current with lower frame voltage and the limits of the fluctuations encountered.

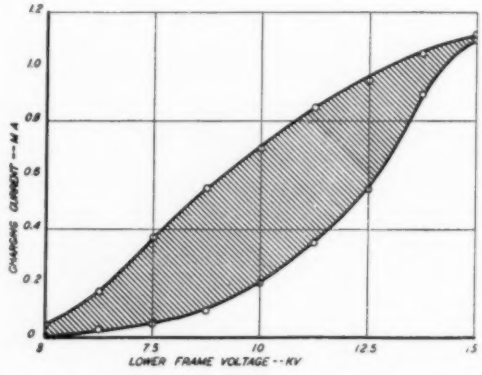

Fig. 6. Limits of the 1.6-c.p.s. current fluctuation encountered with the original belt-charging system at reduced charge densities.

Elimination of Current Fluctuations

Apparently these fluctuations were initiated by the electrical irregularity in the belt at the glue joint and were amplified in effect by the inherent instability of the upper frame voltage. As a first step in the elimination of the current fluctuations, the electrical irregularity in the belt was greatly reduced by making the joint with a celluloid-base cement instead of glue. Then the instability of the upper frame voltage was corrected by a series of alterations in the design of the charging assembly.

The instability of the upper frame voltage was due partly to the shape of the current-voltage characteristic curves of the spray wires. Current-voltage characteristic curves for spray wires at two different spacings from a grounded metal cylinder are shown in Fig. 7a. Two corresponding curves obtained with a spray comb of fine needles are given for comparison. The spray comb consists of a steel ribbon 0.010 inch $\times \frac{1}{2}$ inch with No. 16 beading needles soldered $\frac{3}{8}$ inch apart and extending $\frac{1}{2}$ inch from the edge of the ribbon. Whereas the ideal characteristic curve of a corona device for belt-charging would begin at the origin and rise linearly with voltage, the actual curves are nonlinear and may be expressed quite accurately by empirical relations of the form

$$I = k(V - V_0)^2.$$

From Fig. 7a it appears that combs and larger spacings are to be preferred because of the lower corona threshold voltage of the combs and because of the flatter over-all characteristics obtained with larger spacings. The curves of Fig. 7b show the marked improvement obtained by adding resistance in series with the positive or negative comb. If it were not for other considerations a still flatter characteristic could be obtained by further decreasing the spray gap and increasing the series resistance, i.e., by increasing the ratio of ohmic to non-ohmic resistance in the circuit.

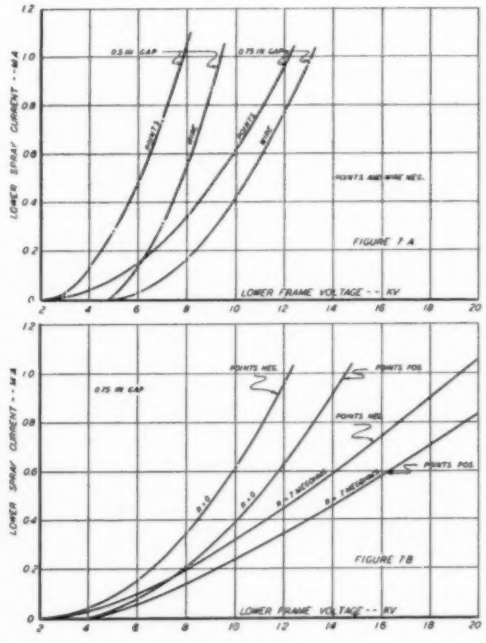

FIG. 7. Current-voltage characteristic curves; a, for negative spray wires and combs with different corona gaps; b, for positive and negative combs with and without series resistance.

Another factor contributing to the instability of the upper frame voltage was the method of limiting that voltage. In this connection the charge density on the ascending and descending sides of the belts should be equal in order to realize maximum current from the belts and to prevent corona loss of unbound charge from the more heavily charged side. That is, the upper frame should be maintained at such a voltage that the current carried away by the descending belts is approximately equal to that delivered by the ascending belts for a wide range of current values. This condition is realized by placing in parallel with the belt spray combs a voltage control comb of the same design to deposit charge directly on the metal frame. It is desirable to make the proper choice of control comb length, corona gap, and series resistance, though these factors are not critical.

The lengths of the control comb and of the combined belt spray combs should be in proportion to their relative currents. These currents would be equal but for the fact that the collector removes only about two-thirds of the charge from the ascending belt, the remainder being neutralized by the belt spray combs. Since the control comb should have approximately the same current-voltage characteristic as the com-

bined belt spray combs, its corona gap should be the same as theirs and its series resistance should equal their series resistances combined in parallel.

These conditions are expressed more precisely by the following relations

$$(R_v+r_v)/(R_s+r_s)=I_s/I_v\simeq 2.0$$

and

$$R_v/r_v=R_s/r_s,$$

where R_v, r_v, and I_v are the external series resistance, the internal nonlinear resistance, and the corona current, respectively, of the voltage control corona gap, and R_s, r_s, and I_s refer similarly to the combined spray corona gaps. The second relation is necessary in order that the first relation may hold for a wide range of values of frame voltage. The application of these conditions can be made more readily understandable by reference to Fig. 8, in which the current network existing in the upper charging system is shown schematically.

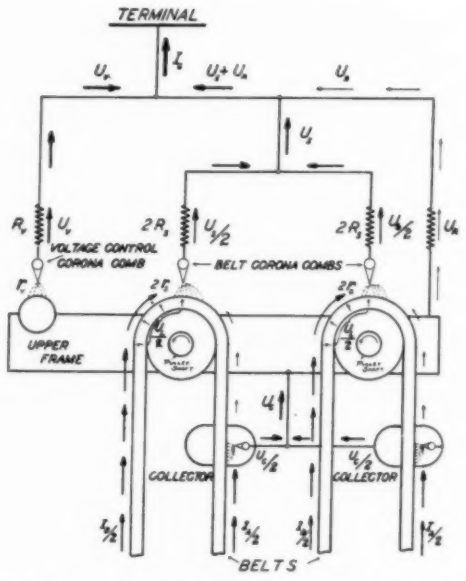

FIG. 8. Schematic diagram of the upper belt-charging system for single excitation.

MODIFIED BELT-CHARGING SYSTEM: SINGLE EXCITATION

The alterations indicated in the preceding section have been incorporated in the belt-charging system described in this section and shown schematically in Fig. 9a. Point spray combs have replaced the spray wires and collector wires. The belt spray combs are used with $\frac{1}{2}$-inch corona gaps and 7-megohm series resistors. The collector combs are placed within $\frac{1}{4}$ inch of the belt, this being the closest safe distance for mechanical reasons. The voltage control comb has half the length of the combined upper spray combs, about the same corona gap, and half the series resistance. In practice minor adjustments in the characteristic of the control comb are made by altering its corona gap. Let us suppose, for example, that saturation charge density on the ascending belts, as indicated by discharge at the point where the belts leave the lower pulleys, is not accompanied by saturation on the descending belts. The corona gap of the control comb should be increased, with a resultant increase in upper frame voltage and current on the descending belts, until discharge appears where the belts leave the upper pulleys. Because of the similarity of the characteristics of the control comb and the belt spray combs, the charge densities on the ascending and descending belts will then be approximately equal for all values of charge density.

The upper and lower frames are connected to the terminal and to ground, respectively, through 200-megohm resistors to prevent the generator from operating self-exciting because of the slight frictional charge generated on the paper belts. These resistors together with those in series with the spray combs are carbon-line resistors of approximately linear response developed in this laboratory for use at high voltage, and will be described in a later publication. The voltage applied to the lower frame is continuously variable from 0 to 20 kv by means of a small adjustable auto-transformer[9] in the primary of the power transformer of the a.c. power supply.

In order to write down in compact form the current relations involved in the operation of this belt-charging system, the following symbols are defined.

I_C = total charging current to the terminal
I_A = current carried by ascending belts
I_D = current carried by descending belts
U_C = corona current at upper collectors

[9] Variac, General Radio Co., Cambridge, Mass.

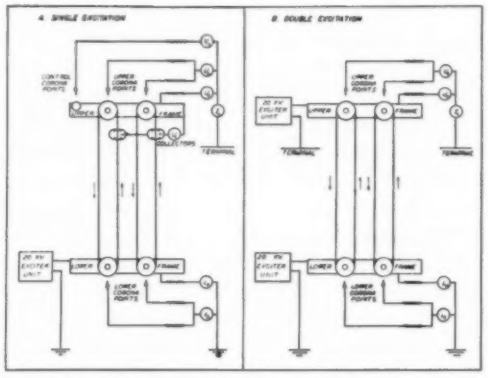

FIG. 9. Schematic diagram of the modified belt-charging systems; a, single excitation; b, double excitation.

U_S = corona current at upper spray combs
U_V = corona current at upper voltage control comb
U_L = leakage current through belts at upper pulleys
U_R = current through grounding resistor on upper frame
L_S = corona current at lower spray combs
L_L = leakage current through belts at lower pulleys

The following exact current relations are then obvious from an examination of Figs. 8 and 9a.

$$I_C = I_A + I_D = U_S + U_V + U_R$$
$$= U_S + U_C - U_L = L_S - L_L.$$

Since in practice U_R is always relatively small and U_L and L_L are small except at saturation charge density, the above relations may be written, approximately,

$$I_C = I_A + I_D = U_S + U_V = U_S + U_C = L_S.$$

These relations give a concise description of the operation of the charging system and are useful in connection with initial design and adjustments.

The belt-charging system described in this section was used for the major part of the current and voltage measurements to be described. It has proved capable of giving very steady currents over a wide range of current values. This system will probably be used here considerably in the future, in spite of certain advantages offered by the belt-charging system which employs double excitation.

MODIFIED BELT-CHARGING SYSTEM: DOUBLE EXCITATION

The necessity for obtaining excitation at the upper charging system from charge on the ascending belt introduces certain complications and adjustments which can be avoided if an independent voltage source for excitation is employed in the terminal. The resulting charging system is shown diagrammatically in Fig. 9b.

It is unnecessary that the upper and lower exciting voltages have the same value except at small charge densities, when they must be kept the same within about ten percent in order to realize steady currents. Thus the current can be adjusted over rather wide limits by varying either exciting voltage independently. For most convenient operation, however, the controls on the two exciting voltages should be operated in tandem by means of a cord or insulating rod connection.

In Fig. 10 several comparative charging current curves are given. These curves show that

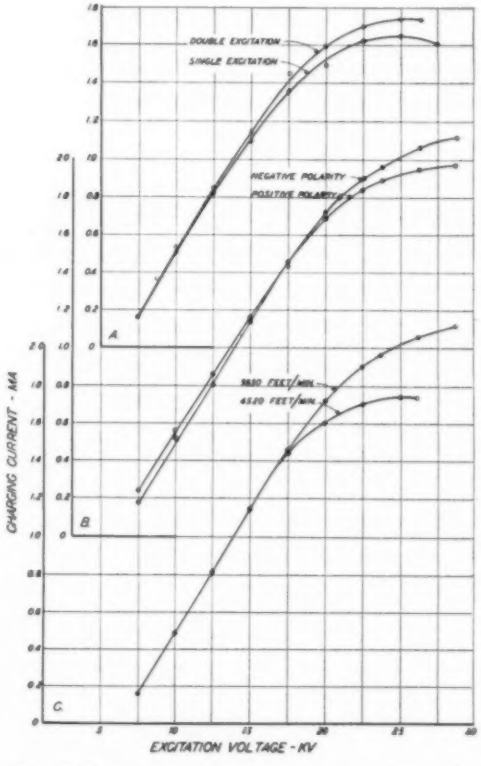

FIG. 10. Comparative charging current curves; a, single and double excitation with negative polarity and 4520 f.p.m. belt speed; b, positive and negative polarity with 5650 f.p.m. belt speed and double excitation; c, 4520 f.p.m. and 5650 f.p.m. belt speeds with negative polarity and double excitation.

greater currents may be obtained with double excitation than with single excitation, that greater currents may be delivered to a negative terminal than to a positive terminal, and that the current increases with belt speed, though not quite proportionally under the conditions obtaining. In addition, the amplitude of fluctuations in the charging current with double excitation is about half that obtained with single excitation.

The maximum charge density on the belts realized experimentally is 30 percent of the theoretical limit which corresponds to a charge density of 2.65×10^{-9} coulomb per sq. cm on each surface of the belt. Actually, since the charge is practically limited to one side of the belt at the time that the belt leaves the pulley, this charging current represents 60 percent of the theoretical limit available with the present charging arrangement.

The results described above indicate that a charging system employing double excitation is to be preferred when the second voltage supply can be obtained without inconvenience.

Voltage Measurement

The problem of obtaining a convenient and reliable measurement of the high voltage has received considerable attention. Several possible methods of voltage measurement have suggested themselves: high resistance, attracted disk, generating voltmeter, magnetic deflection of ions, and proton range. The high resistance method requires a resistance difficult to construct, difficult to shield from corona, and almost necessarily nonlinear because of the dimensions of the apparatus and the magnitude of the voltage involved. An attracted disk voltmeter is subject to large calibrating errors because of the squared scale and the relatively low available calibrating voltage. The magnetic deflection and proton range methods are more complicated than is desirable for many purposes, but may serve to confirm and standardize the results of some more direct method.

The generating voltmeter method has been used with good results for a variety of purposes.[10] Conflicting results have been obtained, however, concerning the reliability of generating voltmeter measurements made on belt electrostatic generators.[11] Because of the advantages offered by its relative simplicity and its independence of the ion beam, the method has been experimentally tested in this laboratory with special attention to systematic errors.

The generating voltmeter consists essentially of an electrostatic alternator excited by the field associated with the voltage to be measured, together with an amplifier and an output meter. In the alternator shown in Fig. 11, a two-bladed grounded rotor plate is mounted in front of a grounded stator plate on a shaft extending through a small hole in the stator plate to a synchronous motor. Two diametrically opposite

[10] P. Kirkpatrick and I. Mayake, Rev. Sci. Inst. **3**, 1 (1932); Ross Gunn, Phys. Rev. **40**, 307 (1932); P. Kirkpatrick, Rev. Sci. Inst. **3**, 430 (1932); G. P. Harnwell and S. N. Van Voorhis, Rev. Sci. Inst. **4**, 540 (1933); J. E. Henderson, W. H. Goss and J. E. Rose, Rev. Sci. Inst. **6**, 63 (1935).

[11] M. A. Tuve and L. R. Hafstad, Phys. Rev. **45**, 651 (1934); M. A. Tuve, L. R. Hafstad and O. Dahl, Phys. Rev. **48**, 315 (1935); R. G. Herb, D. B. Parkinson and D. W. Kerst, Rev. Sci. Inst. **6**, 261 (1935).

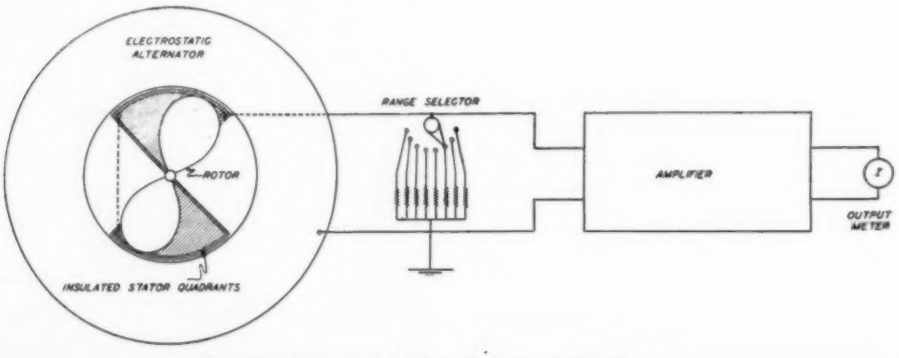

Fig. 11. Component parts of the generating voltmeter.

quadrants are insulated from the remainder of the stator plate and connected to ground through resistors ranging from 300 to 1×10^6 ohms by means of an eight-point selector switch. As the rotor alternately shields and exposes the stator quadrants in the presence of an electrostatic field, an alternating current is produced in the grounding resistor.

In order to avoid harmonics of the fundamental frequency and to simplify calculations, the rotor blades are so shaped that the generated current is sinusoidal. This reduces the effective area of the rotor by a factor of $\pi/2$. Since the alternator arrangement produces an electrical frequency twice the mechanical frequency, the rotor speed of 3600 r.p.m. produces a 120 c.p.s. alternating current.

The peak value of current delivered by the alternator may be written

$$I=\tfrac{1}{2}FAS \text{ statamperes}$$

or

$$I=2\pi CVS \text{ statamperes}$$

where F = electrostatic field on the voltmeter (e.s. volts/cm)
A = effective area of the rotor (cm²)
S = rotor speed (r.p.s.)
C = capacity between area A on the quadrants and the voltage terminal (cm)
V = voltage applied to the terminal (e.s. volts)

The former expression has proved more useful with this type of alternator, while the latter is equivalent to that used by Kirkpatrick. For convenient use the root-mean-square voltage across the resistor is given by the expression

$$E=3.93\times10^{-10}\ FASR \text{ millivolts}$$

where R = grounding resistance for the quadrants (ohms) and F is measured in volts/cm. This expression has been verified experimentally.

The voltage generated across the resistance by the alternator is applied to the input of a three-stage, resistance-capacity coupled amplifier employing type 41 tubes operated at reduced voltages from self-contained B and C batteries. The impedance of the output stage is matched to that of a 10-ma thermocouple meter providing a measured over-all transconductance of 14.0 milliamperes per millivolt at 120 c.p.s. A full-scale reading on the output meter is thus obtained with a field strength on the voltmeter ranging from 0.5 volt/cm to 2000 volts/cm depending upon the input resistance employed.

The alternator and amplifier described above have proved quite useful in the early phase of the voltage measurements because of the sensitivity and wide range afforded. Experience with this voltmeter and earlier models has led to the design of a much simplified voltmeter which will be described in some detail in a future publication.

In order to obtain a measure of the linearity of the voltmeter response, known voltages were applied to an insulated metal plate temporarily mounted at a known distance in front of the voltmeter surface. The output current from the amplifier proved to be accurately proportional to the gradient over the entire range within which measurements are to be taken. This calibration served to determine the constant in the expression

$$F=k_1\cdot I/R$$

for the gradient on the voltmeter in any location, where I is the current in the output meter and R is the input resistance.

For a particular location of the voltmeter and high voltage terminal a known calibrating voltage, separately measured by means of a precision high resistance[12] and milliammeter, is employed to determine the constant in the expression

$$V=k_2\cdot I/R.$$

Serious errors in voltage measurement, especially at calibrating voltages, may result from the large effect on the voltmeter of charged insulating surfaces. The first step in avoiding these errors is to locate the voltmeter as favorably as possible. Even with the voltmeter mounted in the top of the terminal opposite the grounded metal roof, the effect of charge on the surface of the supporting column must be taken into account at calibrating voltages to obtain an accurate calibration constant. If the current output from the generating voltmeter, I_0, due to column charge, is measured with the terminal grounded, it may be taken into consideration by modifying the above expression as follows

$$V=k_2\cdot(I\pm I_0)/R,$$

the sign being determined by the sign of the

[12] Taylor high voltage resistor, Shallcross Mfg. Co., Collingdale, Pa.

charge on the column. With this correction it is possible to obtain results with a probable error of less than one percent for individual readings.

When no correction is made for column charge, the apparent value of k_2 varies with calibrating voltage as is illustrated by the curves of Fig. 12, taken at low calibrating voltages for two different positions of the generating voltmeter at the top port hole of the high voltage terminal. An examination of these curves in the light of the expression just above indicates that in the case of the upper pair of curves the column charge was of the same polarity as the terminal, whereas in the case of the lower pair of curves the column charge was negative for both curves. This difference is correlated with the past history of the generator in the two cases.

The voltmeter has been used also, high on the side wall of the building, directly opposite the terminal. Whereas this position might appear to be quite favorable, the column effect is considerable. For example, with 25 kilovolts applied to the terminal the uncorrected reading of the voltmeter may gradually increase from 25 kilovolts to 50 kilovolts over the period of an hour. Since the change is very slow it is still possible to get accurate results by taking the value of I_0 by grounding the terminal after each voltage reading. The difficulty is that this correction must be made even at voltages as high as one megavolt with the voltmeter in this relatively unfavorable location.

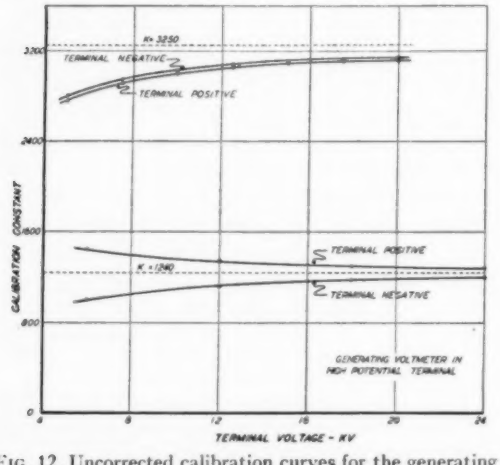

FIG. 12. Uncorrected calibration curves for the generating voltmeter, obtained with low calibrating voltages.

It should be mentioned that these corrections for the effect of charged insulators depend critically upon the humidity and may become quite negligible in damp weather.

The presence about the high voltage terminal of a space charge of ions produced by corona has been suggested[13] as a possible source of systematic error in generating voltmeter measurements. With certain simplifying assumptions, the approximate magnitude of this effect may be readily calculated. If we assume as one of the two extreme cases that all the corona is produced at the surface of the terminal, and therefore that the space charge is all of the same sign, we can calculate the maximum space charge effect.

The geometry is simplified by assuming a spherical terminal in a spherical metal room. Then the current through a spherical surface about the terminal is

$$i = dvA$$

where i = corona current between terminal and ground (amperes),
d = density of charge (coulombs/cc),
v = velocity of ions (cm/sec.),
A = area of spherical surface (sq. cm).

Then, if we make the substitutions

$$v = FM = F_0 r_0^2 M / r^2$$

and

$$A = 4\pi r^2,$$

we obtain the expression for the density at any point in the intervening space:

$$d = i/4\pi M F_0 r_0^2,$$

where M = mobility of ions in air $\simeq 1.6$ cm/sec./volt/cm,
F_0 = gradient at the surface of the terminal (volts/cm),
r_0 = radius of the terminal = 230 cm.

At the maximum generator voltage

$$F_0 \simeq 20{,}000 \text{ volts/cm}, \quad i \simeq 5 \times 10^{-4} \text{ ampere},$$

so that

$$d = 2.3 \times 10^{-14} \text{ coulomb/cc}.$$

Then the total charge in the intervening space between the terminal and the wall of the room, $r_1 = 800$ cm, is

$$Q_1 = (4/3)\pi(r_1^3 - r_0^3)d = 4.9 \times 10^{-5} \text{ coulomb}.$$

[13] M. A. Tuve, L. R. Hafstad and O. Dahl, Phys. Rev. **48**, 315 (1935).

For the sake of comparing this total quantity of space charge with the charge, Q_2, on the surface of the terminal with regard to their effects on the voltmeter in the wall of the room, both charges may be considered to be concentrated at the center of the sphere. For the conditions assumed above,

$$Q_2 = F_0 r_0^2 \times 1.1 \times 10^{-12} = 1.16 \times 10^{-3} \text{ coulomb},$$

so that $Q_1/Q_2 = 4.2$ percent. This effect would be smaller on a smaller generator in proportion to the linear dimensions of the apparatus. With a given apparatus the voltmeter should be as near the terminal as possible, since the effect depends upon r_1^3.

As an indication of the relative importance of space charge to surface charge on insulators, the surface charge density corresponding to a field of 20,000 volts/cm is 1.8×10^{-9} coulomb/sq. cm. Since the total space charge, Q_1, is equivalent to this surface charge on 27 sq. ft. of insulation and since the surface exposed by one supporting column is 400 sq. ft., space charge might be expected to have a considerably smaller effect than insulator charge.

An experimental search for space charge is possible since the effects on the gradients at the terminal and at the wall of the room would be of opposite sign. With a uniform space charge of the same polarity as the terminal, a voltmeter at ground potential would read too high, while a voltmeter in the terminal would read too low. Measurements based on these considerations have been made to ascertain whether space charge produces an appreciable effect under the conditions existing in this laboratory.

The curves of Fig. 13 represent the positive terminal voltage as a function of charging current. For one curve the voltmeter was located at the top of the high voltage terminal as indicated in Fig. 2, while for the other the voltmeter was mounted in the side port hole of the grounded terminal facing the high voltage terminal at a distance of 25 feet. Since one of these curves was taken several weeks before the other, the small difference between them may be explained as due to a slight change in the charging current necessary to realize the corresponding voltage. Differences as great as these have been obtained from day to day between curves taken under

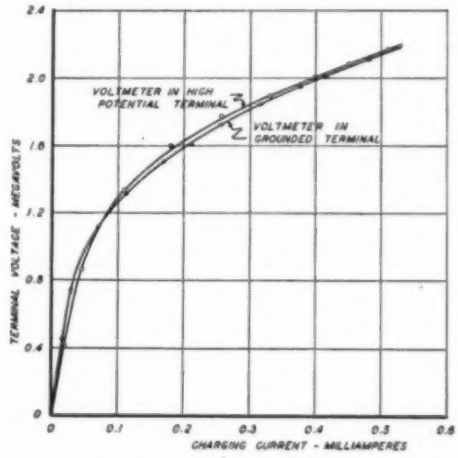

FIG. 13. Voltage-current characteristic curves for the positive terminal measured with the voltmeter in two different locations.

apparently identical conditions. In other pairs of curves similar to that shown in Fig. 13 the relative positions of the two curves have been reversed. The most significant part of the curves is the upper end, where an increasing departure would be evident if there were an appreciable error due to space charge.

These experimental results indicate that the space charge effect does not approach the extreme value calculated above. This is not surprising in view of the inherent uncertainty in the calculations introduced by the simplifying assumptions. In the first place it has been actually observed that, in addition to the corona produced at the surface of the terminal, corona of the opposite sign originates at the hangar wall resulting in a partial cancellation of space charge effects. In the second place the interior surface of the hangar is very irregular and far from spherical.

Finally, generating voltmeter measurements were compared directly with sphere gap measurements up to 1 megavolt using 62-cm spheres. Typical results are shown in Fig. 14. The points represent the sparking voltages as measured with the generating voltmeter. The upper curve was calculated from Peek's formula,[14] but the lower curve, which is two percent lower than the

[14] F. W. Peek, Jr., Trans. A.I.E.E. **33**, 923 (1914).

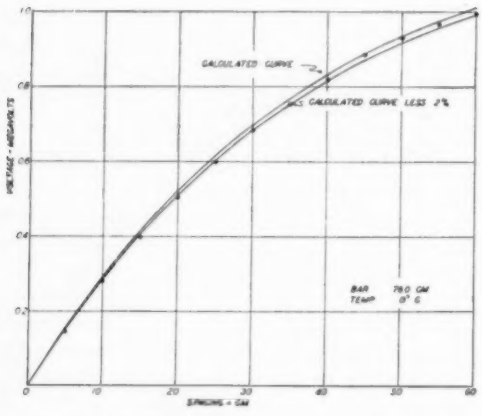

FIG. 14. Sphere gap voltage measurements with 62-cm diameter spheres.

other throughout, gives the best fit for the experimental points to be obtained with a curve of this form. In view of the fact that more recent experimental work[15] has shown that Peek's formula gives results consistently high, it appears that the absolute magnitude of the generating voltmeter results has been confirmed within an estimated probable error of two percent.

The considerations outlined in this section indicate that the generating voltmeter method may be made reliable and reasonably accurate, as well as convenient. A final comparison with proton range and deflection measurements will be made at the earliest opportunity.

CURRENT AND VOLTAGE FLUCTUATIONS

Preliminary current and voltage fluctuation measurements have been made to determine the usefulness of the generator for the study of resonance disintegration effects. Current fluctuations were measured with the terminal at high voltage by means of a cathode-ray oscillograph[16] across a resistor in the connection between the upper charging assembly and the terminal. Current fluctuations with the terminal grounded were made with the oscillograph across a resistor in the terminal grounding lead.

A visual examination showed that the principal component of the current fluctuations may be represented with sufficient accuracy for the present purpose by a single loop of a 12 c.p.s. sinusoidal wave appearing once for each revolution of the belt. It was found to be caused by a slight dip in the charging current at the time that the belt joint was passing over the upper pulley. Since the resulting regularly-spaced pulses were much larger than the irregular background upon which they were imposed, the percentage current fluctuation is defined in terms of the ratio of this a.c. component peak value to the d.c. component. The results for singly-excited and doubly-excited charging systems are given in Fig. 15.

Since the terminal voltage represents an equilibrium between charging current and load current, fluctuations in this voltage may arise from fluctuations in either current. The load current consists of insulator leakage principally down the supporting column, ion current in the accelerating tube, and corona current. Except at the highest voltages, the ion current should be the principal source of load current fluctuations.

If we neglect for the moment load current fluctuations, the percentage fluctuation in terminal voltage is considerably smaller than the associated fluctuation in charging current because of the smoothing effect of the terminal-to-ground capacity. To the extent that the a.c. component of the current can be represented by a sinusoidal wave form of frequency ω, the smoothing effect can be calculated from the

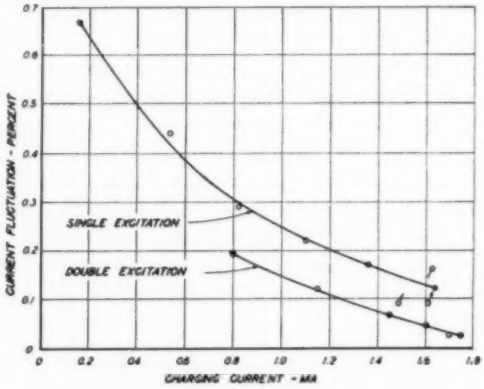

FIG. 15. Fluctuations in charging current with single excitation and double excitation.

[15] J. R. Meador, Elec. Eng. **53**, 942 (1934); J. E. Henderson, W. H. Goss and J. E. Rose, Rev. Sci. Inst. **6**, 63 (1935).
[16] RCA Model TMV-122-B.

expression

$$S=\frac{\text{voltage fluctuation (percent)}}{\text{current fluctuation (percent)}}$$

$$=\frac{R_{ac}}{R_{dc}}\cdot\frac{1}{(R_{ac}\omega^2C^2+1)^{\frac{1}{2}}},$$

where R_{ac}, R_{dc}, and C are, respectively, the terminal-to-ground a.c. resistance, d.c. resistance, and capacity. R_{ac} and R_{dc} for any given voltage may be determined from such curves as those shown in Fig. 13. For example, if we assume an effective frequency of 12 c.p.s. and a terminal capacity of 300 micromicrofarads and take R_{ac} and R_{dc} from Fig. 13, the smoothing factor, S, at 2 megavolts is 0.01 for no ion current and 0.03 for one ma of ion current, and at 1 megavolt the factor is 0.003 for no ion current and 0.06 for one ma of ion current. In view of the assumptions involved in these calculations, the results are useful only in showing the trend of the smoothing effect and in indicating that this effect is considerable.

A direct measurement of voltage fluctuation was made by exposing an insulated 15-cm hemispherical electrode to ground at a port hole of the terminal. With the electrode connected to the terminal through the input resistor of an amplifier and cathode-ray oscillograph, a small fraction of the terminal voltage fluctuation appeared on the oscillograph. The amplitude of fluctuation measured in this way was consistently much smaller than 0.1 percent, but exact values are not given because the calculation of the percentage of the a.c. terminal voltage on the insulated electrode involved uncertainties.

These preliminary current and voltage fluctuation measurements have sufficed to show that the limitation in precision of voltage setting imposed by voltage fluctuations is small compared with other limitations. This point will be confirmed by an improved method for measuring voltage fluctuations at the time that the disintegration experiments are performed.

Voltage variations requiring a time greater than a few seconds may be distinguished arbitrarily from the fluctuations discussed above because of the fact that they can be considerably reduced by automatic or manual control of the excitation voltage. These variations are not large. By the use of a double Variac arrangement for manual control, a given terminal voltage can be maintained constant with a probable error of 0.1 percent.

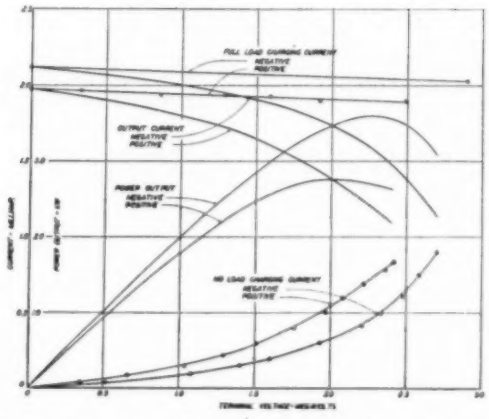

FIG. 16. Generator performance curves for the positive and negative terminals.

GENERATOR PERFORMANCE DATA

The maximum measured voltage of a single generator unit, obtained with a charging current of 1.5 ma, was 2.72 megavolts positive and 3.15 megavolts negative. The highest voltage which has been obtained consistently without sparking is 2.4 megavolts positive and 2.7 megavolts negative, giving a total voltage of 5.1 megavolts between the generator terminals. At this voltage there is still 1.1 ma available for use with an accelerating tube. The humidity control inside the generator column makes it possible to obtain this voltage with an external humidity of 100 percent.

A typical set of generator performance curves for the positive and negative terminals is given in Fig. 16. The full-load charging current, I_c in Fig. 9a, was measured as a function of voltage for the positive terminal with saturation charge density on the belts and the terminal voltage limited by a grounded corona comb mounted in the opposite terminal. Because of the persistent sparking to the corona comb limiting the negative voltage, the full-load charging current for the negative terminal was measured at zero and full voltage only. For both curves the charging current

decreases by only 4 percent between zero and full voltage.

The no-load charging current curves of Fig. 16 were obtained by varying the charge density on the belts and measuring the resulting voltage of the unloaded terminal. Below one megavolt the loss current is largely leakage down the column, as measured by a meter at the base of the column, while above one megavolt loss by corona predominates.

The difference between the full-load and the no-load charging current represents the available output current. Reference to the figure indicates that more than half of the full-load charging current is available at the maximum generator voltage. The reliability of the output current curves obtained in this way has been confirmed for the positive terminal by direct measurement of the current to an external corona comb used for voltage limitation.

The power output curves in the figure represent the product of the output current and the corresponding voltage. The power available from the generator increases with voltage to a maximum of 6.3 kw at a total voltage of 4.4 megavolts.

Acknowledgments

We are pleased to acknowledge our indebtedness to Dr. R. H. Gerke of the United States Rubber Company for his advice in connection with our vibration isolation problems, and to Mr. M. F. Witherell of the Behr-Manning Paper Company for his suggestions and assistance in connection with the problem of jointing and operating the large paper belts.

We are grateful to Mr. E. W. Nickerson, the machinist on this project, for the active interest and the ingenuity with which he has carried out his part of the design and construction of equipment.

We greatly appreciate having had the cooperation of Dr. E. W. Samson who was located at Round Hill during the period, August, 1932 to December, 1933, as a National Research Fellow, and who assisted in the construction and initial tests of the original belt charging system.

We are indebted to Research Corporation for the original grant which made possible the launching of this project, to Colonel E. H. R. Green for the continued use of the extensive facilities at Round Hill, and to Professor E. L. Bowles in administrative charge of these facilities on behalf of the Massachusetts Institute of Technology.

Finally, it is our pleasure to express our profound appreciation for the unfailing support and helpful advice of Dr. K. T. Compton during the long period of generator development.

LETTERS TO THE EDITOR

Prompt publication of brief reports of important discoveries in physics may be secured by addressing them to this department. Closing dates for this department are, for the first issue of the month, the twentieth of the preceding month; for the second issue, the fifth of the month. The Board of Editors does not hold itself responsible for the opinions expressed by the correspondents.

On the Absorption of Slow Neutrons in Boron

Recently attempts have been made[1,2] to measure the energies of neutrons selectively absorbed in elements like Ag, Rh, I. This determination is based on the assumption that, in the case of light elements which are disintegrated with emission of a charged particle, no sharp resonance occurs, and therefore the capture cross section follows the $1/v$ law.[3,4]

It seemed worth while to obtain a direct check of the validity of this law, at least for neutrons of thermal energies, and for this purpose we performed with boron an experiment already used with Ag and Cd for determining the dependence of the capture cross section upon the neutron velocity.[5] An aluminum disk of 50 cm diameter was coated with boron carbide, of such thickness as to transmit about 40 percent of the slow neutrons under the experimental conditions, and was rotated at 5500 r.p.m., all conditions being substantially the same as in the former experiments.[5] By rotating the disk first in one direction and then the other, we observed a change in apparent absorption coefficient of 1.3 percent, with a statistical error of 0.8 percent. This change is so small that it may well be due to experimental error, and we may conclude that our result is not inconsistent with the assumption that there is no change in transmitted intensity depending upon the velocity of the boron absorber. This result, distinctly different from that obtained with cadmium, where a change of as much as 8 percent was found, appears to indicate that the absorption of thermal energy neutrons in boron does not depart appreciably from the $1/v$ law.

Doubt might arise whether this conclusion is still justified in a case like the present one, where on account of their zero-point energy, the random motions of the boron atoms have an average velocity which is higher than the velocity of the rotating disk. Actually, on account of the vibrations in the crystal lattice, the velocities of the boron atoms will roughly correspond to those of free particles of the same mass at the Debye characteristic temperature of the lattice, which we may assume to be about five times higher than room temperature. However, it can be shown that, even with high velocities of the boron atoms, the conclusion is still valid that, under the assumption of the $1/v$ law, the transmitted intensity cannot be appreciably affected by the rotation of the disk.

F. Rasetti
D. P. Mitchell
G. A. Fink
G. B. Pegram

Pupin Physics Laboratories,
Columbia University,
April 15, 1936.

[1] Weekes, Livingston and Bethe, Phys. Rev. **49**, 471 (1936).
[2] Rasetti, Fink, Goldsmith and Mitchell, Bull. Am. Phys. Soc., Washington Meeting, April 30, 1936.
[3] Wigner and Breit, Phys. Rev. **49**, 519 (1936).
[4] Bohr, Nature **137**, 344 (1936).
[5] Rasetti, Segrè, Fink, Dunning and Pegram, Phys. Rev. **49**, 104 (1936).

The Infrared Spectra of H_2S, HDS, and D_2S

Nielsen and Nielsen have just published a preliminary account[1] of an investigation of the above spectra. We have been occupied with this subject for some time, and it is interesting to contrast the two sets of results, since we find some measure of disagreement between them. It must be confessed, however, that the peculiarities of the spectra coupled with their weakness leave room for doubt in their interpretation.

The existence of the H_2S band at 8μ is confirmed, and for the three molecules we find $\omega_2 = 1236$, 1078, and 898 as compared with 1266, 1111, and 926 cm^{-1} (N. and N.). The band in both H_2S and D_2S is peculiar in exhibiting no resolution into P and R branches, although possessing rotational structure; we do find for HDS that there is a strong peak at 998 cm^{-1} which is apparently unobserved by Nielsen and Nielsen. If this is the P branch of this long wave band, we must regard it as missing in the other two molecules.

ω_2 for H_2S is given by Nielsen and Nielsen at 2703 cm^{-1}. We consider a more likely value for the center is 2632 cm^{-1}. In D_2S these authors find a band at 2198 cm^{-1} which they attribute to the same mode: This frequency is much too high, and without correcting for anharmonicity gives a force constant of some 5.3×10^5 dynes per cm, whereas Badger's rule makes it certain that it should be of the order of 4.2×10^5 dynes per cm. We find a band at 1940 cm^{-1} which fulfills this requirement, and conforms with the Raman spectra of H_2S and D_2S.

We have made an estimate of the anharmonic coefficients and using the mechanical frequencies corresponding to infinitesimal amplitude, find in the notation of Van Vleck and Cross,[2] that k_1, k_{12}, k_3, and k_{13} are, respectively, 4.25, 0.07, 0.24 and 0.04×10^5 dynes per cm for H_2S; and 4.34, 0.07, 0.23, and 0.04 for D_2S. These values are for a vertical angle of 110° which fits the admittedly crude deductions made from the vibrational spectrum, as compared with 92° 20′ obtained by Cross[3] from the rotational analysis of the band at 9910 cm^{-1}. The difference between the values of k_1 for H_2S and D_2S is not unlikely, since it is only the energy of dissociation, D, reckoned from the level (0,0,0) which we may expect to be the same to a high degree of approximation in polyatomic molecules and their isotopes.

C. R. Bailey
J. W. Thompson
J. B. Hale

The Sir William Ramsay Laboratories
of Inorganic and Physical Chemistry,
University College, London,
April 8, 1936.

[1] A. H. Nielsen and H. H. Nielsen, J. Chem. Phys. **4**, 229 (1936).
[2] J. H. Van Vleck and P. C. Cross, J. Chem. Phys. **1**, 357 (1933).
[3] P. C. Cross, Phys. Rev. **47**, 7 (1935).

The Disintegration of Nitrogen by Slow Neutrons

The disintegration of nitrogen by slow neutrons was attributed independently by Chadwick and Goldhaber[1] and by ourselves[2] to the reaction

$$_7N^{14}+{}_0n^1\rightarrow{}_5B^{11}+{}_2He^4+Q_1. \quad (1)$$

However, the value of Q_1 obtained by Chadwick and Goldhaber by an ionization method was 0.5 MEV, while we deduced the value 2.33 MEV from our range measurements of tracks observed in a cloud chamber. Our value was calculated from the 1.06-cm range of the disintegration particles by assuming that the disintegration particles were B^{11} nuclei and alpha-particles. In a private communication Dr. Goldhaber has suggested that this apparent disagreement can be eliminated if we interpret the disintegration in a different way as postulated in the reaction

$$_7N^{14}+{}_0n^1\rightarrow{}_6C^{14}+{}_1H^1+Q_2. \quad (2)$$

The energy of the disintegration Q_2 calculated from our range measurements then becomes 0.58 ± 0.03 MEV which agrees with Chadwick and Goldhaber's ionization value. We have now found another reason why the former interpretation is impossible. We have just measured the energy released in the reaction

$$_5B^{11}+{}_1H^2\rightarrow{}_6C^{12}+{}_0n^1+Q_3 \quad (3)$$

and found Q_3 to be 13.5 ± 0.3 MEV.[3] Combining this result with that of Cockcroft and Lewis[4] in their investigation of the reaction

$$_7N^{14}+{}_1H^2\rightarrow{}_6C^{12}+{}_2He^4+Q_4 \quad (4)$$

one obtains $Q_1=Q_4-Q_3=-0.28\pm0.3$ MEV.

This is quite different from the value 1.5 MEV which was calculated from Bethe's masses and which appeared to agree fairly well with the value 2.33 MEV. However, our value of $Q_1=-0.28$ MEV agrees quite well with the respective values $Q_1=-0.3$ and $Q_1=-0.2$, calculated from the recent list of masses given by Oliphant[5] and by Cockcroft and Lewis.[4] This new value of Q_1 necessarily eliminates reaction (1) from further consideration in regard to the 1.06 cm particles resulting from the disintegration of nitrogen by slow neutrons.

Recently McMillan[6] has obtained evidence of a radioactive C^{14} with a half-life of about 3 months and a maximum beta-ray energy of about 0.2 MEV. From reactions (2) and (5)

$$_6C^{14}\rightarrow{}_7N^{14}+e^-+Q_5 \quad (5)$$

we see that ${}_0n^1-{}_1H^1=Q_2+Q_5$; hence from these data the mass difference between a neutron and a hydrogen atom appears to be 0.8 MEV. This is in good agreement with Aston's new masses of $_1H^1$ and $_1H^2$, and Feather's binding energy of the deuteron (2.26 MEV).

T. W. Bonner*
W. M. Brubaker

W. K. Kellogg Radiation Laboratory,
California Institute of Technology,
April 22, 1936.

[1] Chadwick and Goldhaber, Proc. Camb. Phil. Soc. **31**, 612 (1935).
[2] Bonner and Brubaker, Phys. Rev. **48**, 469 (1935); **49**, 223 (1935).
[3] To be published in Phys. Rev.
[4] Cockcroft and Lewis, Proc. Roy. Soc. **A154**, 261 (1936).
[5] M. L. E. Oliphant, Nature **137**, 357 (1936).
[6] E. McMillan, Bull. Am. Phys. Soc., April, 1936.
* National Research Fellow.

Isotopic Constitution of Strontium, Barium, and Indium

Mass spectrograph analyses have been made of the ions of strontium, barium, and indium, emitted when oxides of these elements are heated on tungsten filaments. Evidence has been obtained for two new isotopes, one of strontium and one of barium. No new indium isotopes were found. The observations reported below have been checked on two different instruments.

In the case of strontium, a peak was observed at mass 84 whose height corresponded to 0.5 percent of the total strontium emission. The masses of the known isotopes of strontium are all greater than 84 so the possibility is excluded that the effect is due to a strontium compound. Since the only known isotope of mass 84 belongs to krypton and the other krypton isotopes do not appear, we believe that this peak is due to a new isotope of strontium. A small impurity of rubidium was present initially but disappeared with continued heating of the filament. The relative abundance of the known strontium isotopes was found to be 9.6 percent of mass 86, 7.5 percent of mass 87, and 82.4 percent of mass 88, differing slightly from the rough values given by Aston.[1] Assuming a packing fraction of -8.2 this gives 87.62 for the atomic weight of strontium, in good agreement with the chemical value of 87.63. A search for other isotopes revealed that masses 82, 83, 85, 89, and 90 were present to less than 1 in 2000, 1 in 1000, 1 in 2000, 1 in 500 and 1 in 2000, respectively.

The curves for barium showed a peak at mass 134 making up 1.8 percent of the total emission. The same considerations which applied in the case of strontium lead us to believe that this is due to a new isotope of barium. Accepting Aston's relative abundance for the known isotopes 135, 136, 137, and 138, and assuming packing fractions of -6.1 we deduce an atomic weight for barium of 137.36 in exact agreement with the international atomic weight. Barium isotopes of masses 132, 133, 139, and 140 were shown to be present to less than 1 in 2000, 1 in 1000, 1 in 400, and 1 in 1000, respectively.

Evidence for the possible existence of a third isotope of indium is given by the observation[2] of three artificially radioactive periods induced in indium by neutron bombardment. However, only two of these periods are water sensitive. Mass spectrograph analyses revealed only the two known isotopes. A search over the mass range from 110 to 119 showed that masses 110, 111, 112, 114, 116, 117, 118, and 119 were present to less than 1 in 5000, 1 in 10,000, 1 in 5000, 1 in 200, 1 in 5000, 1 in 10,000, 1 in 8000, and 1 in 30,000, respectively. The ratio of the abundance of mass 115 to that of mass 113 was found to be 21 ± 1 in agreement with Aston's observation.[3] If we assume a packing fraction of -6 we obtain for indium an atomic weight of 114.81 in agreement with Aston's value. The international atomic weight for indium is 114.76.

J. P. Blewett
M. B. Sampson

Palmer Physical Laboratory,
Princeton University,
April 28, 1936.
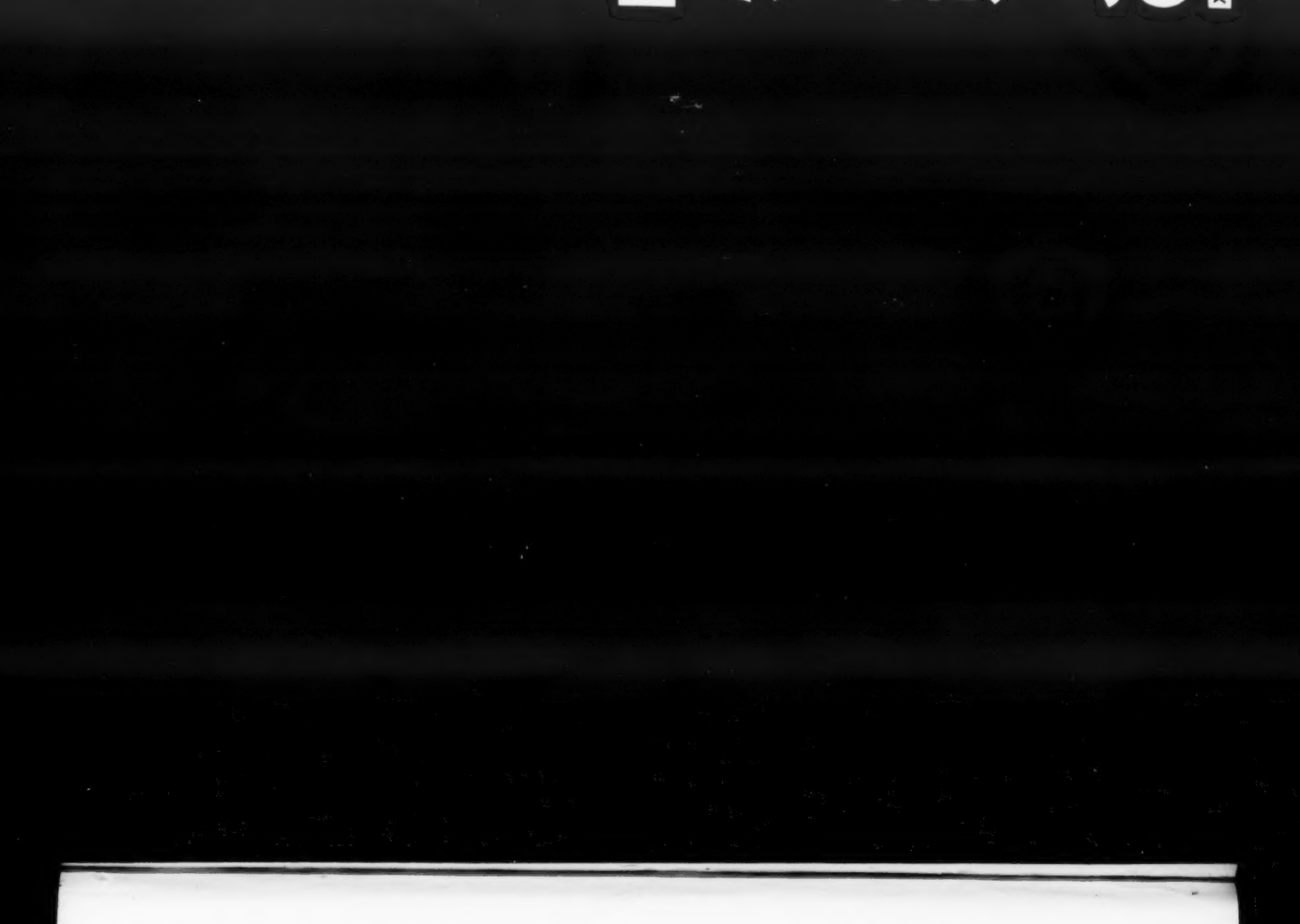
[1] Aston, *Mass Spectra and Isotopes* (Arnold, 1933).
[2] Szilard and Chalmers, Nature **135**, 98 (1935).
[3] Aston, Proc. Roy. Soc. **A149**, 403 (1935).